MUNI
PŘÍRODOVĚDECKÁ
FAKULTA

PERTURBED STELLAR MOTION IN THE GALACTIC CENTER DURING ITS ACTIVE PHASES

BC. KRISTÝNA JANOUŠKOVÁ

Školitel: RNDr. Michal Zajaček, Ph.D.
Konzultant: Mgr. Matúš Labaj
Ústav teoretické fyziky a astrofyziky
Přírodovědecká fakulta
Masarykova Univerzita

Brno – 2024

BIBLIOGRAFICKÝ ZÁZNAM

Autor:	Bc. Kristýna Janoušková Přírodovědecká fakulta, Masarykova Univerzita Ústav teoretické fyziky a astrofyziky

Název práce:	Perturbovaný pohyb hvězd v galaktickém centru během jeho aktivní fáze
Studijný program:	Fyzika
Obor:	Astrofyzika
Vedoucí práce:	RNDr. Michal Zajaček, Ph.D.
Konzultant:	Mgr. Matúš Labaj
Akademický rok:	2023/2024
Počet stran:	xiv + 93
Klíčová slova:	galaktické centrum, hvězda S2, Galaxie, Mléčná dráha, nukleární hvězdokupa, nebeská mechanika

BIBLIOGRAPHIC ENTRY

Author:	Bc. Kristýna Janoušková Faculty of Science, Masaryk University Department of Theoretical Physics and Astrophysics

Title of Thesis:	Perturbed stellar motion in the Galactic center during its active phases
Degree Programme:	Physics
Field of Study:	Astrophysics
Supervisor:	RNDr. Michal Zajaček, Ph.D.
Co-supervisor:	Mgr. Matúš Labaj
Academic Year:	2023/2024
Number of Pages:	xiv + 93
Keywords:	Galactic center, S2 star, Galaxy, Milky Way, nuclear stellar cluster, celestial mechanics

ABSTRAKT

Centrum Mléčné dráhy je nejbližším galaktickým centrem a zároveň jediným centrem, ve kterém je možné současnými pozorovacími metodami rozlišit objekty jako jsou samostatné hvězdy hustých jaderných hvězdokup. Přímo se nabízí jeho pozorování a detailní popis fyzikálních jevů probíhajících v tomto nehostinném prostředí okolo supermasivní černé díry SgrA*. Tato práce popisuje pohyb hvězdy S2, jednou z nejjasnějších S hvězd blízkých k SgrA* s excentricitou dráhy 0.88, a jeho vývoj v plynoprašném prostředí s některými relativistickými vlivy. Stáří S2 a podobných S hvězd je několik milionů let a během této doby se pohybovala v téměř sféricky rozloženém horkém plazmatu. Příležitostně se mohl vytvořit hustší a tenčí akreční disk. Zkoumali jsme, jaké otisky mohly tyto plynně-prachové struktury zanechat na hvězdné dráze a zjistili jsme, že i při maximální pozorované hustotě těchto struktur dráha hvězd není nijak zásadně ovlivněna.

ABSTRACT

The centre of the Milky Way is the closest galactic centre and the only centre where objects such as single stars in dense nuclear clusters can be resolved with current observational methods. Its observations and a detailed description of the physical phenomena occurring in this inhospitable environment around the supermassive black hole SgrA* are directly available. This paper describes the motion of a star, such as the bright star S2, one of the closest stars to the black hole with an orbital eccentricity of 0.88, and its evolution in a gaseous-dusty environment, including most relevant relativistic effects. The age of S2 and similar S stars is a few million years and during that time it has been moving through nearly spherically distributed hot plasma. Occasionally, a denser and thinner accretion disc could have formed. We investigated what imprints these gaseous-dusty structures could have left on the stellar orbit and we found out that even with the highest observed density of these structures the orbit of stars is not substantially affected.

MUNI
SCI

MASARYKOVA UNIVERZITA
PŘÍRODOVĚDECKÁ FAKULTA
KOTLÁŘSKÁ 2, 611 37 BRNO
IČ: 00216224
DIČ: CZ00216224

ZADÁNÍ
DIPLOMOVÉ PRÁCE

Akademický rok: 2023/2024

Ústav:	Ústav teoretické fyziky a astrofyziky
Studentka:	Bc. Kristýna Janoušková
Program:	Fyzika
Specializace:	Astrofyzika

Ředitel *ústavu* PřF MU Vám ve smyslu Studijního a zkušebního řádu MU určuje diplomovou práci s názvem:

Název práce:	Perturbed stellar motion in the Galactic center during its active phases
Název práce anglicky:	Perturbed stellar motion in the Galactic center during its active phases
Jazyk závěrečné práce:	angličtina

Oficiální zadání:
To the first approximation, the motion of a star bound to the supermassive black hole (SMBH) in the Galactic center can be treated as a two-body problem with relativistic corrections. There are different factors that perturb this well-defined motion. First, these are other stars in the nuclear star cluster (NSC) that affect the test star motion via the fast resonant relaxation and the slower two-body non-resonant relaxation. Second, there are environmental effects (accretion disk, jet, giant molecular clouds) that can perturb the stellar motion, especially during the enhanced accretion of the SMBH. The student will review these processes by making analytical estimates of the effects of different components of the NSC, in particular by comparing characteristic timescales of different processes. Subsequently, the student will focus on the environmental effects of an accretion disk-jet system – they will study the motion of a star bound to the SMBH perturbed by the combined influence of the disk-jet system. The timescales and the magnitude of this perturbation will be discussed taking into account different disk densities, jet kinetic luminosities, duration of the activity, and different stellar types. In particular, the potential relation to the detected stellar disks in the inner parts of the NSC in the Galactic center will be discussed.

Vedoucí práce:	RNDr. Michal Zajaček, PhD.
Konzultant:	Mgr. Matúš Labaj
Datum zadání práce:	4. 11. 2021
V Brně dne:	3. 5. 2024

Zadání bylo schváleno prostřednictvím IS MU.

Bc. Kristýna Janoušková, 3. 5. 2024
RNDr. Michal Zajaček, PhD., 3. 5. 2024
Mgr. Dušan Hemzal, Ph.D., 3. 5. 2024

ACKNOWLEDGEMENTS

Here I would like to thank especially my supervisor, Michal Zajaček, thanks to whose patience and time I was able to finish this work, Filip Hroch, who pulled me out of a last-minute trouble with the code, and Matúš Labaj for his help with Python. Furthermore, I would like to thank all the members of the High Energy Astrophysics group in Brno who were helpful every time I bothered them again and again with my questions. Especially during the completion of the thesis, another very important people were Lukáš Vorobok and Eva Baťková, who supported me through every breakdown I had during the writing process.

DECLARATION

Hereby I declare that I have prepared my Master's thesis independently under the guidance of the supervisor with the use of cited works.

Brno, 2024

Bc. Kristýna Janoušková

Hakuna matata.

— Timon and Pumbaa, *The Lion King*

CONTENTS

INTRODUCTION

Over many centuries, mankind gazed into the skies with astonishment thinking about our place in the universe. It was not earlier than in the twentieth century that we finally found our place at least in the nearby neighborhood. From there, the journey to the discovery of the Galactic center took several more decades.

The center of the Milky Way galaxy is our nearest possible laboratory for testing some of the processes that cannot be seen anywhere else. These phenomena include, for example, some relativistic mechanisms, or fundamental processes important for the formation and shaping of galaxies. The strongest influence on the evolution and formation of galaxies are undoubtedly the black holes at their hearts. These environments are crucial for expanding our knowledge of physics and can be a great opportunity to enhance our understanding of the fundamental laws of the Universe.

The Galactic center is a region containing a vast amount of stars where we can observe the effect of extreme gravitational potential found nowhere else in the Universe; one of the greatest motivation to study this inhospitable environment is to fill the gap in our knowledge of the gravitational potential physics. The S2 star is a great candidate to explore this new region in parameter space of gravitational potential against the mass of the gravity generator (Fig. 0.1).

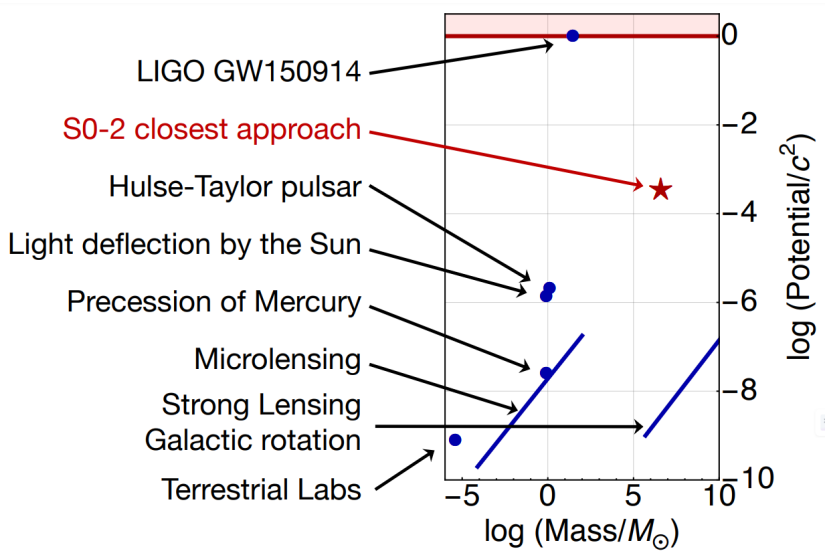

Figure 0.1: A logarithmic parameter space showing the gravitational potential probed by different potential-generating bodies. The S2 star extends the coverage of this space. Image taken from Hees et al., 2017.

The theoretical part of this thesis is divided into two chapters. Chapter one gives a brief overview of the structures in the galactic center with their scales and a list of observatories that were the greatest contributors to the exploration of this magnificent region. In Chapter two we present the most important section of celestial mechanics needed for computing the orbits of the S2 star with a short historical window. In Methodology part we cover two methods for obtaining the orbits; the analytical approach and numerical methods with tests of our codes. Finally, in the Results part of this work we present orbits computed with our codes for various scenarios in the galactic center such as a dusty environment with several layouts or post-Newtonian correction due to the strong gravitational potential.

Part I

THEORY

1

GALACTIC CENTER

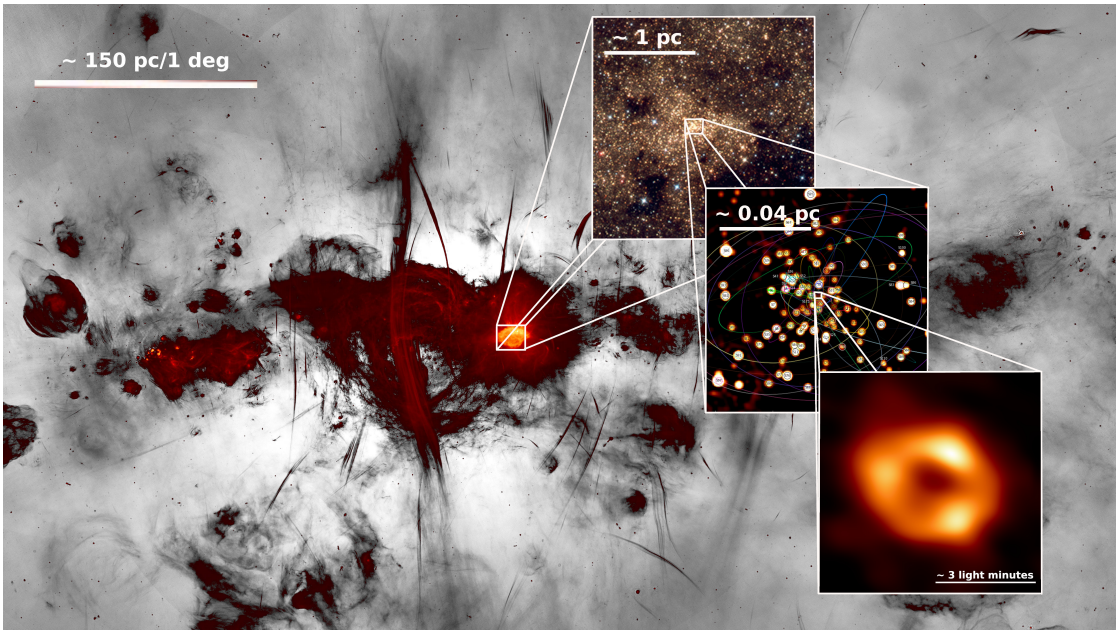

Figure 1.1: A MeerKAT mosaic of inner 6.5 square degrees of the Galactic Center of the Milky Way (*background*), nuclear star cluster (*top zoomed image*), S star cluster (*middle zoomed image*) and the black hole SgrA* (*bottom zoomed image*). To the left of the Sgr A complex (brightest region in the center of the image) the Radio Arc (Sec. 2.4.2) lies perpendicular to the Galactic Plane. Credit: Heywood et al., 2022, UCLA Galactic group, Eckart group, Ph1-UniKoeln, EHT Collaboration.

The long and fascinating journey that led to the discovery of the Galactic Center (GC) spans over several centuries.

Even the ancient Greeks knew about the condensed belt of stars that they later named the Milky Way, since the appearance reminded them of milk spilled over the table. For many centuries the mysteries of the Galactic center (GC), however, remained unveiled. It was in the late 18th century that Sir William Herschel started systematic observations of globular star clusters and debated about the structure of the Milky Way and the universe itself. He discovered that stars were more concentrated towards the GC, and with increasing distance from the center the distribution decreased. Unfortunately for him, infrared and radio astronomy were not accessible at that time.

In early 20th century Harlow Shapley and Heber Curtis got into the "Great Debate" on the nature of "spiral nebulae" and the size of the Milky Way. Shapley, whose work

was mainly focused on the size and structure of the Milky Way galaxy, used observations of the globular clusters to estimate the size of the galaxy and stated that the Sun does not lie in the center of the Galaxy. He realized that around one-third of all the globular clusters lay in the constellation Sagittarius, using the (newly discovered concept) RR Lyrae stars to calculate the distances of the clusters. He discovered that all of the clusters form a roughly spherical distribution whose center lies in the Sagittarius constellation. He argued in favor of a disk-shaped galaxy with the Sun located in the remote part of the galaxy.

On the other hand, Heber Curtis was well known for his work on nebulae and novae. He opposed Shapley's view and proposed the idea that the spiral nebulae were extragalactic systems from our Milky Way. The evidence needed for the determination of the right opinion was presented by Edwin Hubble's discovery of Cepheid variable stars in Andromeda Galaxy M31 stating that it is, indeed, an extragalactic system.

Later in time, in the 1970s, radio, infrared, and X–ray astronomy became a crucial part of many astronomical observations including those of the Galactic center. For the first time, we observed some features that were obscured in the optical fields by interstellar dust.

There are many features in the Galactic nucleus - different types of stars, dust, gas (both ionized and neutral), supernovae, and in the very center the black hole SgrA*. In this thesis, we will mainly focus on the inner 1 arcsecond (in angular diameter) or 0.04 parsec (in linear diameter).

1.1 NUCLEAR STAR CLUSTER

Nuclear star clusters (NSCs) are compact luminous, dense, and massive objects located at dynamical and photometric centers (Neumayer et al., 2011) of about 75% early- to late-type galaxies of the local Universe (Böker et al., 2002; Côté et al., 2006; Neumayer et al., 2011). NSCs are the most massive stellar objects known in the Universe, of the order of more massive than globular star clusters (Böker et al., 2004; Neumayer et al., 2020). They often also coexist with supermassive black holes that lie in their hearts (Graham and Spitler, 2009).

To define the size of the nuclear star cluster, the effective radius $r_{\rm eff}$ is used. Within this radius, half of the cluster's light is contained. Another characteristic that can be directly measured is the NSC's luminosity. Preferred method to measure the luminosity is to integrate the model parametrization of the surface brightness distribution (Carollo et al., 2002; Côté et al., 2006). The last fundamental characteristic is the mass. However, this quantity is not as straightforward to measure. Most mass measurements come from photometric studies (mass is derived from the relations between the color and the mass-to-light ratio).

Most late-type galaxies NSC's consist of a mix of stellar populations. The mass of the cluster is mainly dominated by the oldest stellar populations (ages in Gyrs), whereas the luminosity is dominated by the youngest. Young stars are concentrated in the inner few tenths of a parsec in most galaxies, including M 31 (Bender et al., 2005) and other early-type galaxies (Nguyen et al., 2019).

How such clusters form is still a matter of research. Two main mechanisms are currently being discussed - the migration of the globular cluster to the centre of the galaxy due to the dynamical friction (Lotz et al., 2001; Tremaine et al., 1975) was confirmed with N-body simulations of Oh and Lin, 2000; however Milosavljevic, 2004 argued that the infall of the globular cluster time scale is too long and instead proposed the in-situ formation caused by very high gas density in the spiral galaxies. A combination of both hypotheses is the most probable: the relaxation time is of the order of Gyrs at the half-mass radius (Merritt, 2009) and close to the Hubble time beyond 1pc (Merritt et al., 2010).

These astrophysical objects are of huge interest for tests of general relativity and study of tidal disruptions, stellar collisions, stellar orbit's evolution in the immediate vicinity of a black hole or a very exotic event – extreme mass ratio inspiral (EMRI). In these rare phenomena, gravitational radiation is released with the infall of the mass onto the black hole (Amaro-Seoane et al., 2007).

MILKY WAY'S NSC. One of these structures was found in 1968 in the inner few tens of parsecs of the Milky Way at a distance 8.0 ± 0.25pc (Malkin, 2013) due to the development of infrared cameras (Becklin and Neugebauer, 1968), along with several components of neutral and ionized hot gas (Genzel and Townes, 1987; Reid et al., 2013). The central parsec is dominated by mostly ionized HII region known as Sgr A West (see section 1.4.3. There can also be found a concentration of low-density gas found by Lo and Claussen, 1983 denoted as 'mini-spiral' surrounded by the orbiting, dense molecular cloud, the 'circum-nuclear disk' (section 1.4.2) (Christopher et al., 2005). Further away from the center, the young supernova remnant, Sgr A East (see section 1.4.1), forms a border and on a scale from 5 to 100 pc several molecular clouds reside (Güsten and Downes, 1980; Mezger et al., 1996).

As discussed above, NSC in the center of our Galaxy also contains both stars of young stellar population and a dominant old population which points to repeating episodes of star formation (Walcher et al., 2006) with the latest episode in the last few millions of years (Bartko et al., 2010; Krabbe et al., 1995). About 80% of the stellar mass comes from old stars (more than 10 Gyr) – e.g. late-type giants, helium-burning stars on the horizontal branch with lower masses, and a few more massive red supergiants (two in the inner $R \leq 0.5\,\mathrm{pc}$ and 15 within the radius of $R = 2.5\,\mathrm{pc}$) (Blum et al., 2003).

Apart from the old stars, there is a confirmed presence of more than 200 massive young stars, dominated by Wolf-Rayet and O and B stars, in the central 0.5pc

(Feldmeier-Krause et al., 2015; Ghez et al., 2003). Their ages fall within an interval of $3 - 8$Myrs (Lu et al., 2013; Paumard et al., 2006). The presence of this young population confirms the in-situ formation scenario, because the time for their infall to the Galactic center would take much longer than is their age. Another evidence for the in-situ formation is the lack of these young stars further than 0.5 pc.

From the ratio v/σ (where v is the rotational velocity and σ is the velocity dispersion), we can get a sense of whether the motions in the NSC are dominated by rotation or random motion. The typical value of this ratio is between 0 and 0.5 for early-type galaxies. The Milky Way nuclear star cluster has $v/\sigma = 0.6$ (Feldmeier et al., 2014), leading us to the determination of a rotating object with rotation parallel to the Galactic plane (GP). Schödel et al., 2014 showed for the first time that our NSC appears intrinsically elliptical, rather than spherically symmetric, with an ellipticity of $\epsilon = 0.29 \pm 0.02$ elongated along the GP.

The whole stellar cluster exhibits a solid-body rotation in the sense of the rotation of the Galaxy with a slow pace of around 1.4km/s/arcsec (Feldmeier et al., 2014; Genzel et al., 1996; Schödel et al., 2009). The rotational velocity increases with the distance from SgrA* while the velocity dispersion decreases.

Since galactic conditions do not allow for optical observations (because of the reddening, and a high extinction $A_V \sim 30$mag), researchers have to operate in the range between near-infrared and radio wavelengths, where the minimum of the extinction is around $\lambda = 5\mu$m with $A_{4.5\mu m} \approx 0.5$ (Fritz et al., 2011).

From the work of Fritz et al., 2016; Schödel et al., 2014 the effective radius of the Milky Way's NSC falls to the range between $r_{\text{eff}} = 4.2 \pm 0.4$pc and $r_{\text{eff}} = 7.2 \pm 2.0$pc, depending on the wavelength of the observation. Mass derived from photometric and dynamical measurements by Feldmeier et al., 2014; Fritz et al., 2016; Schödel et al., 2014 is between $M = (2.1 \pm 0.7) \times 10^7 M_\odot$ and $M = (4.2 \pm 1.1) \times 10^7 M_\odot$, which is in agreement with the first work on mass estimates of Galactic center's NSC of Becklin and Neugebauer, 1968.

Altogether, the main characteristics of the nuclear star cluster that resides in the center of our very own Galaxy are summarized in table 1.

–	Spitzer 4.5μm	K-band
Reference radius r_{eff}	4.2 ± 0.4pc	7.2 ± 2.0pc
Luminosity L	$4.1 \pm 0.4 \times 10^7 L_\odot$	$5.2 \pm 3.0 \times 10^7 L_\odot$
Mass M	$(2.1 \pm 0.7 - 4.2 \pm 1.1) \times 10^7 M_\odot$	
Ellipticity ϵ	0.29 ± 0.02	

Table 1: Characteristics of the Milky Way galaxy's nuclear star cluster derived from the Spitzer data and in K-band. The mass range is the result of photometric and dynamical methods.

STELLAR DISKS Galactic centers, including those of the Milky Way, frequently exhibit disc-shaped morphologies, characterized by the presence of massive young O and B stars exhibiting distinctive radial velocity shifts. This pattern logically suggests the existence of a rotating disc composed of these massive stars. This hypothesis gained further credence through proper motion measurements conducted in the late 1990s, which revealed that the majority of bright early-type stars within the central arcseconds predominantly follow a clockwise motion pattern (Genzel et al., 2000). Subsequent investigations have unveiled the likelihood of an additional stellar disc or ring, moving in a counterclockwise direction. In particular, the clockwise system exhibits a more defined structure and is seemingly encapsulated by this counterclockwise ring of stars (Genzel et al., 2003; Paumard et al., 2006; Tanner et al., 2006).

Genzel et al., 1996 observed that approximately 20 stars within the inner 12 arcseconds display a clear rotational pattern, with their radial velocities being significantly blue-shifted north of the GC and red-shifted to the south of the center of gravity, presenting a motion directly opposite to the general rotation of the Milky Way and its NSC (Genzel et al., 1996; Schödel et al., 2014; Seth et al., 2006; Tanner et al., 2006). This stellar structure was termed the clockwise (CW) disk. Over subsequent years, additional research has expanded the catalog of stars confirmed to participate in this structure, simultaneously refining its orbital parameters (Genzel et al., 2000; Genzel et al., 2003; Levin and Beloborodov, 2003a; Paumard et al., 2001). The inclination of the CW disk relative to the plane of the sky was determined to be $i = 12^\circ \pm 7^\circ$, with its line of ascending node positioned at $\Omega = 120^\circ \pm 15^\circ$.

In a detailed analysis by Genzel et al., 2003, a counterposed system was proposed, with an inclination of $i = 40^\circ \pm 15^\circ$ and a line of ascending nodes at $\Omega = 160^\circ \pm 15^\circ$. This counterclockwise (CCW) disk is believed to encompass 10-12 stars.

A comprehensive dynamical study of roughly a hundred stars within the inner 1 parsec of the Milky Way, undertaken by Paumard et al., 2006, has elucidated further details of these enigmatic structures. According to their findings, the CW disk comprises 40 stars, whereas the less densely populated CCW disk contains 17. This analysis facilitated refined estimates of their inclinations and ascending nodes: $i = 127^\circ \pm 2^\circ$, $\Omega = 99^\circ \pm 2^\circ$ for the CW system and $i = 24^\circ \pm 4^\circ$, $\Omega = 167^\circ \pm 7^\circ$ for the CCW disk.

The distinguishing features of these two stellar disks are their markedly different eccentricity distributions. The CW disk primarily features stars on low to medium eccentricity orbits (< 0.5), indicative of near-circular trajectories. Conversely, the CCW disk is predominated by stars on high eccentricity orbits, with a notable peak around $e = 0.8$ (Paumard et al., 2006).

Moreover, Paumard et al., 2006 have determined that a significant majority of early-type stars are associated with one of these two stellar structures, suggesting their formation occurred within the past 2 million years.

1.2 S-STAR CLUSTER

On the smallest scales of the nuclear star cluster, just a few hundredths of parsec around the supermassive black hole SgrA*, the cluster of high-velocity B-type stars reside (Bartko et al., 2010; Do et al., 2013; Ghez et al., 2003; Paumard et al., 2006). Their presence is a vital piece of the puzzle, confirming the existence of a supermassive black hole, Sagittarius A*, within the core of the Milky Way. Several of these bodies trace paths within mere tens of light-hours from Sgr A*, achieving velocities close to 2% of the speed of light.

This spectacular array of stars constitutes a particularly dense cluster, occupying a region less than 1 arcsecond in angular measure, or a mere 0.04 parsecs across (Ghez et al., 2008). This cluster boasts a mix of young B-type stars amidst aged stars — giants, supergiants — and the energetic Wolf-Rayet class. These stars appear to reside in at least one disk-like structure.

One of the disks is the inner edge of the clockwise disk described in section 1.1. The second disk, not fully confirmed yet, is orthogonal to the clockwise one and the stars belonging to it are rotating in counter-clockwise direction (Ali et al., 2020).

Proximity of this cluster to such a destructive force poses a compelling paradox: How did these young stars emerge or arrive so close to a black hole? This puzzle is colloquially termed the 'paradox of youth'.

PARADOX OF YOUTH. The 'Paradox of Youth' posits a conundrum: stars are typically born in dense molecular clouds, yet such clouds cannot hold up against the shearing tidal forces of a nearby black hole. They would, instead, spiral inexorably towards the black hole long before star formation could commence. To remain unscathed by tidal disruption, a molecular cloud's radius should theoretically exceed a certain threshold, given by:

$$r > \left(\frac{M_{\mathrm{BH}}}{m_p n} \right)^{1/3}, \tag{1.1}$$

where M_{BH} is the black hole's mass, m_{p} is the mass of a proton, and n is the cloud's density. With a black hole mass $M_{\mathrm{BH}} = 4 \times 10^6 M_\odot$ and cloud density $n = 10^4 cm^{-3}$, the safe radius turns out to be around 25 parsecs (Ghez et al., 2003).

To facilitate star formation in the vicinity of such tidal forces, one would expect the gas cloud to have a density exceeding the critical Roche density, which outpaces the observed molecular cloud densities by orders of magnitude.

One theory that explains the presence of these stars is that of in situ formation in which intense star formation is triggered by the infall of a dense gas cloud into the inner few parsecs (Levin and Beloborodov, 2003b; Paumard et al., 2006).

On the contrary, the migration hypothesis considers the globular clusters to have been gravitationally seized from a different locale and pulled inward by dynamic friction over time (Tremaine et al., 1975). The dynamical friction depends on the mass of the cluster linearly, and thus the most massive clusters are most likely to be dragged to form the NSC. As evidence for this theory we can consider the lack of globular clusters in the central parts of many galaxies (Capuzzo-Dolcetta and Mastrobuono-Battisti, 2009; Lotz et al., 2001) that indicates many of these were driven to the nucleus.

Among the more unconventional proposals is one that implicates dark matter in star formation. In this scenario, regions rich in dark matter could enhance the environmental density sufficiently to support the birth of stars (Hassani et al., 2020).

THE S CLUSTER Turning our gaze to the S cluster itself, we find a spectrum of stellar types: 16 (52%) lighter B-stars of about 3.5 to 20 $M_\odot$, alongside three O stars and 12 late-type stars. The O stars, which hug tightly around the inner 0.9 arcsecond radius, form part of a clockwise-rotating disk. The computed orbits of 19 such stars within an arcsecond semimajor axis reinforce this structure (Gillessen et al., 2009).

Drawing from spectral analyses, the estimated lifespan of the S-star cluster fits between 6 to 400 years, positioning these stars' spectral properties in close kinship with the B2-9 types found in our solar neighborhood (Eisenhauer et al., 2005).

Incorporating all B stars outside the clockwise disk into our calculations suggests that the distribution of their angular momenta resonates with an isotropic configuration (Eisenhauer et al., 2005; Ghez et al., 2005; Gillessen et al., 2009; Schödel et al., 2003). Meanwhile, their mean eccentricity soars around 0.8 (Ghez et al., 2005; Gillessen et al., 2009; Schödel et al., 2003) —above thermal isotropic distribution levels—hinting at a formative mechanism that favors the production of highly eccentric orbits.

Stellar motions within the black hole's sphere of influence adhere to near-Keplerian dynamics. Although the precession periods far outpace the orbital periods, enabling resonant interactions visible over numerous revolutions (Rauch and Ingalls, 1998), the Lense-Thirring precession proximal to the black hole's axis of spin may hold sway in this context (Levin and Beloborodov, 2003a).

S2 The star with the shortest orbital period, around 16 years, and the closest approach to SgrA*, is S2 / S02. It is the brightest member of the B-star cusp, a main-sequence dwarf of spectral type B0-2.5V and of zero-age main-sequence mass (ZAMS) of $m_{\mathrm{ZAMS}} \sim 19.5 M_\odot$ (Martins et al., 2007) with an age estimated to be $6.6^{+3.4}_{-4.7}$Myr (Martins et al., 2007) and a highly elliptic orbit with an eccentricity of $e = 0.88$. The He/H abundance is relatively high, around (0.25-0.5), which makes the star a member of "He-rich" subclass of the B-stars. It also has a low rotational velocity of an O9/B0 young dwarf with an age less than 10^6yr and a mass of around $15 M_\odot$ (Eisenhauer

et al., 2005). In the work of Davies and King, 2005 the possibility that the star is the He-rich core of a stripped AGB star is proposed.

The S2 star orbits Sgr A* with a period of approximately 15.9 years (Sabha et al., 2012); it follows an elliptical path with a semimajor axis of roughly 970 astronomical units (au). At its pericenter, the point in orbit closest to the black hole, S2 barrels to within a mere 17 light hours of Sgr A*, subjecting it to some of the strongest gravitational forces experienced by any star in our galaxy.

It is the brightest among the S-stars and a significant subject of astrophysical study due to its high velocity and close encounters with Sgr A*, which provide a unique opportunity to test laws of physics under extreme conditions.

With a spectral type ranging from B0 to B2.5V, S2 is a massive main-sequence star with an estimated zero-age main-sequence (ZAMS) mass of approximately 19.5 solar masses ($M_\odot$) (Martins et al., 2007). Observations have revealed an unusual abundance of helium in its atmosphere, classifying it within the "He-rich" subgroup of B-type stars and suggesting an advanced stage in its life cycle.

The unique characteristics and orbit of S2 have allowed astronomers to confirm predictions made by Einstein's general theory of relativity. Throughout its orbit, particularly during its close pass to Sgr A* in 2018, careful observations of its radial velocity and positional displacement confirmed the gravitational redshift predicted by the theory. Moreover, the star's orbit has been seen to precess, an effect consistent with the predictions of general relativity, providing further evidence for the presence of a supermassive object embedded in spacetime at our galactic center.

Astronomers using facilities such as the Very Large Telescope (VLT) operated by the European Southern Observatory and the Keck Observatory have collected extensive data on S2. These observations have contributed not only to the study of gravitation in strong fields but also to our understanding of the complicated interactions and evolution of stars in such an inhospitable environment.

1.3 SGRA*

The conception of a "black hole" can be traced back to A.M. Sullivan (1896-1980) who first used the term in "Music of the Spheres", while its formal acknowledgment as a technical term occurred when John Wheeler introduced it within the scientific community in 1967 (Wheeler, 1968). The term refers to a body bound by gravitational forces so strong that the escape velocity from its surface exceeds the speed of light and therefore even the light particles (massless photons) are not able to escape; leading the object to appear as a "dark" mass. The point of no return is known as the event horizon.

The first ones to study the escape velocities from very massive stars based on Newton theory of gravity were John Michell and Pierre-Simon Laplace in the late 18th

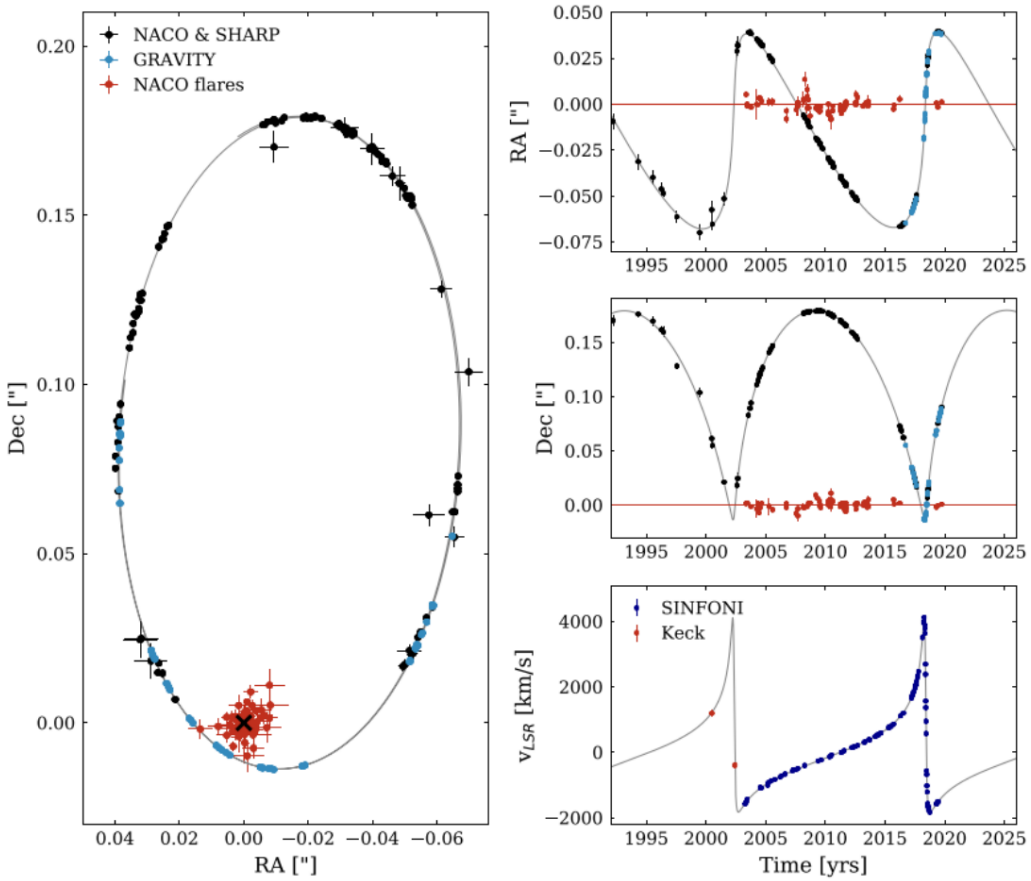

Figure 1.2: Results of the S2 orbital data observations taken between 1992 and 2019. The left panel shows multiple observational instruments' astrometric positions of S2 with best-fitting orbit. The center of mass is denoted by the black cross. The red data points are of the infrared SgrA* emission. Image taken from Genzel, 2021.

century. They noted that for a very massive and compact object, the escape velocity exceeds the speed of light. Mathematically, black holes were described as a solution to Albert Einstein's vacuum field equations from general relativity by Karl Schwarzschild in 1916 and Roy Kerr in 1963 along with several others. Each of these precepts works for different scenarios, as described below.

Black holes are defined by three critical parameters: mass (M), angular momentum ($J = cMa$), and electric charge (q), adhering to the facets of the "no-hair" theorem. The Kerr-Newman solution encompasses all three parameters, assuming nonzero values for each, although the influence of the electric charge is deemed negligible in most astrophysical scenarios. Empirically, the Kerr solution (Kerr, 1963), reliant solely on mass (M) and spin (a), emerges as the most relevant. Characterizing a black hole

necessitates observing the gravitational interactions in its immediate vicinity, which presents the sole approach for determining these defining parameters.

The diameter of the event horizon is calculated as the so-called Schwarzschild radius for a non-rotating black hole without a charge (Schwarzschild, 1916):

$$r_S = \frac{2GM}{c^2}, \tag{1.2}$$

where G is the gravitational constant, M is the mass of a body and c is the speed of light, whereas for Kerr's solution, a solution for spinning black holes, the horizon is located at

$$r_K = \frac{GM}{c^2} + \sqrt{\left(\frac{GM}{c^2}\right)^2 - a^2}. \tag{1.3}$$

Everything within this radius is drawn towards the singularity (region where no longer any physical equations hold) and trapped in an eternal dance with time.

Both these scenarios are, however, assumed to be highly symmetrical, leaving the question whether the reality is the case. Roger Penrose suggested the cylindrical symmetry instead.

The diverse mass spectrum of black holes encompasses a broad astrophysical range. Stellar black holes, typically ranging from ~ 3 to a few tens of solar masses, emerge from the gravitational collapse of massive stars. In contrast, supermassive black holes (SMBHs), prevalent in galactic centers, manifest masses spanning from millions to billions of solar masses. Intermediate-mass black holes, ranging from (10^2) to (10^5) solar masses, represent a less common but significant category. Notably, astronomical observations, as detailed by King, 2015, have established an upper limit to the mass of astrophysical black holes at (5×10^{10}) solar masses, underlining the diverse manifestations of black holes and their influential role across cosmic scales.

Observation of these exotic objects became possible with the development of highly sensitive, high-resolution telescopes. An important point in confirming the existence of a black hole in the center of our galaxy was the detailed observation of the orbit of the star S2 around the gravitational potential, which indicated a mass of over $4 \times 10^6 M_\odot$. From the star's orbit, there was confirmation that the object could not be anything other than a black hole; otherwise the mass would have to be extended, unstable, or emitting much more light than observed (Maoz, 1998).

SGRA* The circumnuclear gas (Crawford et al., 1985; Wollman et al., 1977) and later the S2 star and its measured orbit (Plewa et al., 2015) were used to measure the enclosed dark mass and proved the existence of a $M \sim 4 \times 10^6 M_\odot$ black hole with a

Schwarzschild radius of 10μas. The size of 10μas is equivalent to 2 cm at the distance of the Moon. It is indeed a very compact object with strong emission in the radio and X-ray bands.

The first speculations on the existence of a black hole in our Galaxy were made by Donald Lynden-Bell and Martin Rees in 1971 and only three years later, in 1974, the first detailed radio observation of the inner 1pc core of the Galaxy was made by Bruce Balick and Robert Brown with the Green Bank interferometer (Balick and Brown, 1974). Their findings (high brightness temperature, small angular diameter, association with intense IR and radio continuum) indicated that there must be a massive structure on a subarcsecond scale. However, due to the measurement difficulties and complexity of the instruments, the only experimental proof of the mass concentration are the stellar motions.

Reinhard Genzel's and Andrea Ghez's teams played pivotal role in providing empirical support for SgrA*, concerning the motions of stars around the central mass condensation. Their goal was to detect the gravitational impact on the orbital dynamics of the test particles (the S stars). These studies solidified the idea that the central "dark" mass concentration cannot be just a dense, long-lived cluster of white dwarfs, neutron stars, or stellar black holes but that SgrA* is indeed a black hole (Eckart and Genzel, 1996; Ghez et al., 1998).

Crucial to these revelations are the sensitivity and the angular resolution of the observations. High-resolution VLBI observations (Very Long Baseline Interferometry) in millimeter and radio wavelengths revealed its intrinsic radius between 20 and 50 μas which corresponds to 2 to 5 $R_\odot$ (Bower et al., 2006). Pioneering work by Wollman et al., 1977 provided the first dynamical evidence, estimating a non-stellar mass of 2-4 millions masses that of the Sun through the infrared imaging spectroscopy of interstellar gas clouds.

By the latest measurements, strong variability from radio through infrared to X-ray was detected which can indicate that some energetic processes such as an accretion onto a black hole can take place in that region now.

According to recent findings bolstered by the Event Horizon Telescope observations, the accretion rate of Sgr A* is estimated to be in the range of $(5.2 - 9.5) \times 10^{-9} M_\odot \mathrm{yr}^{-1}$, rather low rate for a supermassive black hole (Collaboration, 2022). This suggests that Sgr A* is accreting at much less than the Eddington limit expressed by Eq. (1.4), which is the theoretical maximum rate of accretion where radiation pressure balances the gravitational attraction (hydrostatic equilibrium). At a higher rate, the radiation pressure would overcome gravity and any material around the black hole would be blown away.

$$\dot{M}_{Edd} = \frac{4\pi G M m_p}{\sigma_T c \epsilon} \tag{1.4}$$

Radiative efficiency (fraction of the rest mass energy of the accreted material that is released as radiation) of SgrA* is quite low. However, studies have found different efficiency values; for instance, accretion models indicate that the radiative efficiency can be as high as approximately 0.9 (Narayan et al., 1995; Quataert et al., 1999). High efficiency implies that a significant fraction of the accreted mass is converted into energy, resulting in strong electromagnetic emissions even for small accretion rates.

These accretion rates and radiative efficiencies inform a wide range of associated astrophysical phenomena. For instance, the low accretion rate of Sgr A* can explain the relatively faint emission across the electromagnetic spectrum when compared to other active galactic nuclei. Additionally, the suspected presence of an outflow or jet from Sgr A* complements the picture; an outflow redistributes the accreted energy, carrying it away from the black hole and potentially impacting the surrounding galactic center environment (Narayan et al., 1998).

Although our Galaxy has a relatively quiescent core, observations have shown variability of this source in the X-ray and near-infrared regions (Do et al., 2009). In the NIR region, we can observe about 4 flares per day with a brightening factor of up to 160, and in the X-ray region, about 1 flare per day occurs, which is brightened by a factor of 27 compared to the continuum radiation (Baganoff, 2003; Dodds-Eden et al., 2011; Eckart et al., 2006). The reason behind these flares is probably a magnetic reconnection in the region of the accretion disc around the SMBH.

The structures around the SMBH in the center of our Galaxy are still being observed as they are a significant contribution to black hole physics. It is a closest known supermassive black hole which makes it an ideal candidate for studying accretion processes in detail. With new possibilities and telescopes the astronomers anticipate more accurate measurements and advanced theoretical models.

PARAMETERS OF SGRA* In this thesis, we will use the following values of some of the characteristic parameters for SgrA*.

The distance to the Galactic center can be derived using two primary methods. The first method utilizes the stellar populations, predominantly globular clusters, while the second method focuses on the motion of stars, particularly the star S2. The approach based on globular clusters assumes a spherical distribution around the galaxy, enabling the determination of the distance (or kinematic properties) of these clusters. By leveraging the symmetry, the center of the galaxy and the position of SgrA* can be determined. Using this approach, a distance of $R = 7.4 \pm 0.28$ kpc was estimated by Francis and Anderson, 2014. The second approach combines proper motions and radial velocities to derive the distance of the stars, resulting in a distance of $R = 8.25 \pm 0.02$ kpc according to observations by Parsa et al., 2017, Abuter et al., 2021, Leung et al., 2022.

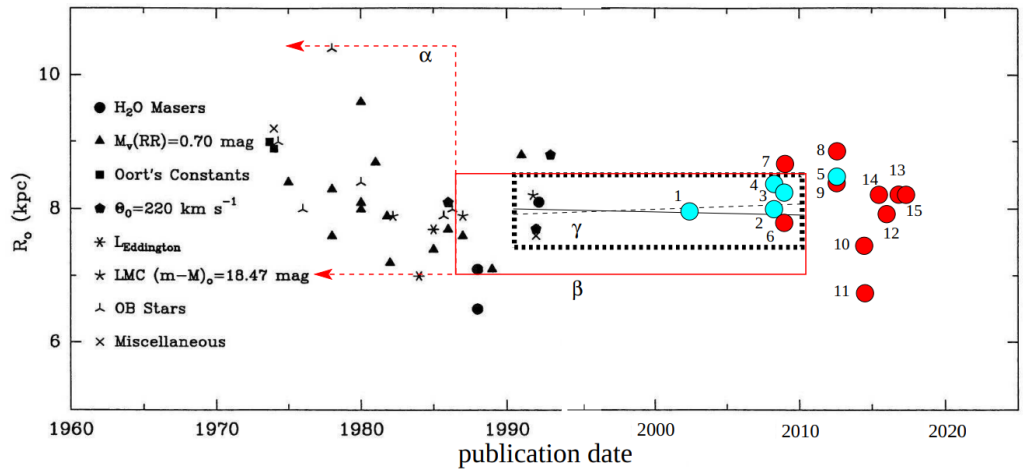

Figure 1.3: Evolution of the measured distance of the Galactic center. Black symbols with comments are taken from Reid, 1993; the data from Genzel et al., 2010 are located in the region α, β; data derived by Malkin, 2013 are in the region γ. Recent results obtained from the stellar orbital analysis are shown by the blue points and labeled by numbers: 1. Horrobin et al., 2004, 2. Ghez et al., 2008, 3. Gillessen et al., 2009, 4. Ghez et al., 2008, 5. Do et al., 2013. Results derived from the stellar populations are shown in red: 6. Majaess et al., 2009, 7. Vanhollebeke et al., 2009, 8. Do et al., 2013, 9. Dékány et al., 2013, 10. Francis and Anderson, 2014, 11. Branham, 2014, 12. Boehle et al., 2016, 13. Parsa et al., 2017. The image was taken from Eckart et al., 2017.

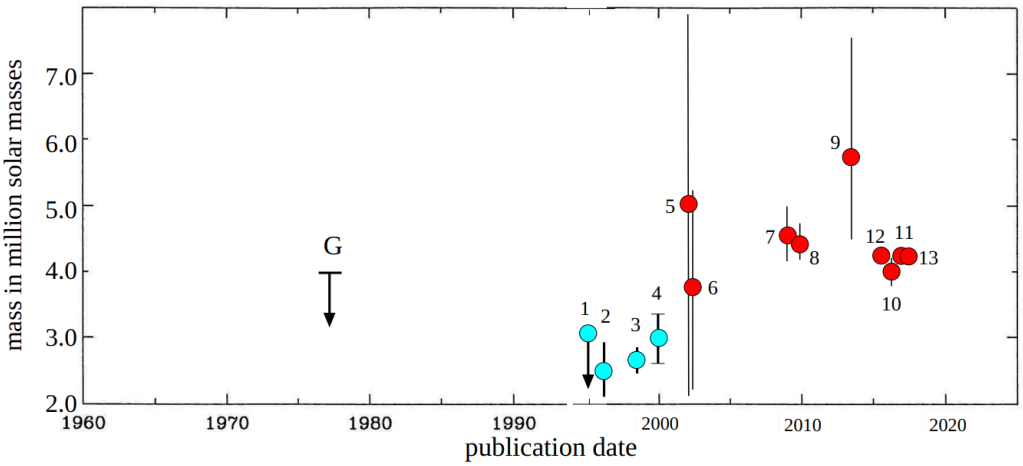

Figure 1.4: Mass measurements evolution of SgrA*. "G" denotes the mass estimate from the minispiral gas by Wollman et al., 1977. Estimates derived from stellar radial velocities and proper motions are shown with blue points: 1. Krabbe et al., 1995, 2. Eckart and Genzel, 1996, 3. Ghez et al., 1998, 4. Genzel et al., 2000. Mass calculations derived from the stellar orbits are shown by red points: 5. Eckart et al., 2002, 6. Schödel et al., 2002, 7. Ghez et al., 2008, 8. Gillessen et al., 2009, 9. Do et al., 2013, 10. Boehle et al., 2016, 11. Parsa et al., 2017. The image was taken from Eckart et al., 2017.

One of the three key parameters for determining the nature of the black hole is its mass. The quest to derive this quantity began in 1977 with the analysis of the 12.8 μm NeII line emission from the ionized gas in the mini-spiral surrounding the black hole by Wollman et al., 1977. Subsequently, with the detection of S stars and their observations, the mass value was confirmed in the work of Abuter et al., 2023, revealing a mass of $M = (4.297 \pm 0.012) \times 10^6\ M_\odot$ enclosed within $9R_g$, corresponding to 0.38 AU (roughly equal to the radius of Mercury orbit).

1.4 OTHER STRUCTURES

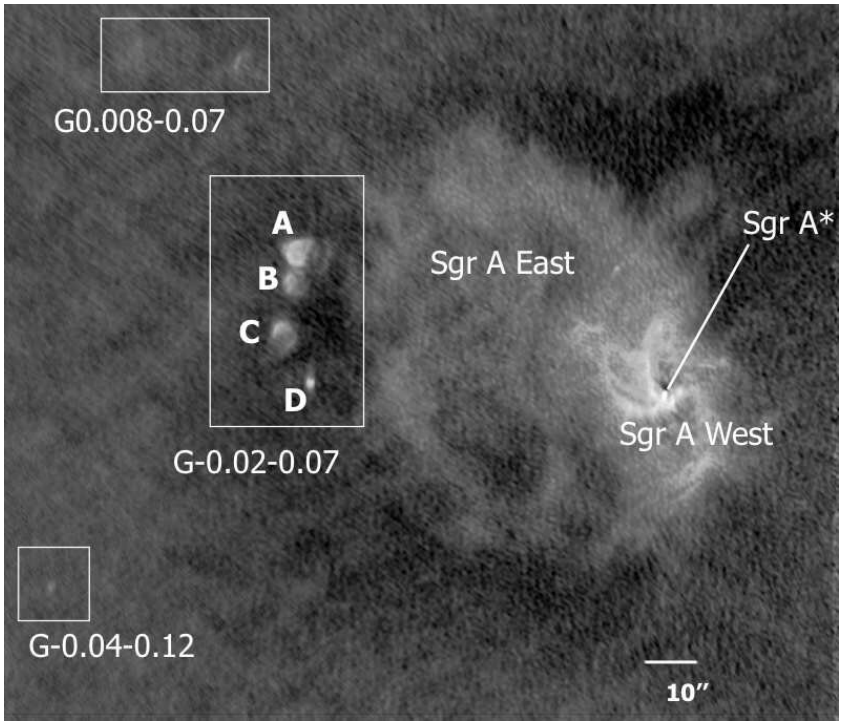

Figure 1.5: Overview of the inner 15 parsecs of the Galaxy - the focus is on the Sgr A East source surrounding the Sgr A West minispiral, at the centre of which lies the black hole SgrA*. The boxes highlight the molecular clouds known as G-clouds with which the supernova remnant interacts. Image adapted from Mills et al., 2011.

Along with the already described NSC in the heart of our Galaxy, there are several other features, such as ionized or neutral gas and dust (Genzel et al., 1994; Genzel and Townes, 1987; Reid et al., 2013).

1.4.1 *Supernova remnant Sgr A East*

At approximately 10 parsecs in scale, the 10^4 years old (Maeda et al., 2002) Sgr A East, thought to be the nearest supernova remnant to the center of our Galaxy (Jones, 1974), emits nonthermal (proposedly synchrotron) radiation in radio wavelengths. Its shell-like configuration lies adjacent to a belt of clusters of molecular gas clouds, distinguished by their velocity along the line of sight.

1.4.2 *Circumnuclear disk*

An asymmetric ring of dense (mainly molecular) gas clumps moving on a quasi-Keplerian orbit around SgrA*, also called the circumnuclear disk (CND) or ring (CNR), is a structure with an inner radius of about 1pc that spans several parsecs. The gas within this disk or torus has significant internal motion and is heated by the central parts from both the old and the young stars' ultraviolet flux.

In the spectrum of the CND, the lines of the carbon monosulfide molecules were found, indicating that the gas clouds are dense enough to be able to form stars. However, such a phenomenon has not been observed. According to a team of researchers, the clouds then have to be stabilized by some other factors such as a strong magnetic field.

1.4.3 *Mini-spiral Sgr A West*

The first observation of a so-called mini-spiral extending over the inner 2 pc at the center of the Galaxy was made with the VLA telescope (1.5.3) by Ron Ekers in 1983 (Ekers et al., 1983). The Lo and Claussen, 1983 image clearly shows the structure of the mini-spiral, consisting of a filamentary HII and neutral gas clouds, and the exact position of SgrA*.

This formation has several distinguishable parts – Northern Arm, Western Arc and Eastern Arm. Recent studies of gas motion suggest that all three arms orbit SgrA* along Keplerian orbits. In addition, the Eastern Arm has been found to collide with the flow from the Northern Arm (Zhao et al., 2009).

The whole system is made up of several molecular clouds of gas and dust that are ionized by massive stars in the central region. The total mass of all the matter enclosed within this structure is estimated to be around $\sim 60 M_\odot$. From the study of kinematics and morphology, Fridman et al., 1996 and Sanders, 1998 concluded that some hydrodynamical instability occurred in the CND and that the fall of part of the mass towards the core created the Northern Arm in the minispiral. The Western arc,

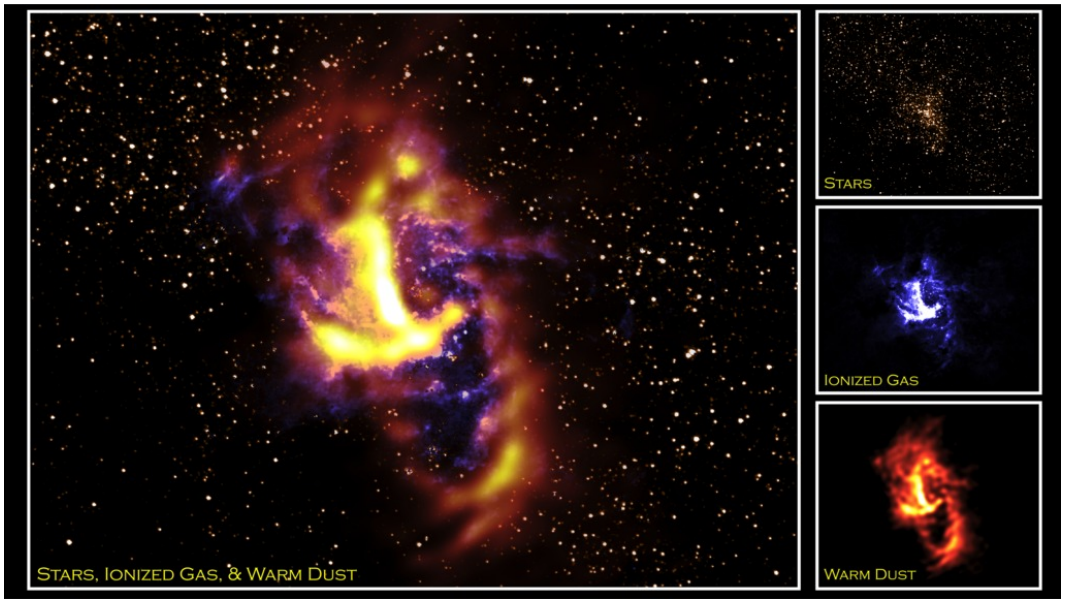

Figure 1.6: A composite image of the circumnuclear ring with Sgr A West minispiral. The infrared emission from stars and ionized gas were observed with the NICMOS instrument on board of the Hubble space telescope and the warm dust image was taken with the FORCAST camera on SOFIA observatory. The stars are responsible for ionization of the gas (middle right image) and heating of the dust (bottom right image). Credit: NASA/HST/NICMOS/DLR/USRA/DSI/FORCAST Team/Lau et al., 2013

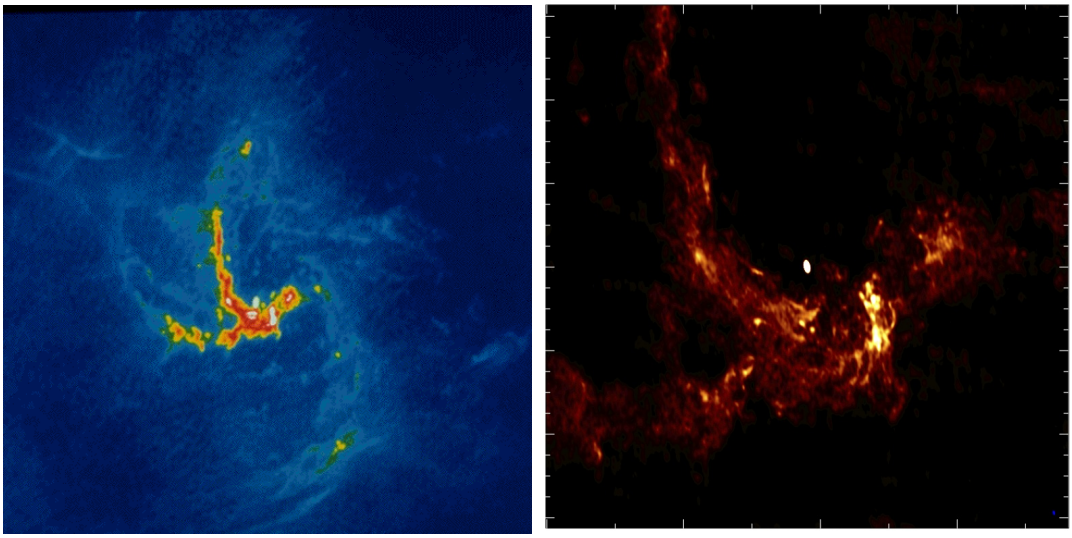

Figure 1.7: Images of the Sgr A West acquired by the VLA at two wavelengths: 6cm (left) and 1.3cm (right). Adapted from Zhao et al., 2009 and UCLA, 2024

visible in the 6cm VLA image below (1.7) is believed to be the ionized inner edge of the CND (Ekers et al., 1983; Lo and Claussen, 1983).

A detailed study of the kinematics of this formation was provided by Paumard et al., 2004. In their work, the arms are interleaved with several points for which motion is modelled using a system of Keplerian equations.

The entire structure of Sgr A West is enclosed within the CND.

1.5 OBSERVATIONS

As noted previously, the Galactic center is obscured by a high extinction in optical wavelengths, leading to the need for alternative observational bands (Oort, 1997), namely infrared, radio and X-ray. Each of the bands can detect different types of matter – infrared observations map cool dust and gas along with stars; radio wavelengths detect hotter gas; x-rays detect extremely hot gas.

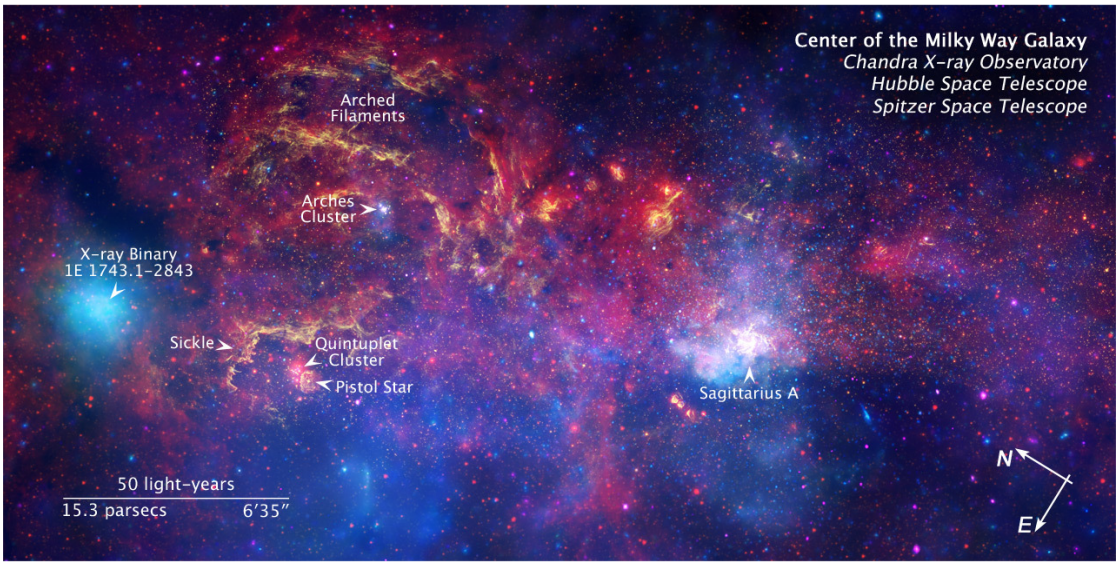

Figure 1.8: A multiwavelength image of the inner 0.5° of the Milky Way galaxy. Yellow color is the image received from near-infrared observation of Hubble space telescope showing the regions of star formation. Red color represents the infrared observations of Spitzer indicating the dust clouds coming from the stellar winds and radiation. Blue and violet colors from Chandra X-ray observatory point out the gas heated to millions of Kelvins by stellar explosions and outflows from the supermassive black hole. The region covered in this thesis is the white portion of the image markes as Sagittarius A. Credit: HubbleSite, 2024

A short list of several observatories that were or are being used to map the Milky Way's nucleus is provided below.

1.5.1 *X-ray*

The X-ray branch of astronomy opens the possibility to observe high energetic processes in the Universe, such as the accretion of matter onto black holes or extremely hot gas. X-ray radiation is absorbed by the Earth's atmosphere and therefore the observatories have to be taken into the orbit. As almost every telescope, X-ray also consists of the optics (mirrors) and the detectors. The difference between the optical and x-ray mirrors is that the x-ray one contains a paraboloidal mirror followed by a hyperbolic, solving the problem with blurry images.

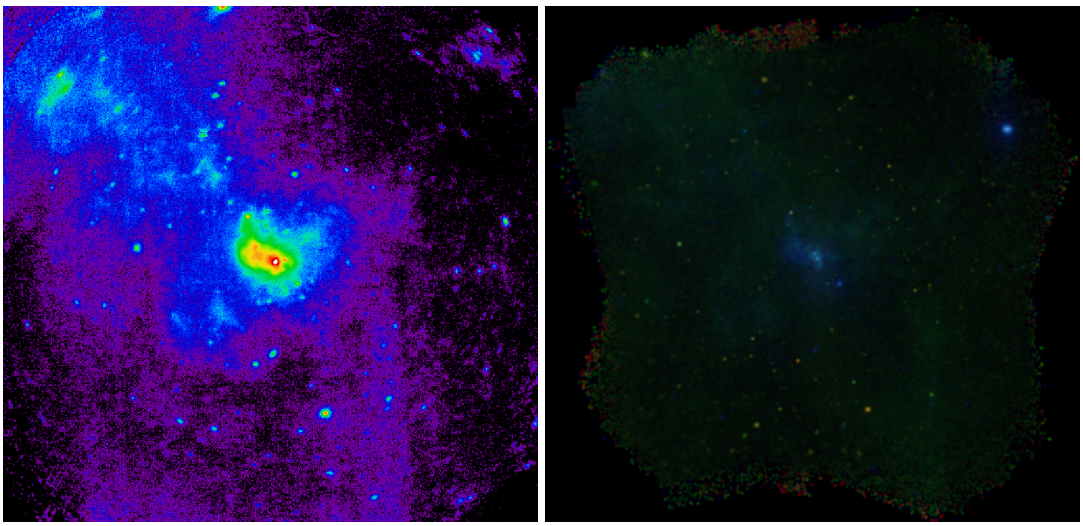

Figure 1.9: Images of the same Galactic Center region taken with XMM-Newton (*left figure*) and Chandra (*right figure*). We can clearly see that the Chandra observatory has much better angular resolution than XMM-Newton. In fact, Chandra is currently one of the best X-ray observatories we have. Credits go to Tomáš Plšek for the Chandra image and Jean-Paul B. R. S. Breuer for XMM, both from our High Energy Astrophysics group in Brno.

CHANDRA X-RAY OBSERVATORY Chandra, formerly known as the Advanced X-ray Astrophysics Facility, started observations after its deployment in 1999. This observatory operates in an energy range of roughly 80 eV to 10 keV, covering a very broad range of astrophysical processes (e.g. star formation in lower energy bands or black hole accretion in high energy bands).

Chandra is equipped with two detectors: Advanced CCD Imaging Spectrometer (ACIS) and a High Resolution Camera (HRC). The ACIS consists of two detectors – ACIS-I for imaging and ACIS-S for spectroscopy. It can be observed with a spatial resolution of about 0.5 arcseconds. This detector can measure in the energy range from 0.3 to 8.0 keV. On the other hand, the HRC, although also having two detectors (HRC-I

for imaging and HRC-S for spectroscopy), can observe energies between 0.08 and 10.0 keV.

Some of Chandra's contributions to the galactic center's study is the latest discovery of the magnetic reconnection (Wang, 2021) or the observations of the flares from SgrA* (Baganoff et al., 2001).

XMM-NEWTON As one of the most powerful X-ray telescopes ever placed in orbit, XMM-Newton's primary mission has been to observe some of the hottest, densest, and most energetic phenomena in the universe.

Its three main instruments include the European Photon Imaging Cameras (EPIC), which provide detailed imaging capabilities; the Reflection Grating Spectrometer (RGS), which dissects the light to study the properties of matter; and the Optical/UV Monitor (OM), which extends observations into the ultraviolet and visible bands. Together, these devices provide a multi-wavelength view on various astrophysical processes.

One of the XMM-Newton's most notable contributions to the knowledge about the Galactic Center has been thanks to the study of X-ray transients (Porquet et al., 2005).

1.5.2 *Infrared*

For infrared astronomy, usually the same telescope is used as for the optical wavelengths, since the IR radiation behaves in the same way as the optical radiation and can be detected with the same designs and materials of the device.

Principal limitation to the infrared observations is the Earth's atmosphere. Most of the radiation is absorbed by the water molecules and atmosphere itself radiates in the infrared wavelengths. That is the reason why the ground-based IR observatories are built in high altitudes and very dry locations.

KECK TELESCOPE One of the most productive telescopes in the optical and infrared is the Hawaiian Keck Telescope located on the island of Mauna Kea. It is a twin telescope, each 10 meters in diameter and composed of 36 hexagonal mirrors. Thanks to the highly developed system, each of the hexagonal mirrors can be adjusted to nanometer precision. The first of the twins, Keck I, first began observing in 1993, and was joined by Keck II a few years later in 1996.

In the infrared, the Keck telescope operates at wavelengths of 1 to 5 microns. For greater sensitivity, the telescope is equipped with an adaptive optics (AO) system that compensates for fluctuations in stellar radiation due to light passing through the Earth's atmosphere. This provides improved image quality by a factor of 10 to 20.

It is equipped with several instruments for infrared observations. Some of them are the Near-Infrared Camera (NIRC) and the Near-Infrared Spectrometer (NIRSPEC),

an echelle spectrograph designed for high-resolution observations with the Keck II telescope.

Together, the Keck I and Keck II telescopes achieve high angular resolution never seen before in infrared astronomy.

The Keck observatory's contribution to Galactic center astrophysics was crucial in determining the orbits and properties of the closest stars to the SgrA*. Some of the Einstein's general theory of relativity features were tested in detail by Do et al., 2019.

VERY LARGE TELESCOPE (VLT) VLT is a ground-based 8.2 meters wide telescope located in Atacama Dessert in Chile, operated by European Southern Observatory. It primarily operates in the optical wavelengths but is also equipped with several near-infrared devices. It broadens the astronomical knowledge since 2001.

One of the widely used near infrared tool is the NACO (Nasmyth Adaptive Optics Sustem (NAOS) - Near-Infrared Imager and Spectrograph (CONICA)). NAOS is an adaptive optics system correcting for the atmospheric turbulences and the CONICA apparatus contains the infrared camera and spectrometer. SINFONI is then second most used infrared system in VLT – it is a spectrograph with adaptive optics correction able to observe in three dimensions: each pixel is associated with a full spectrum.

Science made with VLT NACO in the field of Galactic center was, for example, the 16-year-long study of the dynamics of 28 stars in the heart of the Galaxy providing yet another evidence of the SMBH. SINFONI then was the first ever telescope to capture a flare from the black hole.

SPITZER Spitzer telescope, launched in 2003 and deactivated in 2020, was NASA's third infrared telescope. It carries three instruments: Infrared Array Camera (IRAC), Infrared Spectrograph (IRS) and Multiband Imaging Photometer for Spitzer (MIPS). IRAC worked simultaneosly in four wavelenths – 3.6, 4.5, 5.8 and 8 microns. IRS operated in four bands: $5.3 - 14.0\mu$m, $10.0 - 19.5\mu$m, $14 - 40\mu$m and $19 - 37\mu$m. The last instrument, MIPS, ranged from mid- to far-infrared.

All of these three instruments used the liquid helium for cooling. Only the two shorter wavelength modules continued working after the exhaustion of the helium in 2009. The period between 2009–2020 was called the "warm mission".

Spitzer has been instrumental in obtaining detailed mappings of dust structures in the Central Molecular Zone (CMZ) of the Milky Way, and recent studies include flashes of SgrA* and its variability.

JAMES WEBB SPACE TELESCOPE (JWST) JWST, launched in December 2021, represents the next-generation space observatory that has gotten new insights into the new-era astronomy so far. Unlike HST, Web operates primarily in infrared band.

The core of the telescope is its large primary mirror with 6.5 meters in diameter, composed of 18 hexagonal segments made of gold-coated beryllium.

Webb holds four scientific instruments needed for infrared observations: Near Infrared Camera (NIRCam), Near Infrared Spectrograph (NIRSpec), Mid-Infrared Instriment (MIRI) and Fine-Guidance Sensor and Near Infrared Imager and Slitless Spectrograph (FGS/NIRISS). NIRCam operates in the range of 0.6μm to 5μm. It is also used for aligning and focusing the main segments of the mirror. NIRSpec performs the spectroscopy science (using both the principle of the prism and the slit) over the same wavelength range as the NIRCam in three modes of observation: a low-resolution prism mode, multiobject mode, and long-slit spectroscopy mode. On the other hand, MIRI works in the range of 5 to 27 μm. It consists of a mid-infrared camera and a spectrometer. The last tool, FGS/NIRISS, is used to control the orientation and stability of the observatory (FGS), and the NIRISS module provides imaging and spectroscopy between 0.8 and 5 μ m.

One of the latest contributions to the astrophysics of the galactic center is the detailed image of hundreds of massive stars in the galactic nucleus.

1.5.3 *Radio*

Every radio astronomer knows the story of the first detection of a radio signal from the constellation Sagittarius. Karl Guthe Jansky, then working for Bell Telephone Laboratories, was hired to explain and eliminate the various noises that interfere with transatlantic calls. He built his own rotating antenna to investigate various types of noise. Among the strongest noises was storm interference, but also an unknown, regularly recurring noise. At first he thought the signal was coming from the Sun, but later he noticed that the signal had a repetition period of 23 hours and 56 minutes and was synchronised with the movement of the stars. After a thorough examination of astronomical maps, in 1933 (Jansky, 1933) concluded that the unknown signal was coming from the constellation Sagittarius and was probably the source of the Galactic Center (Shapley, 1918 identified the constellation Sagittarius as the center of our Galaxy, see chapter 1).

VERY LARGE ARRAY (VLA) The VLA is among the most productive radio interferometric observatories. It is located in New Mexico, near the town of New Socorro on the San Agustin plateau plains at an altitude of 2124 meters.

There are 27 standalone radio antennas connected by optical fiber, each with a diameter of 25 meters. All antennas are movable and arranged in the characteristic "Y" shape. To avoid unwanted thermal noise, each receiver is equipped with a cryo-cooler.

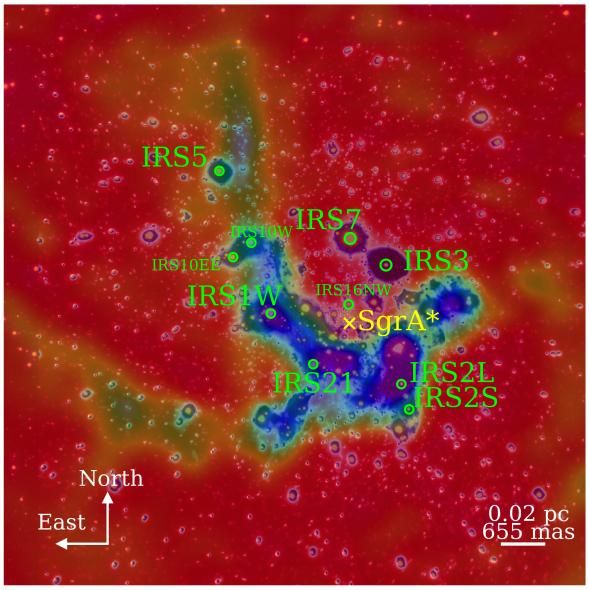

Figure 1.10: A composite image of the inner parsec of the Milky Way. The yellow cross indicates the position of SgrA*; the red image shows observations of hot stars in K-band, the blue image shows dust observed in L-band – both observations obtained from the NACO instrument on the VLT. The green color indicates cool CO gas of ALMA at a wavelength of 1.5 mm. Credit: Florian Peißker/ESO.

An interesting feature of this array is the variable spacing of the antennas, which changes every quarter. Therefore, it is possible to obtain 4 different configurations with corresponding resolutions and fields of view per year.

VLA was one of the first observatories to observe the Galactic center and the first to detect the mini-spiral of the hot gas. Since then, many scientifically significant findings of this array were presented.

ATACAMA LARGE MILLIMETER/SUBMILLIMETER ARRAY (ALMA) ALMA is the world's most powerful radio-interferometer array, located in northern Chile in the Atacama Desert at an altitude of around 5,000 meters above sea level, and consists of 66 relocatable antennas with the longest baseline measuring almost 16 km. This location was chosen precisely because of its altitude and associated advantages, such as low humidity and the absence of interference elements. The 66 antennas mentioned include 50 with a diameter of 25 metres, 4 with a diameter of 12 metres and the last 12 with a diameter of 7 metres. Thanks to the different radii, a larger field of view can be obtained during observation. The operating wavelength ranges from 3.6 to 0.32 millimeters.

The most important contribution of ALMA to the science of the Galactic Center is the participation in the EHT collaboration in obtaining the black hole image (Fig. 1.11).

VERY LONG BASELINE INTERFEROMETER (VLBI) VLBI is a network of radio telescopes spread across the world that form a virtual telescope of the size of Earth developed in the 1960s. With such a distribution, the achieved angular resolution and sensitivity are incomparably high.

In the 1980s, VLBI observations showed that the size of SGRA* in the radio band decreases with decreasing wavelength.

EVENT HORIZON TELESCOPE (EHT) EHT is a specific application of the VLBI telescope with the corrections of the wavelengths. It is an international collaboration founded in 2009 now comprising over 300 members.

This specific setting covers very high radio frequencies starting from submillimeter through millimeter wavelengths.

In March 2024, a new image of the SgrA* from EHT collaboration emerged: it uncovered a strong magnetic-field structure spiralling around the SMBH (1.11).

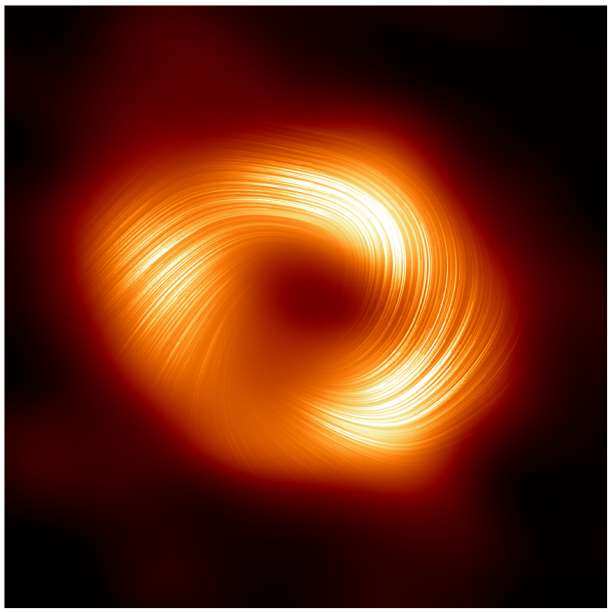

Figure 1.11: Latest image of the SgrA* in the heart of our Galaxy showing a magnetic field seen in polarized light spiralling from the edge toward the black hole. Adapted from Collaboration, 2024

2

ORBITAL MECHANICS

Orbital mechanics is the mathematical study of the motion of celestial objects around their center of gravity. Several physical relations are fundamental for computing the orbits of stars around the supermassive black hole in the center of the Galaxy (or orbits of planets around the Sun).

The beginning of the development of celestial mechanics dates back to ancient civilizations, which include mainly the Greeks, Babylonians, Egyptians and Chinese. The Greeks were most responsible for early observations of bodies in the night sky and descriptions of their movements. Claudios Ptolemy was the first documented thinker to propose a geocentric model of the universe. Much later, in the 16th century, Nicolaus Copernicus came up with a new model that depicted the Sun as the center of our system with the planets orbiting in circles. This model then laid the foundations for modern astronomy as we know it today. This model was also the basis for Johannes Kepler, who accurately described the simplified motion of celestial objects in our Solar System (Chap. 2.1.1) and was followed by Isaac Newton (Chap. 2.1.2), who finally laid the physical foundations for this field. The final step to obtain a detailed description of the motion made Albert Einstein. His Genereal Theory of Relativity (GTR) views gravity as a curvature of spacetime caused by mass. The so-called corrections derived from the GTR can be added to Newtonian mechanics in extreme environments to describe more realistic situations in places with high gravitational potential.

2.1 FUNDAMENTALS OF CELESTIAL MECHANICS

2.1.1 *Kepler's laws*

One of the most important persons in modern orbital mechanics is undoubtedly Johannes Kepler, the German mathematician and astronomer, who, in the early 17th century, formulated three laws describing the orbits of bodies in the gravitational potential of material objects (first two in 1609 and the third one in 1619). These three laws are the building blocks for the development of celestial mechanics as we know it today.

1. LAW OF ELLIPSES "The planets move along ellipses that share the focal point of the Sun."

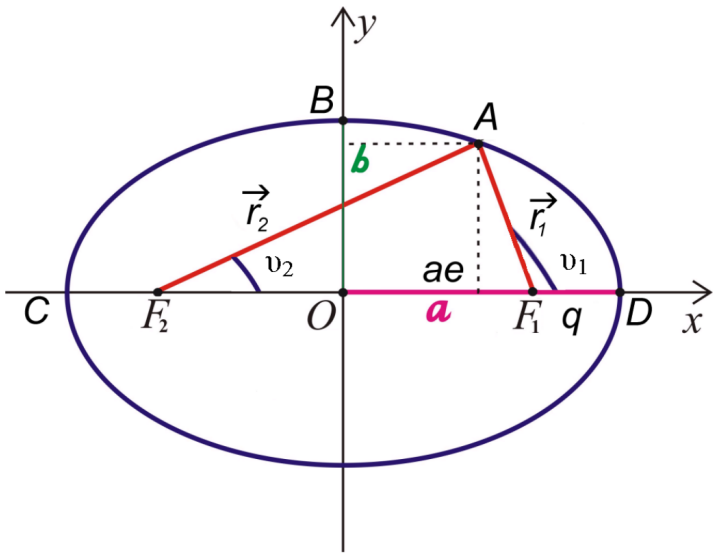

Figure 2.1: Elliptic trajectory of the orbitting body with elliptic parameters. Credit: Jan Janík, 2022

2. LAW OF EQUAL AREAS "The imaginary line joining a planet and the Sun sweeps equal areas of space during equal time intervals as the planet orbits."

In other words, this law says that the body moves with different velocities along its path.

3. HARMONIC LAW "The ratio of the third power of the major semiaxis to the second power of the orbital period is constant for all planets."

$$\frac{a^3}{T^2} = \frac{G(m_1 + m_2)}{4\pi^2} \tag{2.1}$$

The solution to the body's orbit is given by the conic equation:

$$r = \frac{p}{1 + e\cos(\phi - \omega)} \,. \tag{2.2}$$

According to the parameter values (see Sec. 2.3), we can arrive at four cases: circle, ellipse, parabola, hyperbola (Fig. 2.2).

For celestial mechanics, the ellipse is the most important solution. Its prescription is as follows:

$$r = \frac{a\left(1 - e^2\right)}{1 + e\cos f} \,, \tag{2.3}$$

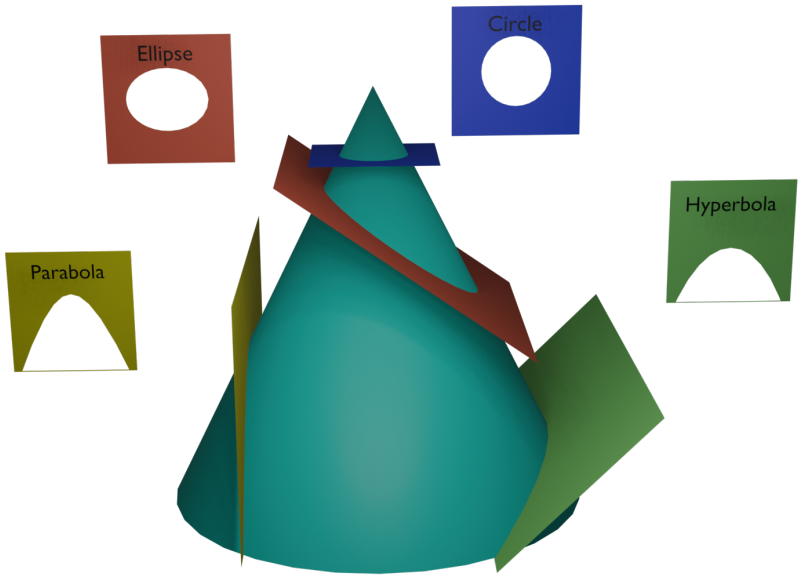

Figure 2.2: A scheme of conic sections described by the Eq. 2.2.

where $f \equiv \phi - \omega$ is called the true anomaly and is measured from the pericenter.

2.1.2 *Newton's laws*

In his work *Principia* from 1687, Isaac Newton added his three laws of motion along with the law of gravitation to Kepler's laws, which opened the door for a detailed study of the two-body problem.

1. LAW OF INERTIA "If there are no external forces, an object will maintain its state of motion, that is, it will stay at rest or continue rectilinear motion at constant velocity."

2. LAW OF ACCELERATION "At any instant of time, the net force on a body is equal to the body's acceleration multiplied by its mass or, equivalently, the rate at which the body's momentum is changing with time."

$$\vec{F} = m\vec{a} \tag{2.4}$$

3. ACTION–REACTION "To every action there is always an opposed and equal reaction; or, the mutual actions of two bodies upon each other are always equal and directed to contrary parts."

$$\vec{F}_{21} = -\vec{F}_{12} \tag{2.5}$$

LAW OF GRAVITATION The first correct relation for classical gravitation states that every two points of mass exert a gravitational force on each other directed along the line of these points. The force then looks as follows (for a mass m_2 acting on a mass m_1):

$$\vec{F}_{12} = Gm_1m_2\frac{\vec{r}_2 - \vec{r}_1}{|\vec{r}_2 - \vec{r}_1|^3} \ . \tag{2.6}$$

All of the Kepler laws can be more or less easily derived from those of Newton.

2.1.3 *Two-Body Problem*

In the chapters above we have given equations describing the orbit of bodies orbiting a fixed center of gravity. However, this is only a theoretically established model, because in real situations, according to Newton's second law, bodies gravitationally interact with each other. Such a model is called the two-body problem.

In the two-body problem, the influence of other objects on the orbit of the observed body is neglected, allowing a complete description of the orbit to be obtained from the initial conditions only.

From Kepler's laws, it is thus possible to obtain an analytical solution for the motion of two bodies in an ideal environment without disturbing elements. In reality, however, everything is a little more complicated. The trajectories of the observed bodies can be disturbed by external influences. Numerical solutions (further described in Ch. 4) are then needed to describe such perturbed motions.

2.2 KEPLER'S EQUATION

The Kepler equation relates the mean anomaly M to the eccentric anomaly E (see Fig. 2.1). It was derived by Johannes Kepler in his 1609 volume *Astronomia nova*. We start with the quantity that gives us the position of the body on the circumcircle of the ellipse. This is the mean anomaly M, which flows uniformly and gives the mean daily angular motion.

$$M = \frac{2\pi}{P}(t - T_0) \ , \tag{2.7}$$

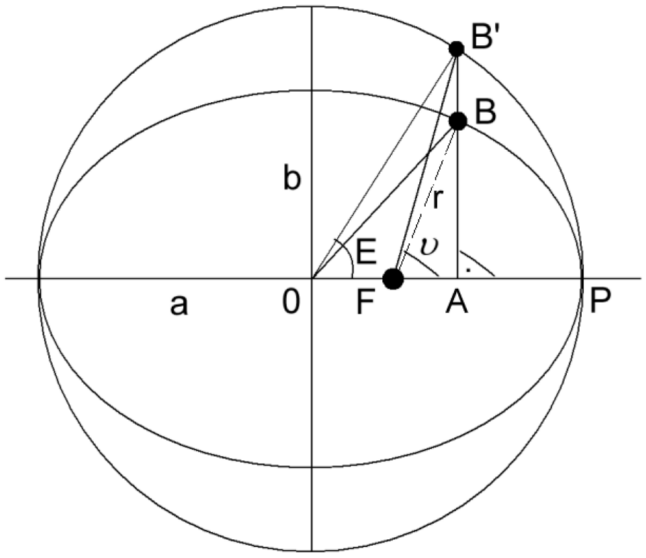

Figure 2.3: Representation of the eccentric and true anomaly on the ellipse and its circumcircle. Credit: Jan Janík, 2022

where P is the period of the orbit, t is the time we measure the body's position at and T_0 is the time of the passage the pericenter.

From Kepler's second law for the guide we obtain the ratio of the sweeped area to the total area of the ellipse:

$$\frac{\Delta S}{S} = \frac{t}{P} \qquad \Longrightarrow \qquad \Delta S = \frac{\pi ab}{P} t$$

Now, from the Fig. 2.3 we can express the area

$$\Delta S = \frac{b}{a} \Delta S_E \ ,$$

where $\Delta S_E = \frac{1}{2} a^2 (E - e \sin E)$ and thus the final area portion is

$$\frac{\pi ab}{P} t = \Delta S = \frac{1}{2} ab (E - e \sin E) \ .$$

After few minor adjustments the equation becomes the proper expression of the Kepler equation

$$E - e \sin E = \frac{2\pi}{P} (t - T_0) \ . \tag{2.8}$$

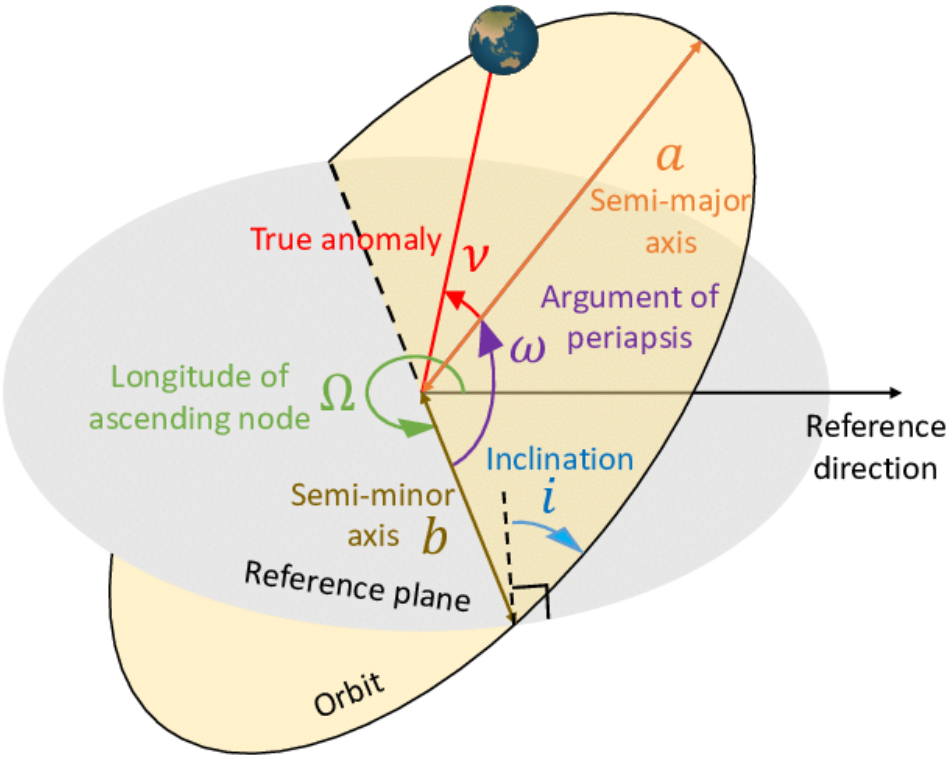

Figure 2.4: The orientation of the orbit is described by the six orbital parameters. In the Galactic center, the reference direction is the north. Credit: Wikipedia, 2024.

2.3 ORBITAL PARAMETERS

Orbital parameters, also known as orbital elements, are quantities that describe the shape and spatial orientation of an osculating orbit (orbit that the body would have without any perturbing effects) in a gravitationally bound system. The first three parameters describe the position of the body in its orbit while the remaining three indicate the spatial orientation of the orbit (Fig. 2.4). In the following paragraphs, we will find their description and relations.

SEMI-MAJOR AXIS a is related to the period of the orbit by the third Kepler's law 2.1. It is half the distance between the pericenter and the apocenter (see Fig. 2.1).

ECCENTRICITY e describes the shape of an orbit along which the body moves; it reflects how much the path differs from a circular path. It is defined as the ratio of the distance between the foci and the size of the main semiaxis:

$$e = \sqrt{1 - \frac{b^2}{a^2}} \,. \tag{2.9}$$

The eccentricity can take four possible values together with the parameter p leading to different orbit shapes:

- circular orbit $e = 0$ $p = a$
- elliptic orbit $0 < e < 1$ $p = a(1 - e^2)$
- parabolic orbit $e = 1$ $p = 2q$
- hyperbolic orbit $e > 1$ $p = a(e^2 - 1)$

After inserting the values into Eq. 2.2, each pathway has its own prescription.

CLOSEST APPROACH T_0 serves as a metric that indicates the location of a celestial body within its orbit at a particular moment. It is represented as an angle that increases steadily over time. This parameter is crucial for forecasting the positions of stars within their orbits at any given time.

INCLINATION i of an orbit is the angle between the orbit's plane and a reference plane, in our case the plane of the sky.

$$i = \cos^{-1} \frac{L_z}{L} \tag{2.10}$$

LONGITUDE OF THE ASCENDING NODE Ω is an angle that defines the rotation of an orbit within its plane. This parameter is crutial when desribing the spatial orientation of an orbit.

ARGUMENT OF PERIAPSIS ω specifies the angle between the ascending node and the closest point of approach of the orbit to the primary focus.

2.4 ORBITAL PERTURBATIONS

So far we have only discussed orbiting bodies in an ideal environment without any disturbing elements. However, the real path differs from the osculating orbit due to the perturbing effects and the orbital elements become time dependent. Now we will introduce several different disturbers affecting the orbits of the bodies - among the most important are hydrodynamic drag caused by the surrounding gas and dust, encoun-

ters with massive bodies (other stars in the case of a star cluster), and post-Newtonian effects in the case of velocities and conditions close to those of General Relativity.

In a two-body problem, the acceleration of the star originates from the gravitational force along with the external forces:

$$\vec{a} = -G\frac{m_\bullet}{r^2}\frac{\vec{r}}{r} + \frac{\vec{F_{ext}}}{m} \,. \tag{2.11}$$

Each perturber has its own description of the external force $\vec{F}_{ext}$.

2.4.1 *Nonmagnetic gaseous medium*

In the extreme surroundings of the supermassive black hole at the center of our Galaxy, we can find a lot of gas and dust, along with plasma from the stellar winds of distant stars. This matter directly affects the orbits of orbiting stars in two mechanisms – hydrodynamic drag force and gaseous dynamical friction. Both of these interactions dissipate orbital energy and transfer angular momentum to the surrounding environment. These mechanisms were derived from Ostriker, 1999 and Villaver and Livio, 2009.

These interactions have a profound effect on the orbital elements of orbiting stars – apsidal precession, orbital migration and eccentricity changes occur. In the case of hydrodynamical drag force, the formula for the external force in Eq. 2.11 becomes (Szolgyen et al., 2022)

$$\vec{F_{hyd}} = -\frac{1}{2}C_d R^2 \pi \rho v^2 \frac{\vec{v}}{v} \,, \tag{2.12}$$

where R is the radius of the orbiting body and C_d is a dimensionless drag coefficient.

The coefficient C_d quantitatively describes the resistance of the fluid on the passing object. It depends on the Mach number $\mathrm{Ma} \equiv v/c_s$ (the ratio of the speed of the object to the speed of sound c_s in the medium) and the Knudsen number Kn (the ratio of the mean free path in the gaseous medium to a length scale of the problem, e.g. the size of the body passing through). From the definition, this applies only to the compressible gas described by the Reynolds number $\mathrm{Re} = 4\frac{\mathrm{Ma}}{\mathrm{Kn}}$ or

$$Re = \frac{\vec{v}_{rel} \cdot L}{\nu} \,, \tag{2.13}$$

where L is the dimension of the area and ν is the kinetic viscosity

$$\nu = \frac{\alpha c_s^2}{\Omega_R} \,.$$

Ω_R here denotes the Keplerian angular velocity and α is the viscosity parameter. For the GC, the viscosity parameter takes the value $\alpha = 0.1$.

The Eq. 2.12 applies for linear or circular motions when the moving body causes small density fluctuations only and does not accrete the matter.

Depending on the body size and velocity, the Mach number can take three different values, which have different effects on the behavior of the body:

- **Subsonic regime** Ma < 1**:** The compressibility can be neglected for the lowest conditions.
- **Transonic regime** Ma ≈ 1**:** In this regime, compressibility is the most important effect for transonic flow.
- **Supersonic regime** Ma > 1**:** In supersonic regime, the body's surface creates the shock waves

By particle-fluid interactions (and thus the characteristics of the fluid and the particles) we can distinguish two mostly used regimes – Epstein and Stokes. Epstein regime is used in a low-density mediums with a mean free path comparable in size with the dimensions of the particles. In astrophysics such environments can be the stellar disks or interstellar medium. The condition for this case is Kn > 1. Second most discussed regime in astrophysics is the Stokes regime used when the fluid is dense enough to consider it a continuum (the mean free path is much smaller than the sizes of the particles). The condition is Kn < 1. In this thesis, we approximate $C_d = 1$ as for our conditions (relative velocities and area dimensions), the Reynolds number becomes very large and in the Fig. 2.5 we move to the Newton regime.

On the other hand, the relation for dynamical friction is (Szolgyen et al., 2022)

$$\vec{F_{df}} = -4\pi(Gm)^2 \frac{\rho \mathrm{Ma}}{v^2} \,. \tag{2.14}$$

Both of these relations use the relative velocity of the body with respect to the movement of the gas, that is, in a direction opposite to the motion of the body. Under the influence of these forces, the orbits change their parameters, such as eccentricity and inclination.

All of the quantities used in the force equations depend on local conditions. We covered two scenarios: (i) a spherically symmetric cloud of gas around the system of SgrA* and the stars, and (ii) an accretion disk.

(i) A spherical accretion reffered to as the Bondi accretion is characterized by the relations below:

$$R_{\mathrm{Bondi}} = \frac{GM}{c_s^2} \tag{2.15}$$

is the Bondi radius from within the matter (gas and dust mainly) is likely to be gravitationally drawn to the central body and accreted. The accretion is then spherically

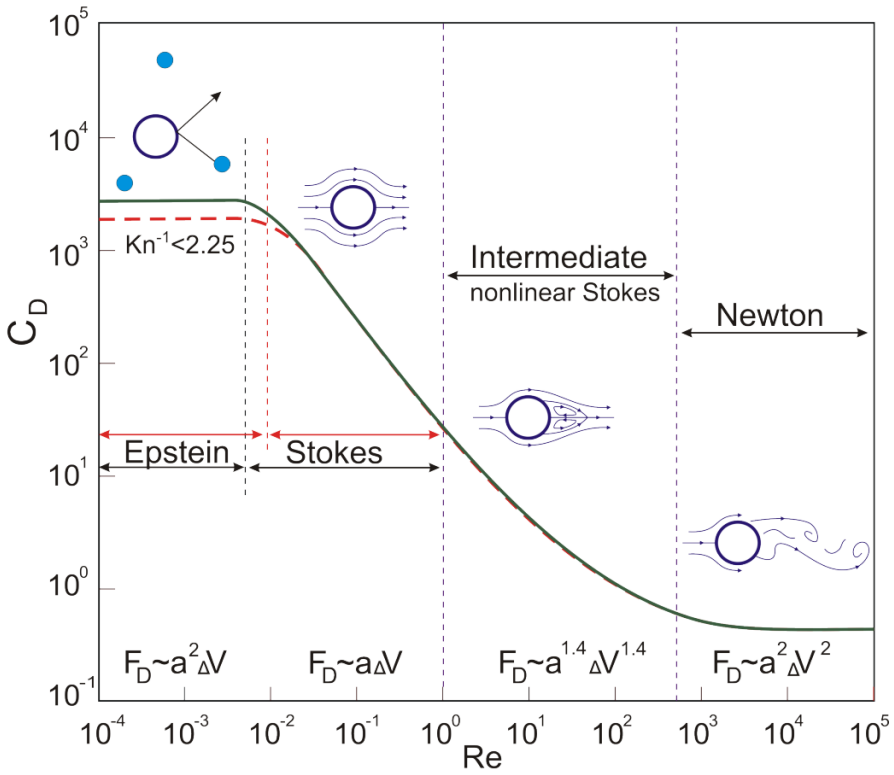

Figure 2.5: Dependence of drag coefficient on Reynolds number. Credit: Stoyanovskaya et al., 2020

symmetric with the infalling medium (described by the free fall) having the acceleration

$$a_{\text{infall}} = -\frac{2GM}{r^2}. \tag{2.16}$$

The density gradient in the Eq. 2.12 of the medium then follows this relation:

$$\rho(r) = \rho_0 \left(\frac{r}{R_{Bondi}}\right)^{-3/2}. \tag{2.17}$$

(ii) For the case of an accretion disk characterized by its height H

$$H = c_s \left(\frac{R}{GM}\right)^{1/2} R\,, \tag{2.18}$$

we can make an approximation to a thin disk that satisfies the condition $H \ll R$ and thus the Eq. 2.18 gives the requirement on the Keplerian velocity of the gas in the disc:

$$c_s \ll \left(\frac{GM}{R}\right)^{1/2}. \tag{2.19}$$

With this condition satisfied, we can parametrize the disc with the Shakura-Sunyaev solution (Frank et al., 2002) for a steady thin disc

$$\begin{aligned}
\Sigma &= 5.2\alpha^{-4/5}\dot{M}_{16}^{7/10}m_1^{1/4}R_{10}^{-3/4}f^{14/5}gcm^{-2}\,,\\
H &= 1.7\times10^{8}\alpha^{-1/10}\dot{M}_{16}^{3/20}m_1^{-3/8}R_{10}^{9/8}f^{3/5}cm\,,\\
\rho &= 3.1\times10^{-8}\alpha^{-7/10}\dot{M}_{16}^{11/20}m_1^{5/8}R_{10}^{-15/8}f^{11/5}gcm^{-3}\,,\\
T_c &= 1.4\times10^{4}\alpha^{-1/5}\dot{M}_{16}^{3/10}m_1^{1/4}R_{10}^{-3/4}f^{6/5}\mathrm{K}\,,
\end{aligned} \tag{2.20}$$

where

$$f = \left[1-\left(\frac{R_*}{R}\right)^{1/2}\right]^{1/4}\,,$$

R_* is the innermost stable circular orbit and α is the viscosity parameter.

Consider a star with a general inclination. When the star intersects the disc, it is gradually dragged into the plane of the disc and once fully embedded in the disc, the orbit becomes more and more circular. During the passage within the disc, the body is migrating towards the center and then it eventually moves to the tidal radius where it is torn apart by the gravitational forces. Under some circumstances, the migrating star can start to accrete the matter from the disc.

2.4.2 *Magnetic gaseous medium*

With the discovery of a radio continuum filament named Radio Arc, or just Arc (see Fig. 1.1) in the GC perpendicular to the Galactic plane (GP) (Yusef-Zadeh et al., 1984), comprehensive studies of the influence of the magnetic field on ubiquitous gas and dust in the GC began. In (Inoue et al., 1984; Tsuboi et al., 1985) they provided the evidence that the magnetic field in the Galactic center indeed is normal to the GP. From several works, mainly the Morris, 2006; Tsuboi et al., 1986; Yusef-Zadeh and Morris, 1987, the magnetic field strenght in the inner 70pc of the GC was estimated to be as high as $\sim (1-2)\times10^{54}$ergs and thus equivalent to $\sim (1000-2000)$ supernova explosions (Ferrière, 2009).

Speculations on how this magnetic field can affect the motions of the gas clouds and probably even stars emerged not long after. In the work of McCourt et al., 2015 they ran Athena simulations of the magnetohydrodynamical system of the gaseous cloud with dimension R_{cloud} and the galactic wind. The magnetic field was frozen to the galactic wind with the strength $\beta_{\mathrm{wind}} \equiv 8\pi P_{\mathrm{wind}}/B_{\mathrm{wind}}^2$ and the magnetic field defined as

$$\vec{B} = \cos(\alpha a)\hat{\vec{c}} + \sin(\alpha a)\hat{\vec{b}}$$

in the right-handed coordinate system $\hat{\vec{a}}$, $\hat{\vec{b}}$ and $\hat{\vec{c}}$. The parameter $\alpha = 10/R_{cloud}$ is the correlation length of the magnetic field.

They found that the strongly magnetized wind ($\beta_{\text{wind}} \lesssim 1$) accelerates the cloud much faster than in the hydrodynamical simulation. The total magnetohydrodynamic drag force is then higher than the hydrodynamic drag force 2.12 by a factor $1 + \frac{v_{\text{A}}^2}{v_{\text{wind}}^2}$ (Dursi and Pfrommer, 2008):

$$F_{\text{MHD}} \sim \rho_{\text{wind}} v_{\text{wind}}^2 R_{\text{cloud}}^2 \times \left(1 + \frac{v_{\text{A}}^2}{v_{\text{wind}}^2}\right) . \tag{2.21}$$

Here, v_{A} is the Alfvén speed of the wind defined as $v_{\text{A}} \equiv \frac{B}{\sqrt{4\pi\rho}}$.

2.4.3 *Post-Newtonian effects*

The Post-Newtonian effects (expansion, correction) are the approximate solutions to Einstein's field equations in General Relativity added to the classical Newtonian description of the gravitating bodies. This correction needs to be considered in environments with very large gravitational fields, which the galactic centre certainly has. Since the fastest stars in the Galactic center reach speeds close to a few percents of the speed of light, this correction has to be taken into account. These effects can be detectable after many revolutions.

One of these effects is the pericentre precession referred as the Schwarzschild precession observed in the closest stars to SgrA* on eccentric orbits. The order of this correction is v^2. The suggestion that other corrections of the order v^2, such as gravitational redshift, may be detectable with current observatories emerged in the work of Zucker et al., 2006. Kannan and Saha, 2008 even proposed the possibility of detection of the frame dragging (order of v^4) with the development of better spectrographs.

The precession of the pericenter is also well known from our Solar System – Mercury exhibits a relatively strong precession of the perihelion (Fig. 2.6). During this phenomenon, the elliptical orbit gradually rotates in the direction of the body's orbit, and after a specific time, called the apsidal period, it can return to its initial position.

In this work, we only consider the Schwarzschild spacetime, a black hole without a spin. The Post-Newtonian correction of the acceleration then takes the following form:

$$\vec{a}_{\text{PN}} = -\frac{GM}{r^3}\vec{r} + \frac{GM}{c^2 r^2}\left[\left(2(\gamma+\beta)\frac{GM}{r} - \gamma v^2\right)\frac{\vec{r}}{r} + 2(1+\gamma)\dot{r}\vec{v}\right] \tag{2.22}$$

which is inserted to the Eq. 2.11. The parameters γ and β arises from the General Relativity and are taken $\gamma = \beta = 1$.

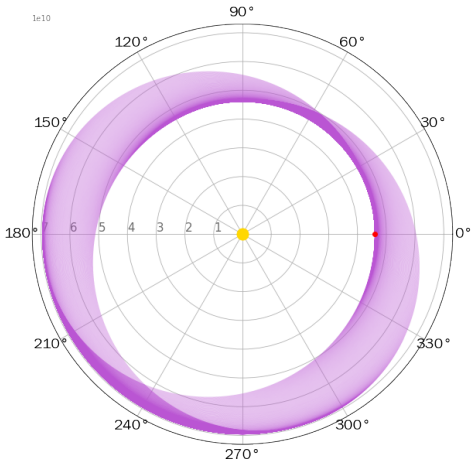

Figure 2.6: Mercury's periapsidal precession due to the General Relativity. The effects is magnified by the factor 10000. Credit: Alena Vanžurová.

For the star S2 the precession changes the orientation of the orbit by $\Delta\Phi \approx 12'$ per one revolution.

Part II

METHODOLOGY

3

ANALYTICAL APPROACH

With a sky as our plane of reference (see Fig. 2.4), we first had to derive the projected positions and velocities of the S stars. This was achieved using the code `poscalc`. This code recalculates the orbital elements specified in Gillessen et al., 2017 (tab. 2) as described below.

After initial conversion to SI units we calculated the real positions and velocities along the star's orbits. From the information in the table we were able to derive the mean anomaly M from which we could find the eccentric anomaly E with the use of the Kepler equation 2.8. From eccentric anomaly we were able to compute the (true) coordinates and velocities of the star along its orbit with these equations:

$$\begin{aligned} x &= a \cdot (\cos(E) - e) & v_x &= -\tfrac{na \sin E}{1 - e \cos E} \\ y &= a \cdot \sqrt{1 - e^2} \cdot \sin(E) & v_y &= \tfrac{na\sqrt{1-e^2} \cos E}{1 - e \cos E} \\ z &= 0 & v_z &= 0 \end{aligned} \tag{3.1}$$

with $n = \frac{2\pi}{P}$ being the mean motion (or mean angular velocity).

These are the physical coordinates and velocities of the star on the orbit's path. Now, we need to transform these to the reference plane, that is the plane of the sky. To do that, we need to multiply our position vector by the transformation matrices for each angle:

$$\begin{bmatrix} x_1 \\ y_1 \\ z_1 \end{bmatrix} = \begin{bmatrix} \cos(\omega) & -\sin(\omega) & 0 \\ \sin(\omega) & \cos(\omega) & 0 \\ 0 & 0 & 1 \end{bmatrix} \begin{bmatrix} x \\ y \\ z \end{bmatrix}$$

$$\begin{bmatrix} x_2 \\ y_2 \\ z_2 \end{bmatrix} = \begin{bmatrix} 1 & 0 & 0 \\ 0 & \cos(i) & -\sin(i) \\ 0 & \sin(i) & \cos(i) \end{bmatrix} \begin{bmatrix} x_1 \\ y_1 \\ z_1 \end{bmatrix}$$

$$\begin{bmatrix} x_3 \\ y_3 \\ z_3 \end{bmatrix} = \begin{bmatrix} \cos(\Omega) & -\sin(\Omega) & 0 \\ \sin(\Omega) & \cos(\Omega) & 0 \\ 0 & 0 & 1 \end{bmatrix} \begin{bmatrix} x_2 \\ y_2 \\ z_2 \end{bmatrix}$$

Now, only the conversion to the parsecs/arseconds for the projected positions and kilometers per second for the velocities is left.

3.1 ANALYTICAL ORBIT OF S2 STAR

The resulting plot of the orbit of the S2 star computed analytically is the following:

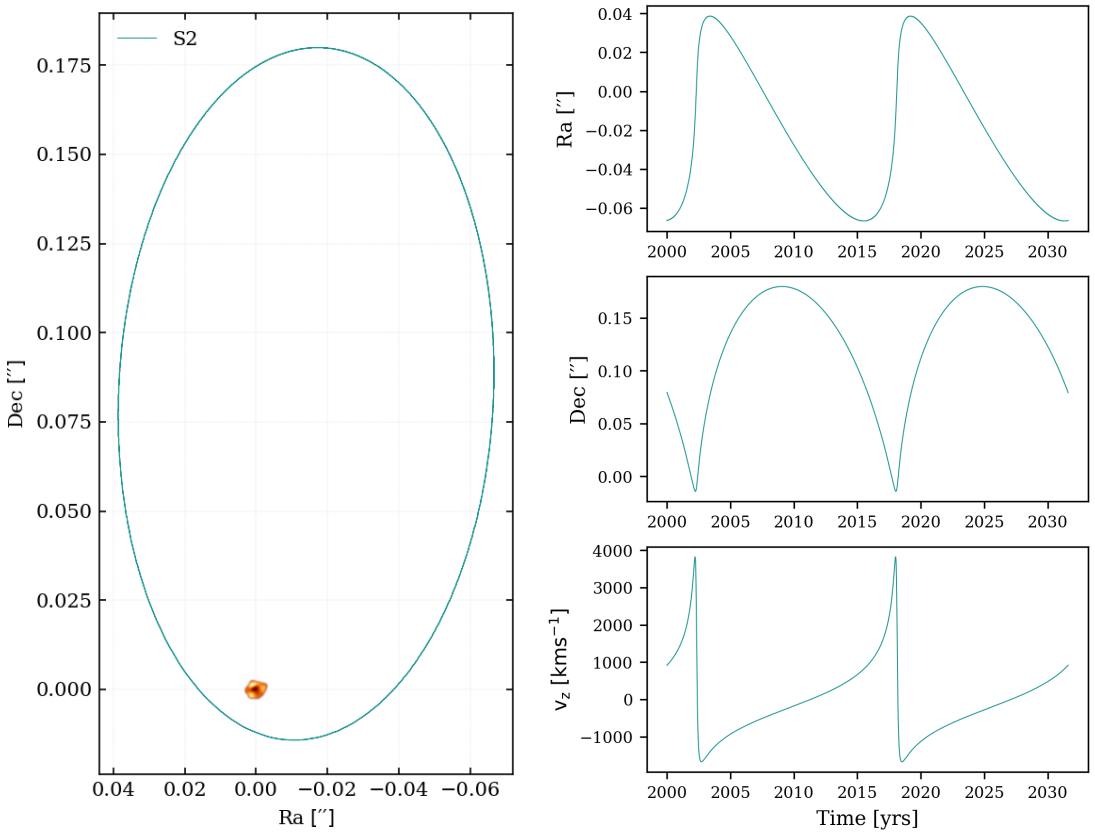

Figure 3.1: A plot of the projected orbit of the S2 star onto the sky plane with a change of the right ascension and declination in time and its radial velocity. One can see that our result is in good agreement / consistent with the ones derived by Genzel, 2021 (Fig. 1.2). Note: The SgrA* black hole location is depicted by the image of the black hole from Collaboration, 2022. The image of the black hole is not up to scale!

3.2 ORBIT OF S STARS IN INNERMOST 1″

With this same code we were able to plot a 3D visualisation of orientations of all the S stars' orbits for which we know the orbital elements and which have the semimajor

axis shorter than 1 arcsecond. The information needed for this plot are written in the Tab. 2.

Table 2: The orbital elements of some of the S stars. For more information see Gillessen et al., 2017.

Star	T_0 [yr]	P [yr]	a [″]	e	i [°]	Ω [°]	ω [°]
S1	2001.80 ± 0.15	166.0 ± 5.8	0.595 ± 0.024	0.556 ± 0.018	119.14 ± 0.21	342.04 ± 0.32	122.3 ± 1.4
S2	2002.33 ± 0.01	16.00 ± 0.02	0.1255 ± 0.0009	0.8839 ± 0.0019	134.18 ± 0.40	226.94 ± 0.60	65.51 ± 0.57
S4	1957.4 ± 1.2	77.0 ± 1.0	0.3570 ± 0.0037	0.3905 ± 0.0059	80.33 ± 0.08	258.84 ± 0.07	290.8 ± 1.5
S6	2108.61 ± 0.03	192.0 ± 0.17	0.6574 ± 0.0006	0.8400 ± 0.0003	87.24 ± 0.06	85.07 ± 0.12	116.23 ± 0.07
S8	1983.64 ± 0.24	92.9 ± 0.41	0.4047 ± 0.0014	0.8031 ± 0.0075	74.37 ± 0.30	315.43 ± 0.19	346.70 ± 0.41
S9	1976.71 ± 0.92	51.3 ± 0.70	0.2724 ± 0.0041	0.644 ± 0.020	82.41 ± 0.24	156.60 ± 0.10	150.6 ± 1.0
S12	1995.59 ± 0.04	58.9 ± 0.22	0.2987 ± 0.0018	0.8883 ± 0.0017	33.56 ± 0.49	230.1 ± 1.8	317.9 ± 1.5
S13	2004.86 ± 0.04	49.00 ± 0.14	0.2641 ± 0.0016	0.4250 ± 0.0023	24.70 ± 0.48	74.5 ± 1.7	245.2 ± 2.4
S14	2000.12 ± 0.06	55.3 ± 0.48	0.2863 ± 0.0036	0.9761 ± 0.0037	100.59 ± 0.87	226.38 ± 0.64	334.59 ± 0.87
S17	1991.19 ± 0.41	76.6 ± 1.0	0.3559 ± 0.0096	0.397 ± 0.011	96.83 ± 0.11	191.62 ± 0.21	326.0 ± 1.9
S18	1993.86 ± 0.16	41.9 ± 0.18	0.2379 ± 0.0015	0.471 ± 0.012	110.67 ± 0.18	49.11 ± 0.18	349.46 ± 0.66
S19	2005.39 ± 0.16	135 ± 14	0.520 ± 0.094	0.750 ± 0.043	71.96 ± 0.35	344.60 ± 0.62	155.2 ± 2.3
S21	2027.40 ± 0.17	37.00 ± 0.28	0.2190 ± 0.0017	0.764 ± 0.014	58.8 ± 1.0	259.64 ± 0.62	166.4 ± 1.1
S22	1996.9 ± 10.2	540 ± 63	1.31 ± 0.28	0.449 ± 0.088	105.76 ± 0.95	291.7 ± 1.4	95 ± 20
S23	2024.7 ± 3.7	45.8 ± 1.6	0.253 ± 0.012	0.56 ± 0.14	48.0 ± 7.1	249 ± 13	39.0 ± 6.7
S24	2024.50 ± 0.03	331 ± 16	0.944 ± 0.048	0.8970 ± 0.0049	103.67 ± 0.42	7.93 ± 0.37	290 ± 15
S29	2025.96 ± 0.94	101.0 ± 2.0	0.428 ± 0.019	0.728 ± 0.052	105.8 ± 1.7	161.96 ± 0.80	346.5 ± 5.9
S31	2018.07 ± 0.14	108.0 ± 1.2	0.449 ± 0.010	0.5497 ± 0.0025	109.03 ± 0.27	137.16 ± 0.30	308.0 ± 3.0
S33	1928 ± 12	192.0 ± 5.2	0.657 ± 0.026	0.608 ± 0.064	60.5 ± 2.5	100.1 ± 5.5	303.7 ± 1.6
S38	2003.19 ± 0.01	19.2 ± 0.02	0.1416 ± 0.0002	0.8201 ± 0.0007	171.1 ± 2.1	101.06 ± 0.24	17.99 ± 0.25
S39	2000.06 ± 0.06	81.1 ± 1.5	0.370 ± 0.015	0.9236 ± 0.0021	89.36 ± 0.73	159.03 ± 0.10	23.3 ± 3.8
S42	2008.24 ± 0.75	335 ± 58	0.95 ± 0.18	0.567 ± 0.083	67.16 ± 0.66	196.14 ± 0.75	35.8 ± 3.2
S54	2004.46 ± 0.07	477 ± 199	1.20 ± 0.87	0.893 ± 0.078	62.2 ± 1.4	288.35 ± 0.70	140.8 ± 2.3
S55	2009.34 ± 0.04	12.80 ± 0.11	0.1078 ± 0.0010	0.7209 ± 0.0077	150.1 ± 2.2	325.5 ± 4.0	331.5 ± 3.9
S60	2023.89 ± 0.09	87.1 ± 1.4	0.3877 ± 0.0070	0.7179 ± 0.0051	126.87 ± 0.30	170.54 ± 0.85	29.37 ± 0.29
S66	1771 ± 38	664 ± 37	1.502 ± 0.095	0.128 ± 0.043	128.5 ± 1.6	92.3 ± 3.2	134 ± 17
S67	1705 ± 22	431 ± 10	1.126 ± 0.026	0.293 ± 0.057	136.0 ± 1.1	96.5 ± 6.4	213.5 ± 1.6
S71	1695 ± 21	346 ± 11	0.973 ± 0.040	0.899 ± 0.013	74.0 ± 1.3	35.16 ± 0.86	337.8 ± 4.9
S83	2046.8 ± 6.3	656 ± 69	1.49 ± 0.19	0.365 ± 0.075	127.2 ± 1.4	87.7 ± 1.2	203.6 ± 6.0
S85	1930.2 ± 9.8	3580 ± 2550	4.6 ± 3.30	0.78 ± 0.15	84.78 ± 0.29	107.36 ± 0.43	156.3 ± 6.8
S89	1783 ± 26	406 ± 27	1.081 ± 0.055	0.639 ± 0.038	87.61 ± 0.16	238.99 ± 0.18	126.4 ± 4.0
S91	1108 ± 69	958 ± 50	1.917 ± 0.089	0.303 ± 0.034	114.49 ± 0.32	105.35 ± 0.74	356.4 ± 1.6
S96	1646 ± 16	662 ± 29	1.499 ± 0.057	0.174 ± 0.022	126.36 ± 0.96	115.66 ± 0.59	233.6 ± 2.4
S97	2132 ± 29	1270 ± 309	2.32 ± 0.46	0.35 ± 0.11	113.0 ± 1.3	113.2 ± 1.4	28 ± 14
S145	1808 ± 58	426 ± 71	1.12 ± 0.18	0.50 ± 0.25	83.7 ± 1.6	263.92 ± 0.94	185 ± 16
S175	2009.51 ± 0.01	96.2 ± 5.0	0.414 ± 0.039	0.9867 ± 0.0018	88.53 ± 0.60	326.83 ± 0.78	68.52 ± 0.40

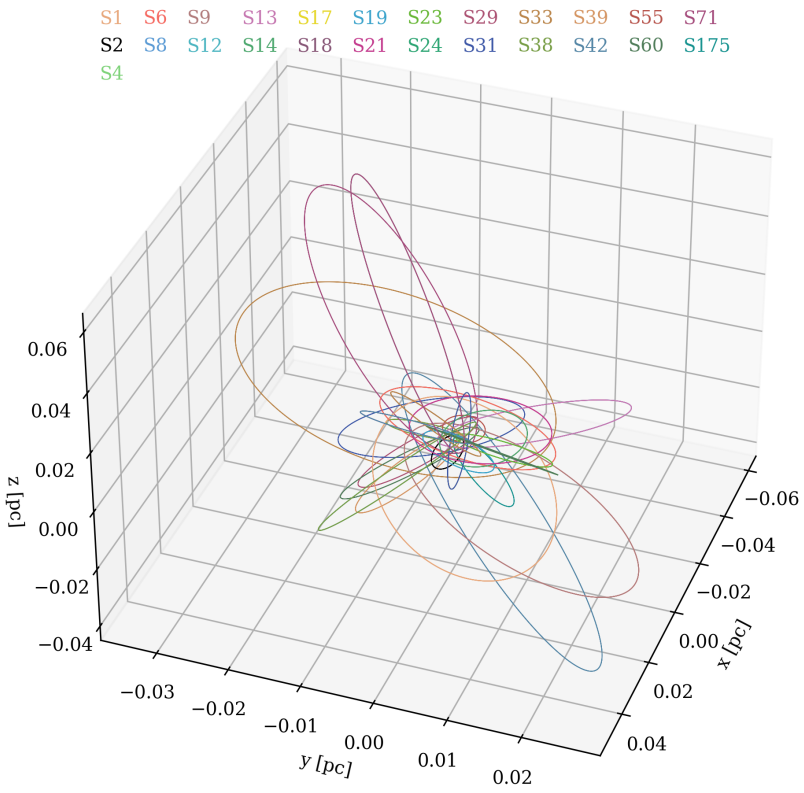

Figure 3.2: A scheme of the S-star cluster stars in the innermost 1″ of the Galaxy. The black hole SgrA* resides in the (0, 0, 0) coordinates. The star of our interest, S2, is denoted in black. The orbital parameters used for this visualization were taken from Gillessen et al., 2017 and are written in Tab. 2.

4

NUMERICAL APPROACH

Unlike in our analytical approach, we can determine the stellar orbits from initial conditions (the position and velocity components at a given time) with the numerical methods that solve ordinary differential equations. The list with a brief description of each integrator used in this thesis follows.

4.1 EULER INTEGRATION

The simplest method for calculating stellar trajectories from the initial conditions is the Euler integrator. In our notation, the prescription of the relations looks like this:

$$\begin{aligned} \vec{v}_i^{n+1} &= \vec{v}_i^n + \vec{a}_i^n \Delta t \ , \\ \vec{r}_i^{n+1} &= \vec{r}_i^n + \vec{v}_i^n \Delta t \ . \end{aligned} \tag{4.1}$$

At the end of each iteration, the time increases by the time step Δt:

$$t^{n+1} = t^n + \Delta t \ .$$

The error in one iteration is as high as $(\Delta t)^2$ and the total error increases to Δt. This method is not ideal for closed orbits, and very often the artificial pericenter precession occurs (see Fig. 4.1).

Since Euler method does not conserve the kinetic energy it is bad to use it for closed orbits (the effect of the lack of conservationcan be seen in Fig. 4.1).

4.2 HEUN INTEGRATION

Heun second-order method is in fact a modified Euler method, also known as explicit trapezoid rule.

Its general prescription is following:

$$y_{n+1} = y_n + \frac{\Delta t}{2} \left(k_1 + k_2 \right) \ , \tag{4.2}$$

with the stages

$$\begin{aligned} k_1 &= f(t_n, y_n) \,, \\ k_2 &= f(t_n + \Delta, y_n + \Delta t k_1) \,. \end{aligned} \tag{4.3}$$

The global error of this method is of order $(\Delta t)^2$ (the local truncation error is of order $(\Delta t)^3$).

4.3 4TH ORDER RUNGE–KUTTA INTEGRATION

Similar to the Heun method, the Runge-Kutta 4th order uses the auxiliary functions k. The prescription then looks like this:

$$y_{n+1} = y_n + \frac{\Delta t}{6} \left(k_1 + 2k_2 + 2k_3 + k_4\right) \,. \tag{4.4}$$

$$\begin{aligned} k_1 &= f(t_n, y_n) \,, \\ k_2 &= f(t_n + \frac{\Delta t}{2}, y_n + \frac{\Delta t}{2} k_1) \,, \\ k_3 &= f(t_n + \frac{\Delta t}{2}, y_n + \frac{\Delta t}{2} k_2) \,, \\ k_4 &= f(t_n + \Delta t, y_n + \Delta t k_3) \,. \end{aligned} \tag{4.5}$$

Again, the local error of this integrator is of order $(\Delta t)^5$ and the global error $(\Delta t)^5$. Even tho this method is significantly more accurate, it still exhibits some inaccuracies, such as unrealistic energy growth of the whole system.

4.4 `python` SOLVERS

All of the first-order differential equations integrators above had to be implemented into the `python` code. However, `python` has its own libraries with ODE solvers, like `scipy.integrate`. We tried some of the internal integrators, for starters the `odeint` integrator which is based on the FORTRAN solver of ODEs called `lsoda`. It is highly adaptive, making the solver suitable for almost all ODE problems.

The `solve_ivp`, standing for "solving initial value problem", also solves for a wide variety of ODEs. The method of integration can be changed with the '`method`' parameter, the allowed options are for example: `'RK45', 'DOP853', 'Radau'`.

In our case, we compared the `odeint` integrator with the `solve_ivp` module with the `'DOP853'` choice for the `method` parameter. This method is an explicit 8th order

Runge-Kutta with the interpolation polynomial of the order 7. We also applied the adaptive time step, enabling us to control the rapid variations of the system.

4.5 INTEGRATORS COMPARISON

In the plots below, we can see the comparison of the integrators described above. To show the errors of the chosen method we had to change the time interval along with the time step.

4.6 NUMERICAL ORBIT OF S2 STAR

Here we tested the code functionality. She orbit of the S2 star is again consistent with the ones in Fig. 3.1 and Fig. 1.2.

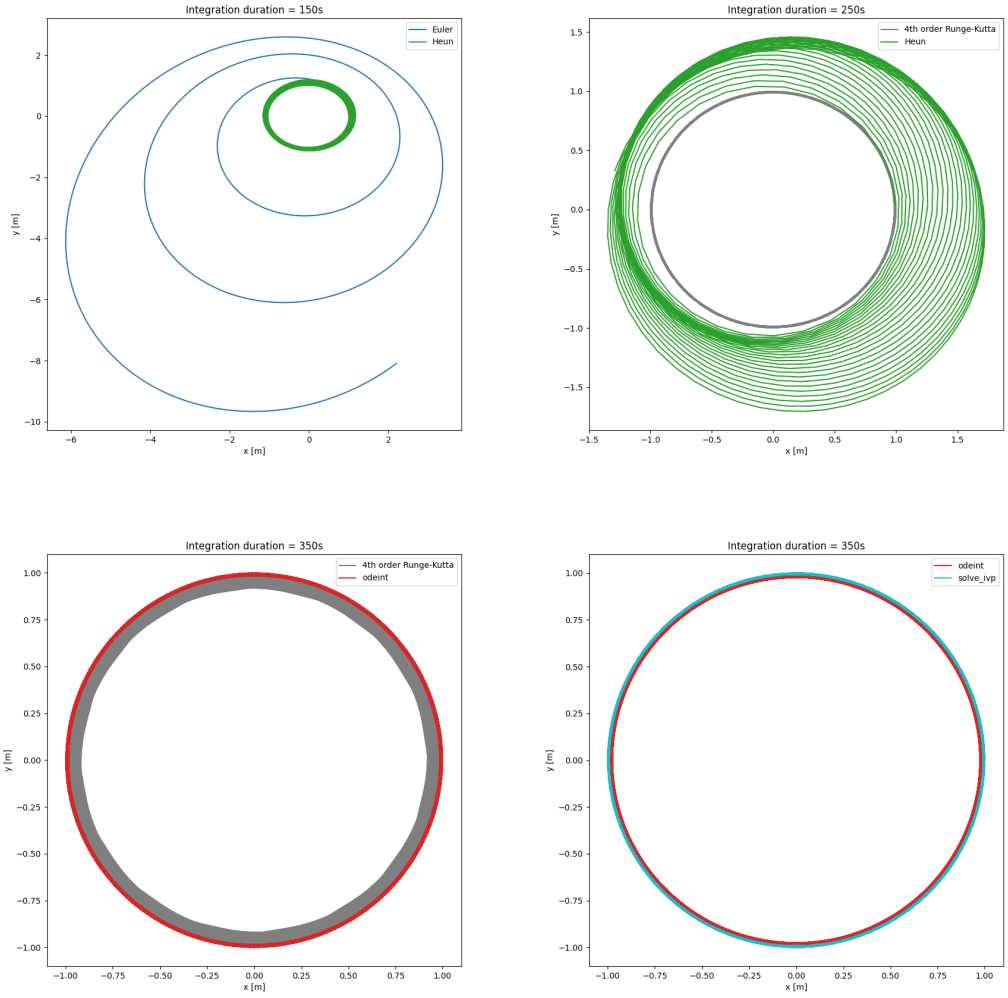

Figure 4.1: Comparison of the simple integrators with the Python's `odeint` and `solve_ivp` libraries. The `solve_ivp` module is used with the method = 'DOP853', that is, the 8th-order Runge-Kutta integrator.

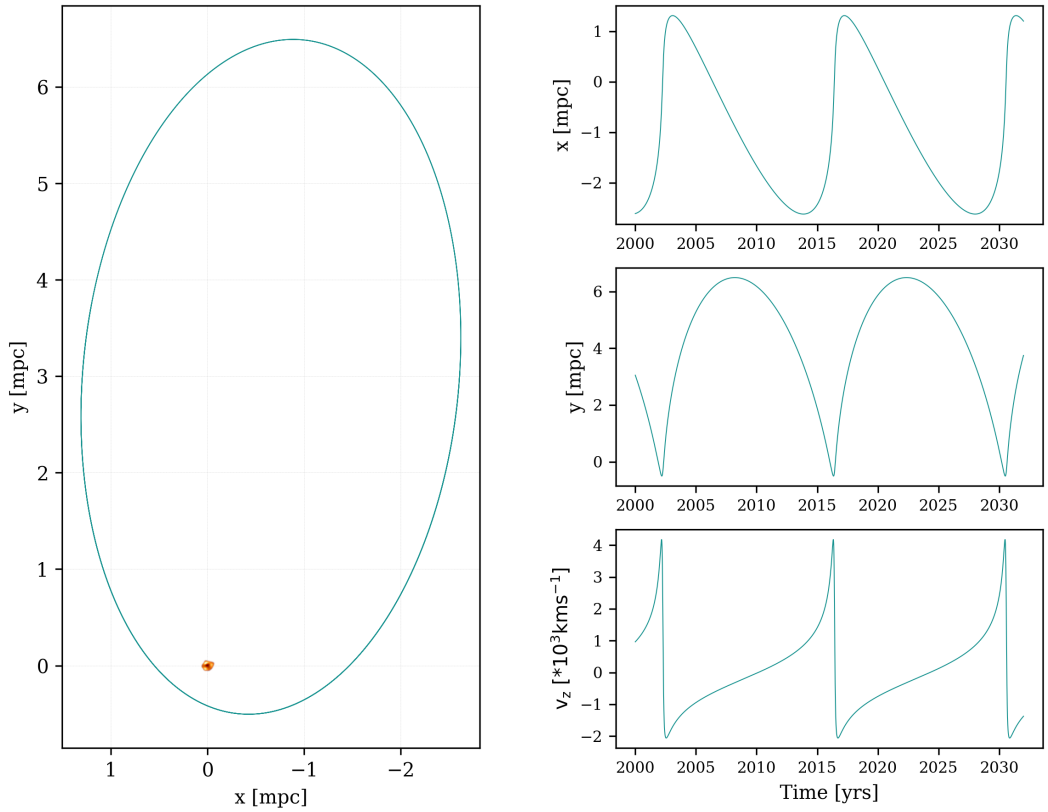

Figure 4.2: The orbit of S2 star computed numerically. Again, we can see that it is consistent with the the figures Fig. 3.1 and Fig. 1.2. The image of SgrA* is not in scale!

Part III

RESULTS & DISCUSSION

5

BONDI ACCRETION

The functionality of the integrator was already tested in the section 4 for only gravitational acceleration. In this section, we will compare the evolution of the system with the hydrodynamical drag force and the post-Newtonian correction for several different cases (varying density, mass) for spherical and disc layout. First we used a hypothetical particle with unrealistic parameters (the diameter was set to $R = 0.005$m and the mass $m = 0.15$kg) so the changes in orbit and parameters would appear quickly. Then the simulations for realistic particles whose parameters were $R = 0.05$m and $m = 0.15$kg were made. Finally, after all the tests with the particles, the orbit of the star S2 itself was simulated with various conditions. The characteristics of the S2 star were derived from spectroscopic observations and are as follows: $m = 13.6 M_\odot$, $R = 5.53 R_\odot$ (Habibi et al., 2017).

5.1 SIMULATIONS IN BONDI ACCRETION SCENARIO

The results of the simulations for the first scenario, Bondi accretion, are shown on the following pages. The hypothetical particle's orbit can be seen in Fig. 5.1. We can notice the rapid inspiral onto the black hole (the simulation was terminated at the distance of $100\, r_{\mathrm{grav}}$ – at this distance the particle would be evaporated). The orbital energy is transferred to the internal energy of the body which leads to the decreasing eccentricity and circularisation of the orbit. At the same time, the change of the argument of periapsis increases exponencially.

Figures 5.2 – 5.4 show the simulations of the realistic particle. In Fig. 5.2 only hydrodynamical drag from the real density distribution (Eq. 2.17) was taken into account. The eccentricity changes with each revolution linearly with the linear change of the argument of periapsis. The post-Newton correction without the influence of the dusty environment is shown in Fig. 5.3. This effect, called precession of pericenter, does not change the eccentricity or the argument of periapsis of the orbit. These two effects were combined in the final simulation for the test particle in this layout (Fig. 5.4) - the PN correction has negligible effect over the period this short (200 years).

In three final figures of this scenario, Fig. 5.5 – 5.7, the orbits of the S2 star were computed. The motion of the star through the medium with the real density distribution without the effect of the strong gravitational field from the black hole can be seen in Fig. 5.5. It does not seem to be affected by this sparse domain at all. However, the effect of the PN precession is very strong (Fig. 5.6). The final simulation was made for

extreme density with PN effect during longer period of 5000 years. Relatively small change in the energy can be detected.

Notice that in this scenario the inclination does not change since it is the spherical problem.

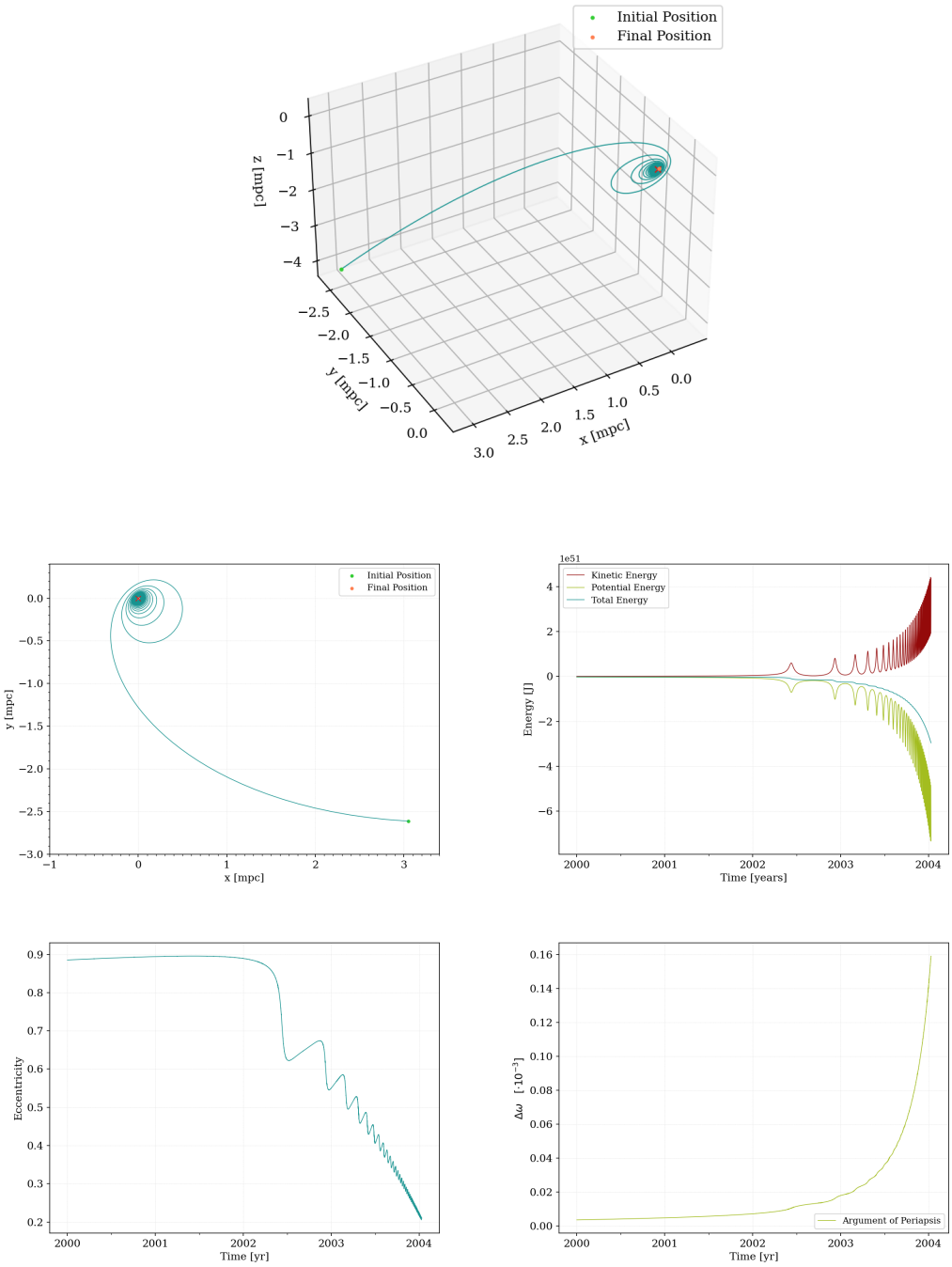

Figure 5.1: Bondi accretion; $m = 0.15\text{kg}$, $R = 0.005\text{m}$, $\rho = 10^{-11}\text{kg/m}^3$, $T = 5\text{years}$
First test simulation was done for an extreme case of hydrodynamic drag force: the characteristics for the hypothetical test particle were $R = 0.5$ cm and $m = 150$ g in an extremely dense environment (the mass density was set to $\rho = 10^{-11}\text{kg/m}^3$). The *upper plot* is the 3D projection of the particle's orbit with markers on the initial and final position. The *middle left* panel shows the projection of the orbit to the x-y plane, the *middle right* plot traces the energy components evolution over time, *lower left* panel depicts the time evolution of the orbit's eccentricity, and the final, *lower right* panel shows the evolution of the argument of periapsis over time. The integration was terminated at a distance of 100 gravitational radii from the center.

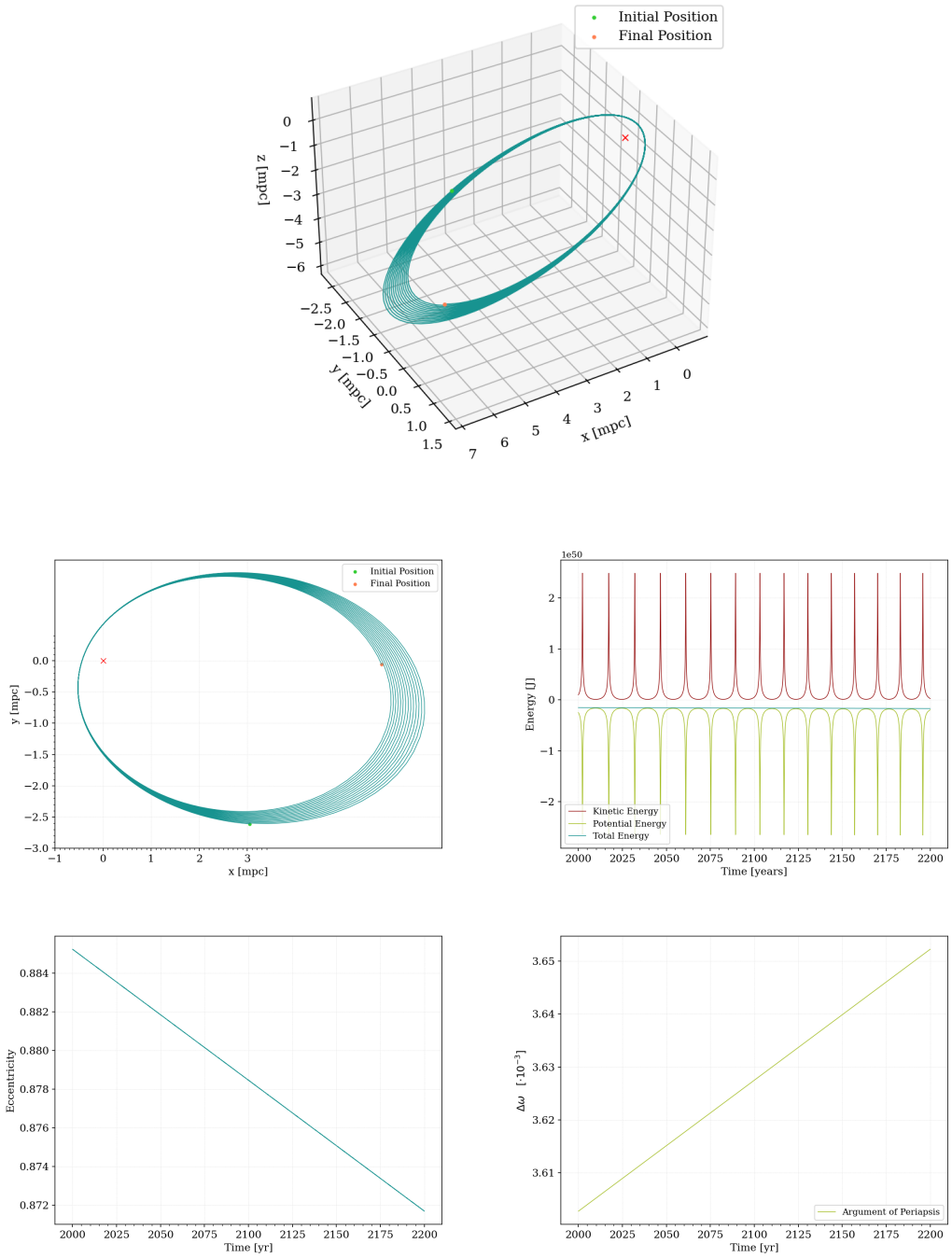

Figure 5.2: Bondi accretion; $m = 0.15\text{kg}$, $R = 0.05\text{m}$, $\rho = 10^{-11}\left(\frac{r}{R_{Bondi}}\right)^{-3/2}\text{kg/m}^3$, $T = 200\text{years}$
Simulation of the movement of realistic particle in the region of Bondi accretion with the density prescribed by Eq. 2.17 without PN correction. The panels are the same as in Fig. 5.1.

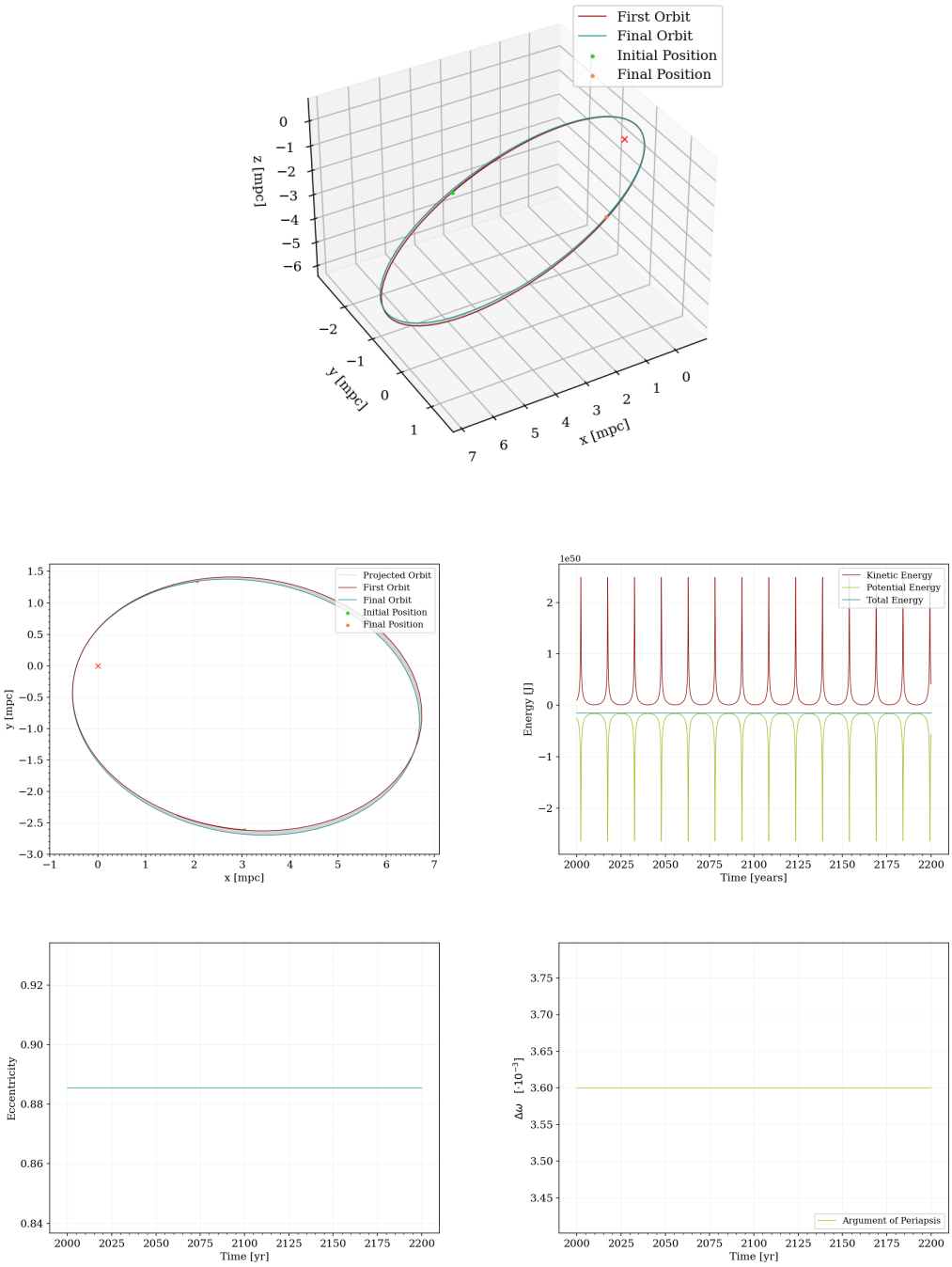

Figure 5.3: Bondi accretion; $m = 0.15$kg, $R = 0.05$m, $T = 200$years
Simulation of test particle movement in the gravitational potential of SgrA* without the dust and gas (only PN correction is taken into account). Again, panels are in the same order as in Fig. 5.1.

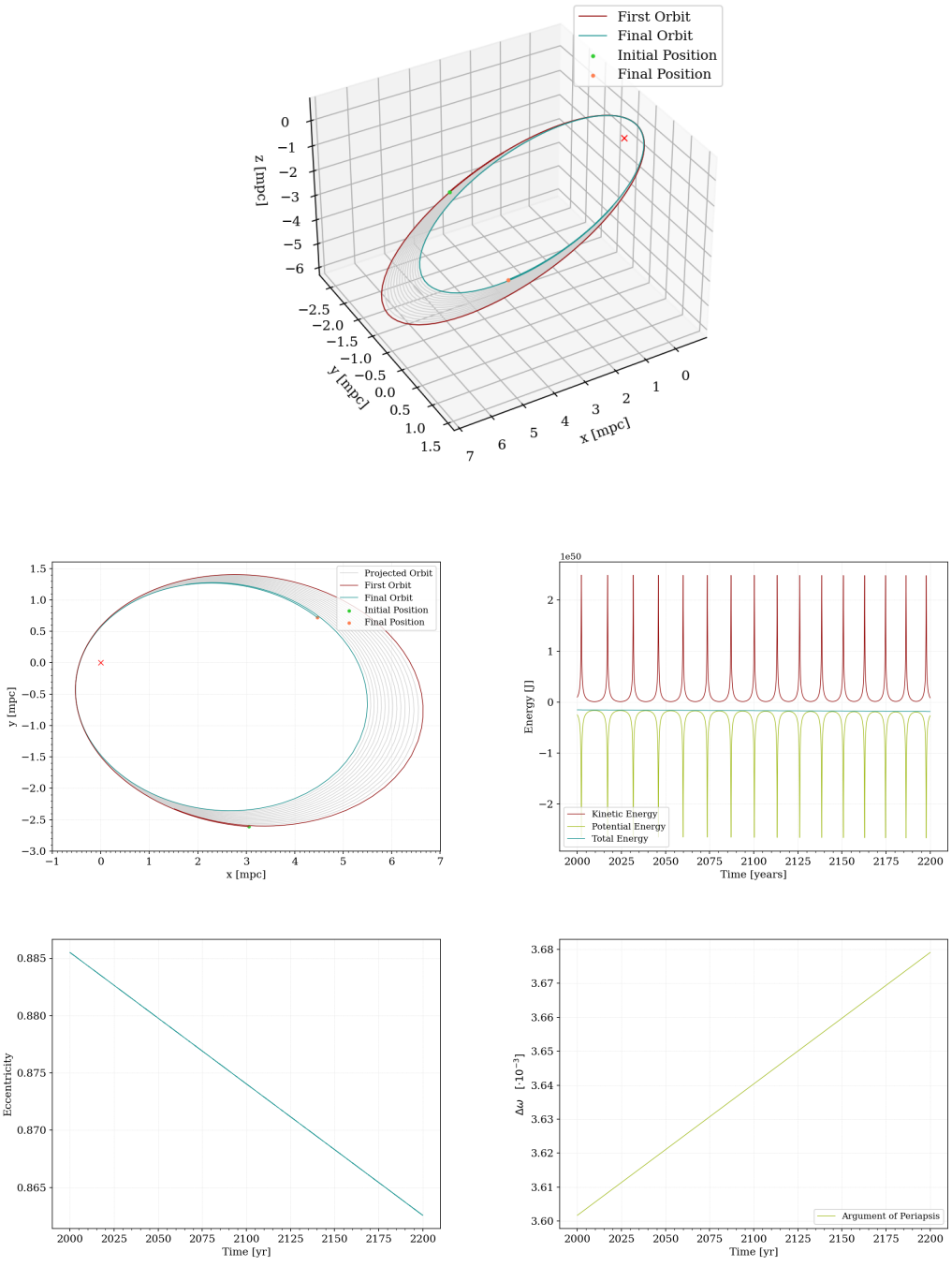

Figure 5.4: Bondi accretion; $m = 0.15\text{kg}$, $R = 0.05\text{m}$, $\rho = 10^{-11}\left(\frac{r}{R_{Bondi}}\right)^{-3/2}\text{kg/m}^3$, $T = 200\text{years}$
Test of the influence of both perturbing effects – the hydrodynamical drag and PN correction. As usual, the panels have the same order as in Fig. 5.1.

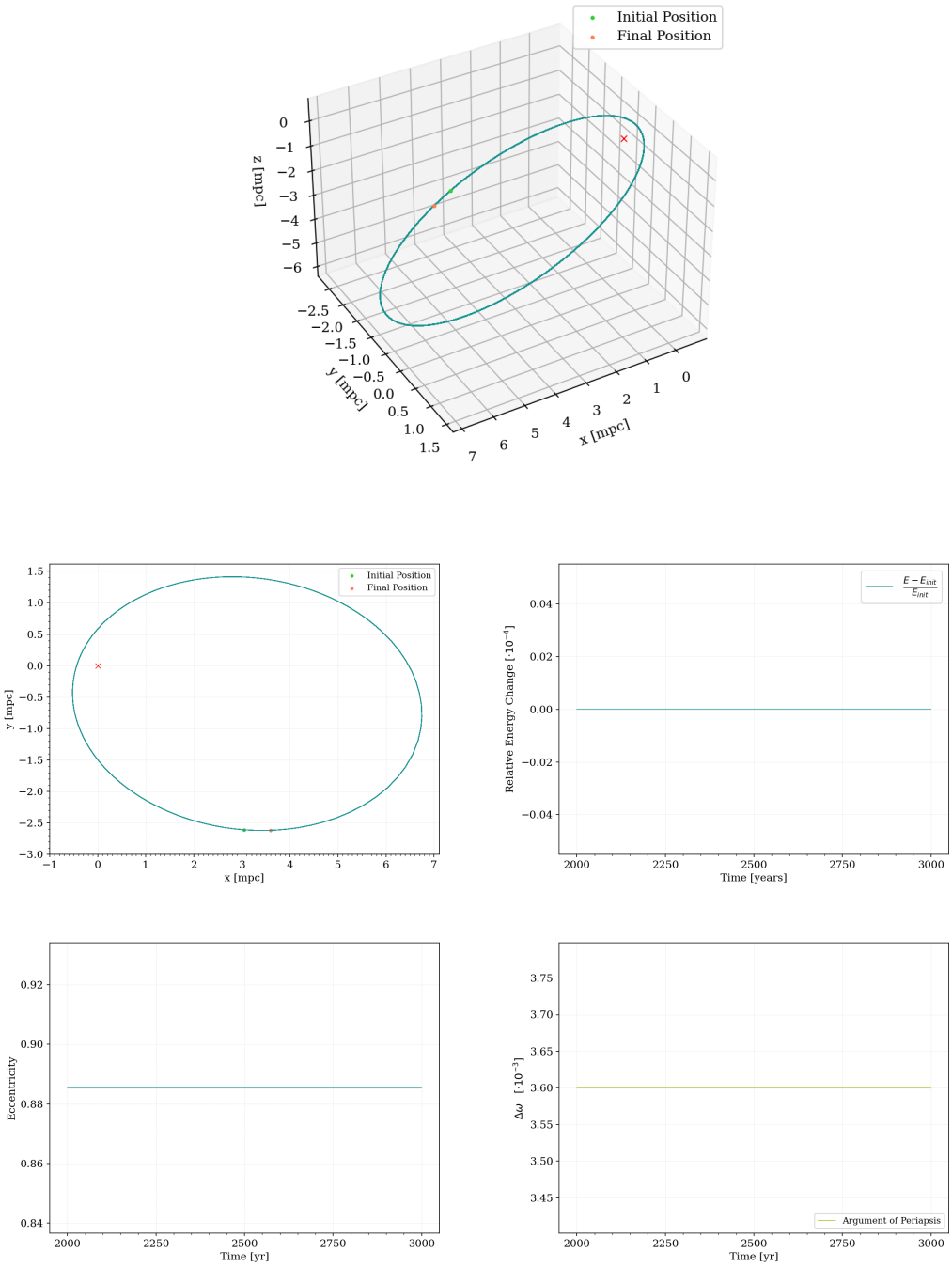

Figure 5.5: Bondi accretion; $m = 13.6M_{\odot}$, $R = 5.53R_{\odot}$, $\rho = 10^{-11}\mathrm{kg/m^3}$, $T = 1000$years
Simulation of the orbit of S2 star in the Bondi sphere without the effect of strong gravitational field. Except the *middle right* panel, that is now showing the relative energy development (the time period is too long to show usual energy evolution) the panels are the same as in Fig. 5.1.

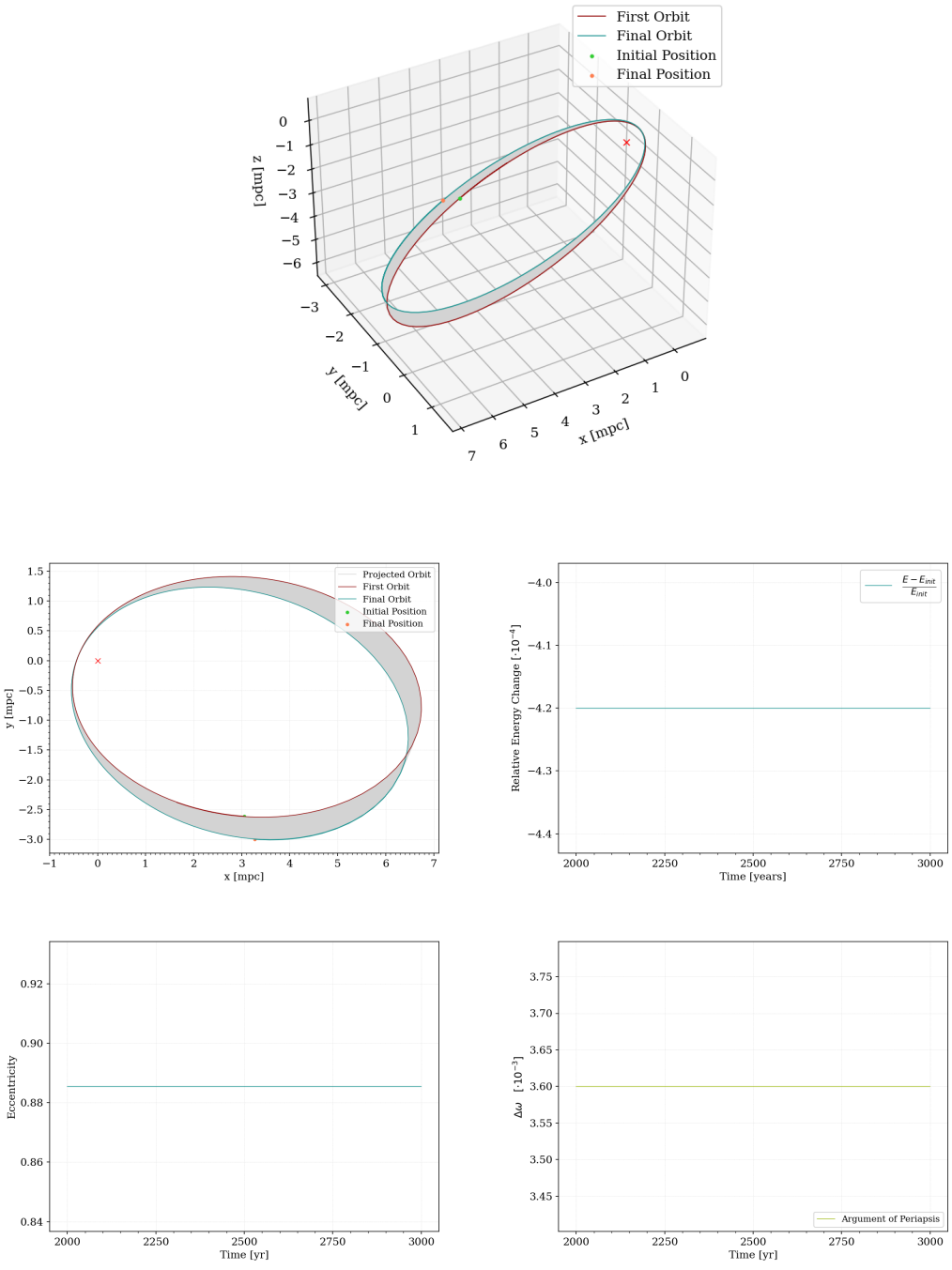

Figure 5.6: Bondi accretion; $m = 13.6M_{\odot}$, $R = 5.53R_{\odot}$, $\rho = 10^{-11}\left(\frac{r}{R_{Bondi}}\right)^{-3/2}\,\mathrm{kg/m^3}$, $T = 1000$years S2 star's PN precession without the influence of the environment. Panel layout is the same as in Fig. 5.1.

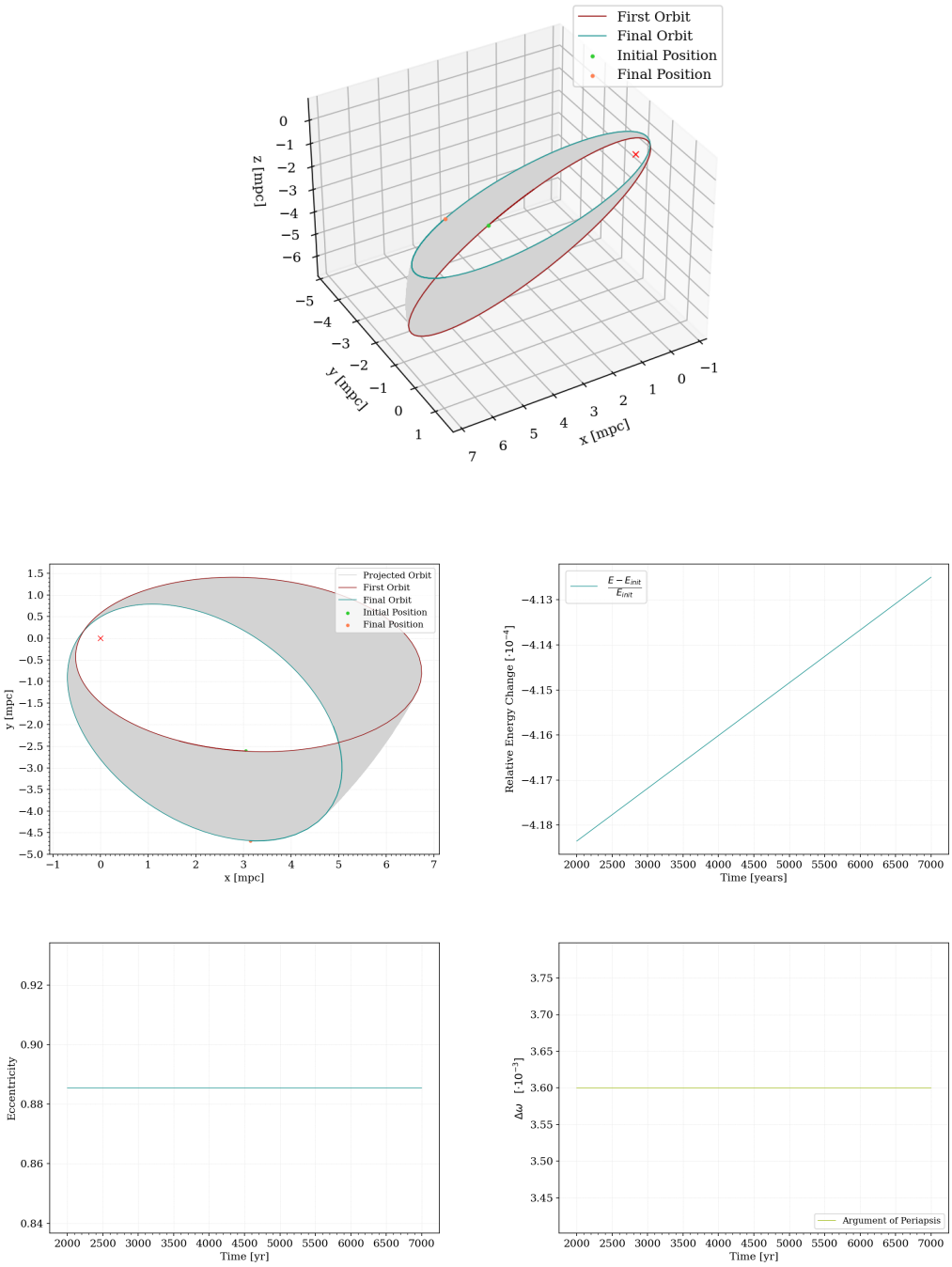

Figure 5.7: Bondi accretion; $m = 13.6M_{\odot}$, $R = 5.53R_{\odot}$, $\rho = 10^{-11}\mathrm{kg/m^3}$, $T = 5000$years
Simulation of the motion of the S2 star during the 5000 year-long period with the hydrodynamical drag and PN1 precession accounted. The density is set to extreme value $\rho = 10^{-11}\mathrm{kg/m^3}$. Again, the layout is as in Fig. 5.1.

6

ACCRETION DISC

Second scenario, the accretion disc, was first tested on "infinitely thick disc" and then the disc was parametrized by the Shakura-Sunyaev approximation to a thin (or alpha) disc (Eq. 2.20).

The characterization of the test particles and S2 star are the same as in Chap. 5.

6.1 SIMULATIONS IN THICK ACCRETION DISC SCENARIO

In this scenario, the height (or thickness) of the disc is set to extremely huge value (so the star or particle is inside the disc at all time steps). The disc rotates in Keplerian motion.

In Fig. 6.1 the result for the hypothetical particle inside this dusty and gaseous medium without the correction on strong gravitational field is depicted. In the panel with the x-z projection we can clearly notice the tendency of the particle to align to the accretion disc plane (the panel with the inclination evolution confirms this observation). Also, the argument of periapsis changes right after the simulation starts very rapidly.

Fig. 6.2 shows the particle enclosed in more realistic scheme (Shakura-Sunyaev density of the disc with physically correct particle size and mass) during the 1000 years long period. Only slight change in the orbit's inclination is detected suggesting that the more massive object, such as the star S2, would not be affected very much by this setup.

Finally, the Fig. 6.3 of both perturbing sources acting on the particle's trajectory shows the expected change in both the inlination and the argument of periapsis.

Final result in this subsection 6.4 was obtained for the actual S2 star under the effect of both perturbing elements in realistic parameters (we already know that the star's orbit will not be changed due to the hydrodynamical drag).

6.2 SIMULATIONS IN SHAKURA-SUNYAEV DISC SCENARIO

After all the simulations within the thick accretion disc were done, the parametrization by Shakura-Sunyaev approximation could be implemented.

In Fig. 6.5 and Fig. 6.6 the thickness of the parametrized disc is too small to be affecting the orbits of any bodies significantly. However, if the accretion rate of SgrA*

changed to $\dot{M} = 10^3 M_\odot/\text{year}$, the disc would be thick enough to change the orbit of the particle again (but the accretion rate this high then does not allow for the Shakura-Sunyaev approximation since it is only for a thin disc).

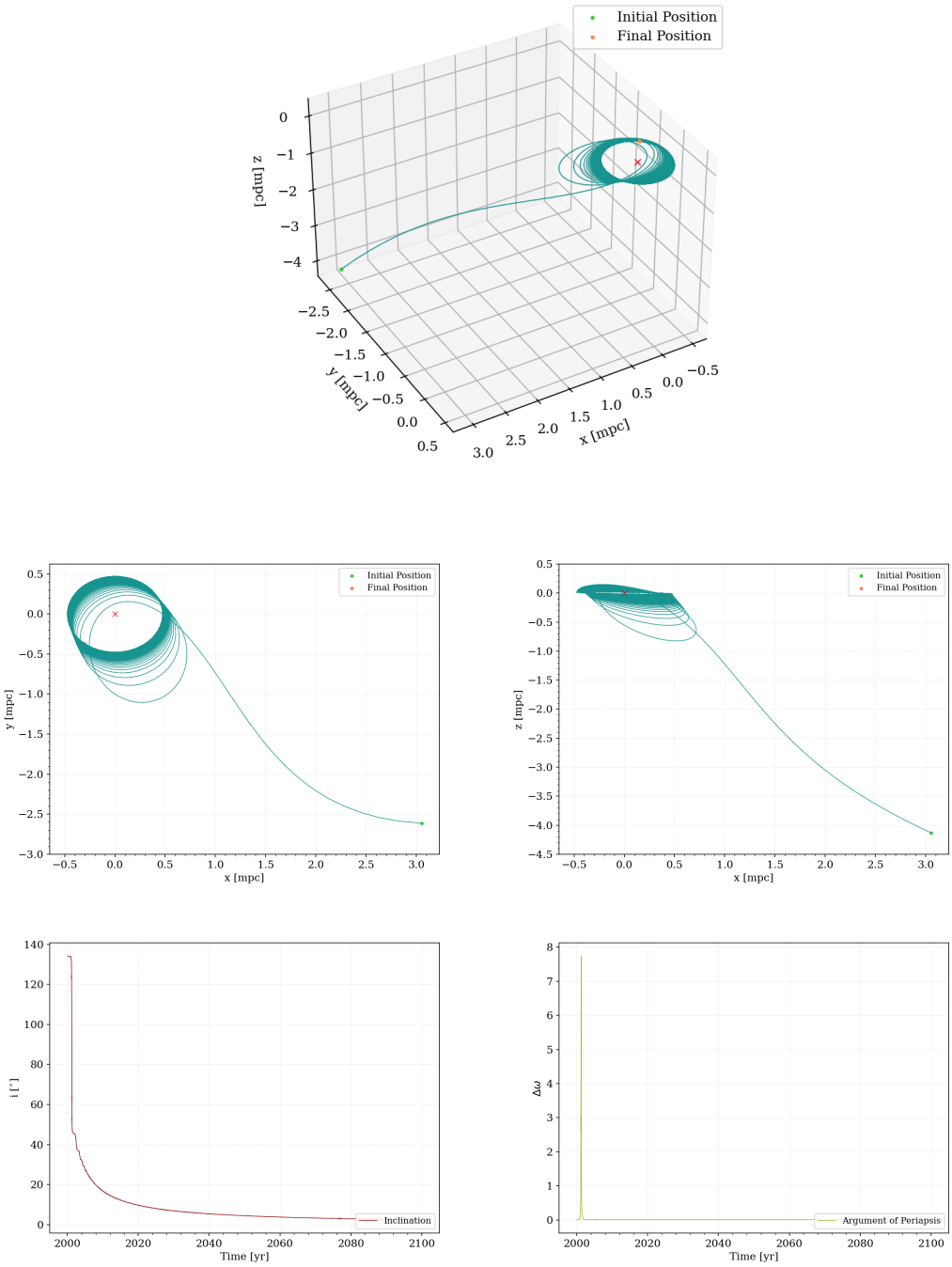

Figure 6.1: Thick disc; $m = 0.15\text{kg}$, $R = 0.005\text{m}$, $\rho = 10^{-11}\text{kg/m}^3$, $T = 100\text{years}$
Simulation of the hypothetical particle in extremely dense and infinitely thick accretion disc in Keplerian motion. PN correction is not taken into account. Here, in the *top* plot the 3D projection of the orbit is shown, the *middle left* shows the x-y plane projection, *middle right* plot is the projection to the x-z plane. The *lower left* panel traces the inclination evolution and the *lower right* chart shows the time evolution of the change in argument of periapsis.

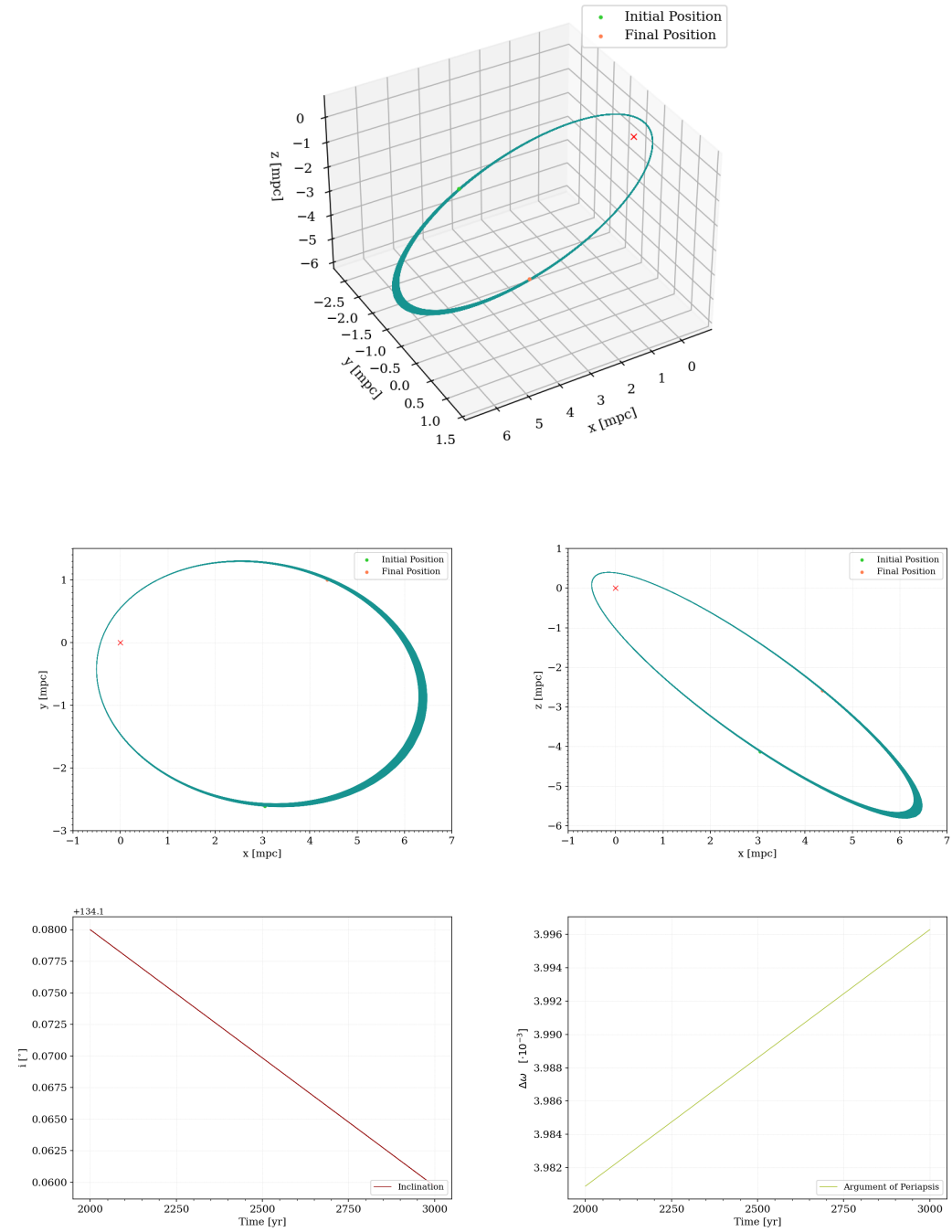

Figure 6.2: Thick disc; $m = 0.15$kg, $R = 0.05$m, $T = 1000$years
The simulation of the realistic particle moving through the realistic density distribution (Shakura-Sunyaev density distribution) without the gravitational field not accounted for. Panels are the same as in Fig. 6.1.

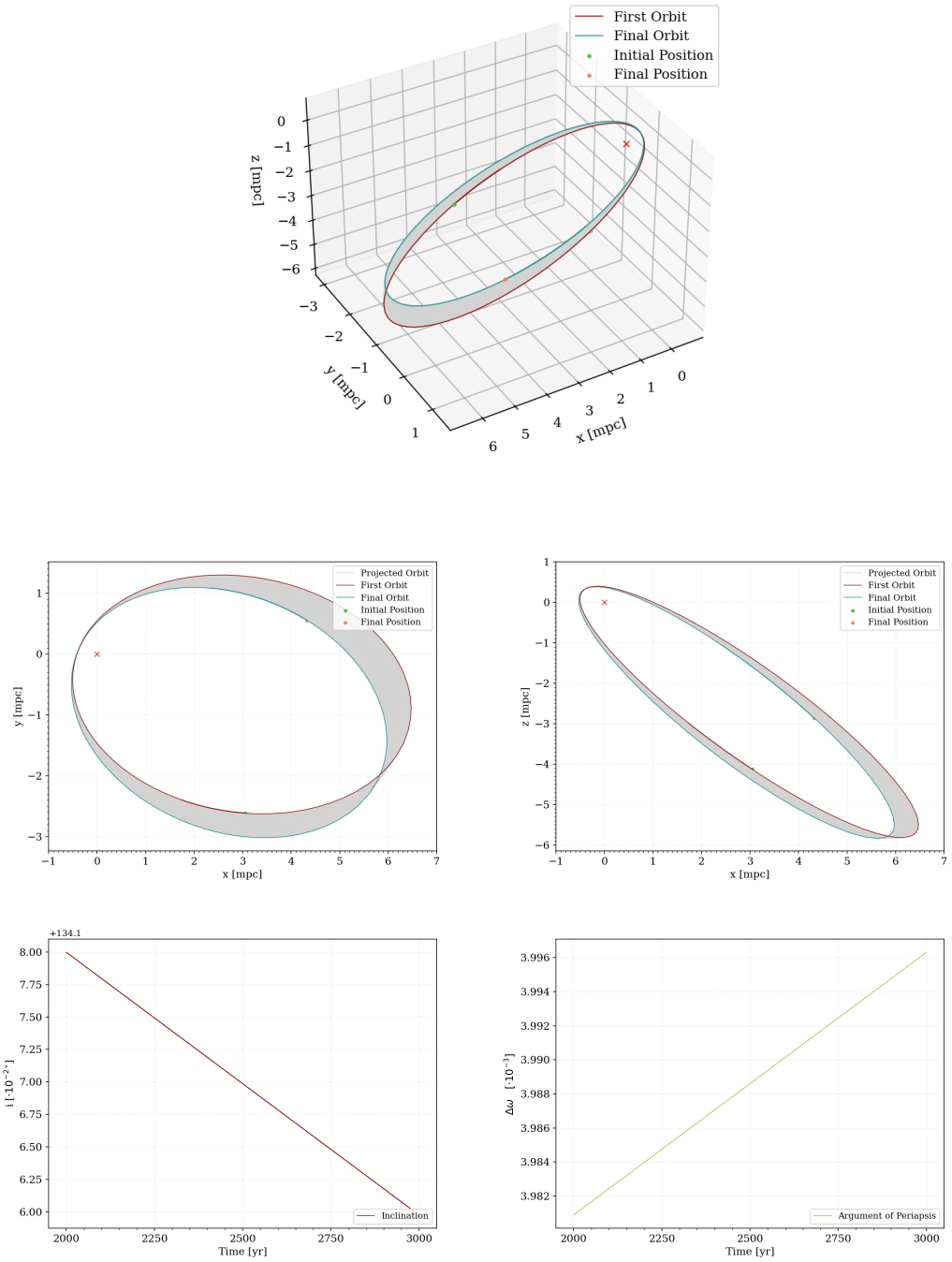

Figure 6.3: Thick disc; $m = 0.15$kg, $R = 0.05$m, $T = 1000$years
Test simulation on realistic particle with both perturbing effects taken into account. Panels layout is as usual the same as in Fig. 6.1.

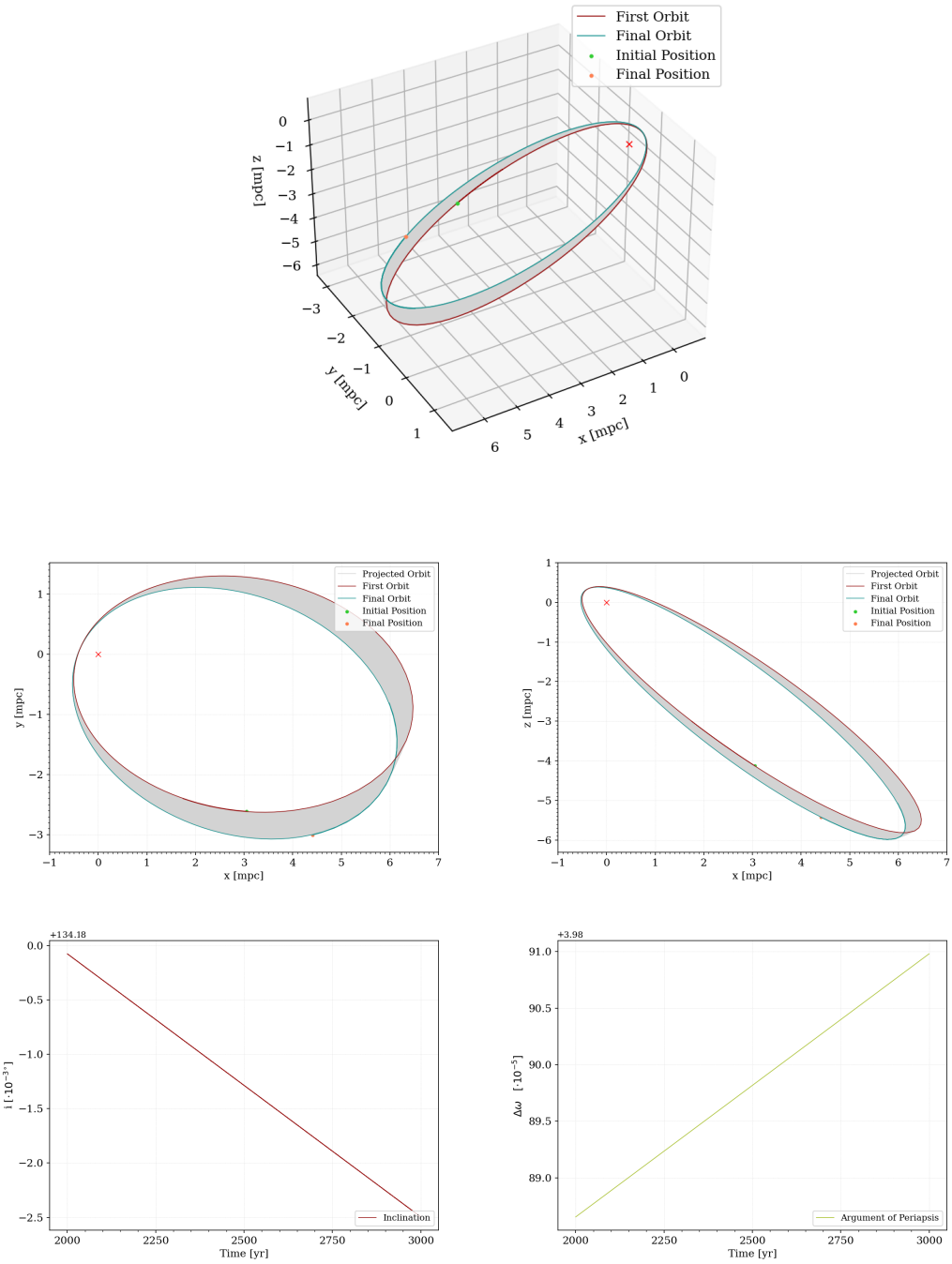

Figure 6.4: Thick disc; $m = 13.6M_{\odot}$, $R = 5.53R_{\odot}$, $T = 1000$years
The simulation of S2 moving through the extremely dense medium with the presence of the strong gravitational field. Panels are the same as in Fig. 6.1.

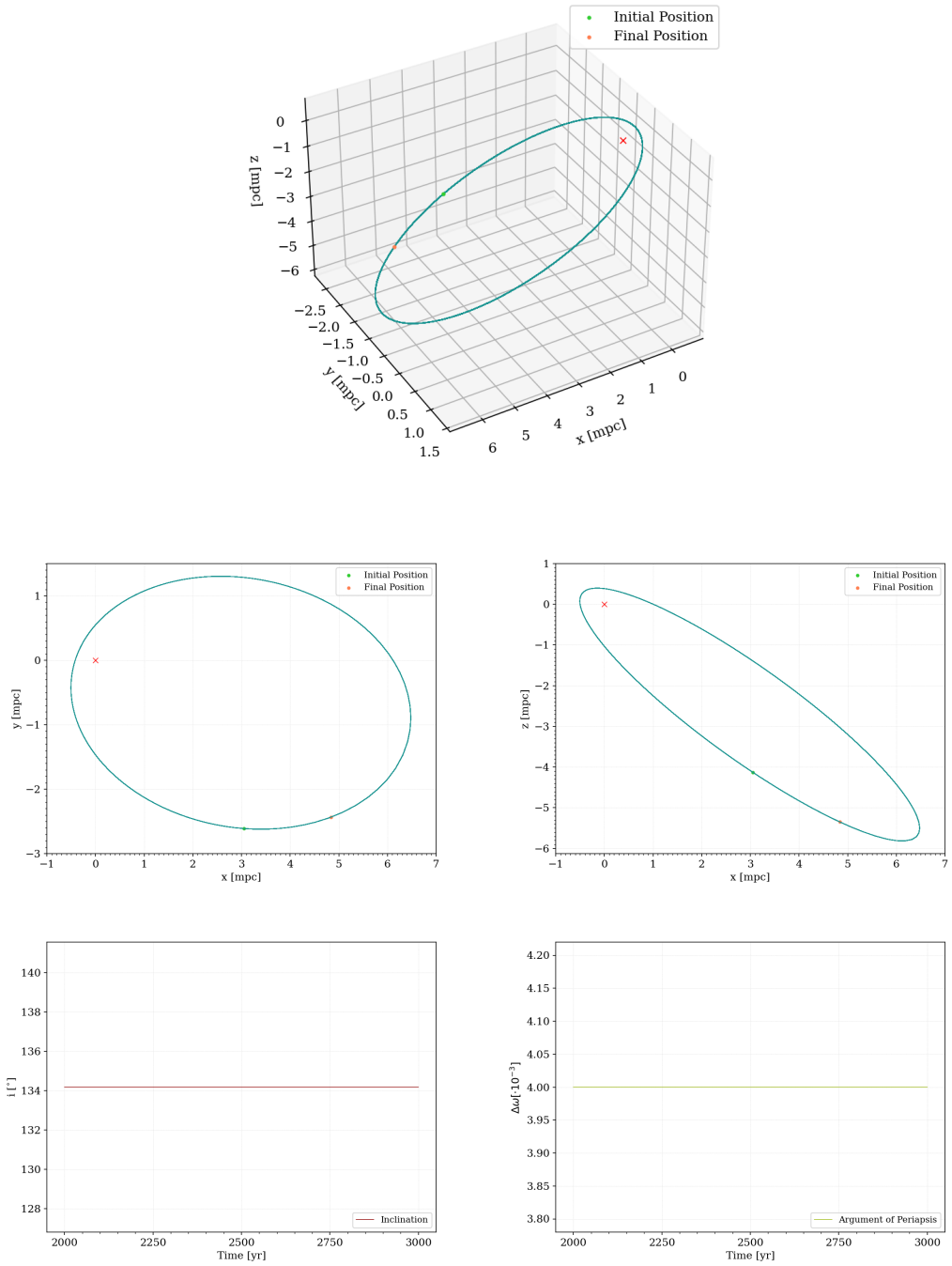

Figure 6.5: Shakura-Sunyaev disc; $m = 0.15$kg, $R = 0.005$m, $\dot{M} = 10^{-6} M_{\odot}/\text{year}$, $T = 1000$years
Simulation of the unrealistic test particle's motion through the accretion disc parametrized by the Shaura-Sunyaev model. The pathway of the test particle is not affected at all by the disc. Panels layout is the same as in Fig. 6.1.

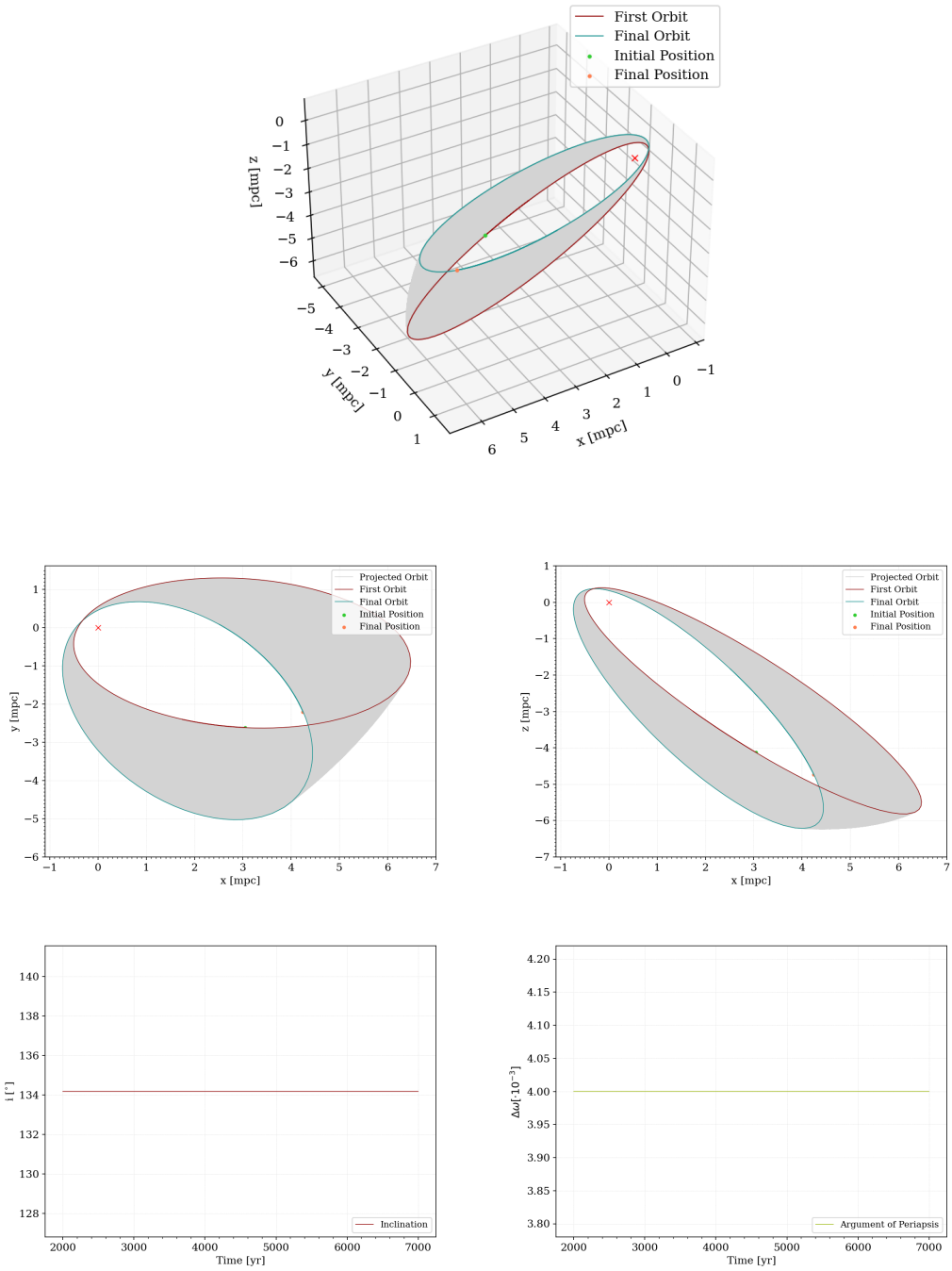

Figure 6.6: Shakura-Sunyaev disc; $m = 13.6M_\odot$, $R = 5.53R_\odot$, $\dot{M} = 10^{-6}M_\odot/\text{year}$, $T = 5000\text{years}$
S2's orbit change when passing through a Shakura-Sunyaev disc during 5000 years period. The orbit is not affected by the disc at all whereas the PN correction is visible very well.

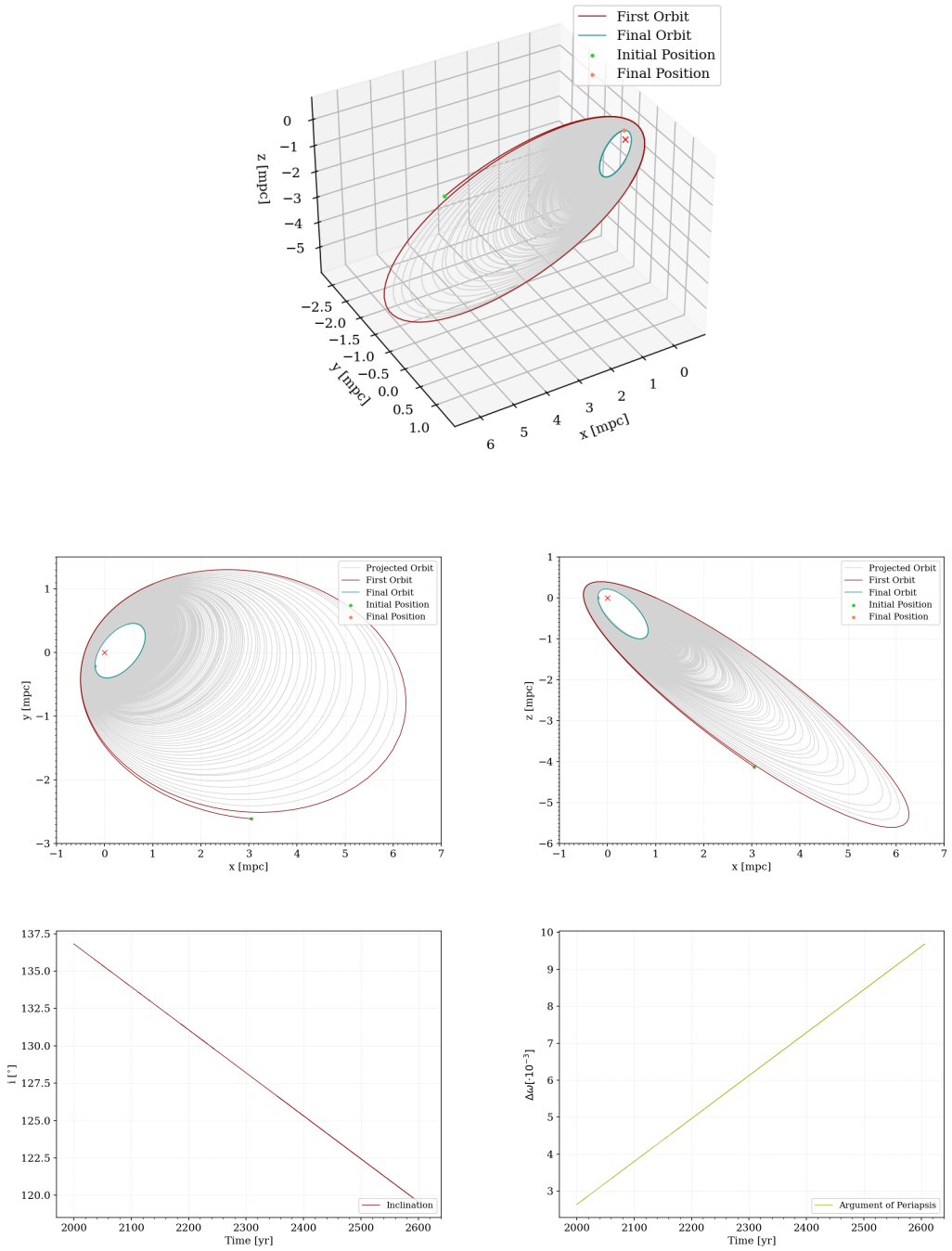

Figure 6.7: Shakura-Sunyaev disc; $m = 0.15$kg, $R = 0.005$m, $\dot{M} = 10^3 M_\odot$/year, $T = 5000$years
Unrealistic particle's movement through the Shakura-Sunyaev parametrization of the disc. The accretion rate was set extremely high, to $\dot{M} = 10^3 M_\odot$/year.

7

DISCUSSION

The results in chapters 5 and 6 proved that the surrounding dusty environment has little, if any, effect on the orbit of S2, but the Schwarzschild precession is very strong in this region and causes the largest change in the orientation of the orbital plane. The angle by which the orbit is shifted by this post-Newtonian correction is approximately $\Delta\varphi \approx 12''$, a perceptible shift already visible in simulations of S2's motion.

In this thesis, we have omitted consideration of the Newtonian precession (due to the gravitational influence of surrounding stars) on S2, since meticulous observations of the Galactic Centre thus far suggest its negligible impact on S2's orbital dynamics. However, on the time scales longer than the resonant relaxation time (for the galactic center about millions to billions of years) the influence proximate stars within the so-called influence radius (stars gravitationally bound to the black hole mutually interact with each other, for the environment at the centre of the galaxy this radius is approximately 2 pc) becomes relevant. These timescales characterize the stochastic processes that can alter the morphological configuration of the cluster Alexander, 2017.

The simulations conducted in the Bondi accretion scenario provide valuable insights into the dynamic behavior of particles and stars near a supermassive black hole. Initial investigations with a hypothetical particle featuring extreme parameters reveal a rapid inspiral towards the black hole, accompanied by a transfer of orbital energy to internal energy, leading to decreased eccentricity and orbit circularization. Subsequent simulations with realistic particle parameters demonstrate the continuous influence of the surrounding medium, evidenced by linear changes in eccentricity with each revolution induced by hydrodynamical drag. Conversely, post-Newtonian corrections exhibit negligible effects on eccentricity or argument of periapsis. Analysis of the S2 star's orbit within the Bondi sphere reveals minimal deviation, underscoring the resilience of massive stellar bodies to external dusty environments.

The investigation into accretion discs, encompassing both thick disc and the Shakura-Sunyaev model parametrization, provides another insight onto the physics of black holes. Initial simulations on infinitely thick discs unveil notable inclinations of particles towards the disc plane and rapid changes in periapsis argument, while subsequent exploration under more realistic parameters suggests minimal impact on larger objects like the S2 star. Incorporating hydrodynamical drag and post-Newtonian corrections further elucidates orbital dynamics, showcasing expected changes in inclination and periapsis argument. Transitioning to the Shakura-Sunyaev approximation reveals limited effects on orbiting bodies due to the thinness of the disc, though the change in SgrA*'s accretion rate demonstrate potential variations in particle orbits.

In the context of our thesis, it's evident that hydrodynamic drag plays a role in the processes influencing the motion of massive bodies. This hydrodynamical drag, or friction, can be studied in the context of the origin of the supermassive black holes. When black holes navigate through densely packed interstellar environments, they encounter hydrodynamic drag, which effectively curtails their motion. This deceleration induces a loss of angular momentum, promoting the merging of these black holes with other massive celestial bodies. Consequently, these mergers contribute to the consolidation of increasingly massive black holes, speeding up the formation of supermassive black holes at the centers of evolving galaxies. This mechanism of gravitational interaction, modulated by hydrodynamic drag, offers insights into the swift formation of SMBHs, a phenomenon that resonates with observations of quasars at exceptionally high redshifts (Kroupa et al., 2020).

The computational framework employed for our simulations has demonstrated remarkable stability and robustness, with computations spanning runs exceeding 50,000 iterations, the software exhibited consistent performance without encountering any significant issues or instabilities. However, these extensive simulations necessitated substantial computational resources, particularly in terms of memory requirements. Despite the larger memory footprint and computational time, the software maintained its stability, highlighting its suitability for tackling complex astrophysical phenomena.

In future investigations, this area of study could be expanded to include several additional factors that were not incorporated in our current simulations. These factors encompass various aspects of stellar evolution, such as the potential loss of momentum and mass resulting from stellar ablation induced by the surrounding environment or jets. This phenomenon is presently under comprehensive examination by Petr Kurfürst and Michal Zajaček of the High-Energy Astrophysics Group in Brno (Zajaček et al., 2020). Additionally, accounting for the Lense-Thirring precession in consideration of the black hole's spin and interactions among neighboring stars could further enhance the fidelity of our models. Moreover, our current system does not factor in the gravitational influence of stars on the accretion disc or the magnetic properties detailed in Chapter 2.4.2. Another very interesting extension could be the confrontation of these simulations with the real observed situation from which the limit on the density of the medium could be derived. Overall, this field presents ample opportunities for future research.

CONCLUSION

In this thesis, we delved into the dynamics of S2, a star orbiting the supermassive black hole SgrA* at the center of our Milky Way galaxy. Our exploration aimed to uncover the influence of various factors, including the gaseous-dusty environment and Schwarzschild precession, on the orbital motion of S2.

Through comprehensive simulations and analysis, we explored two primary scenarios: Bondi accretion and accretion disc environments. In the Bondi accretion scenario, we observed the rapid inspiral of particles towards the black hole, with their orbits gradually circularizing due to the transfer of orbital energy to internal energy. The inclusion of hydrodynamical drag and post-Newtonian corrections revealed significant effects on the orbital parameters, highlighting the importance of these factors in accurately modeling astrophysical systems.

For the star S2, we have demonstrated that the gaseous-dusty environment surrounding the star exerts minimal influence on its orbit. Conversely, our investigation into Schwarzschild precession has revealed a profound effect on the orientation of S2's orbital plane. The substantial shift, approximately $\Delta\varphi \approx 12''$, underscores the significance of relativistic corrections in accurately describing the motion of celestial bodies in the vicinity of massive gravitational sources.

Transitioning to the thick accretion disc scenario, we investigated the behavior of particles within the boundaries of a dense, gaseous disc. Our simulations demonstrated the tendency of particles to align with the disc plane, accompanied by notable changes in the argument of periapsis. However, the dense environment of the accretion disc exerted negligible perturbative effects on S2's trajectory, highlighting the resilience of massive stellar bodies to external gravitational forces within certain configurations.

Furthermore, our exploration extended to the Shakura-Sunyaev disc scenario, where we examined the effects of disc thickness on orbital stability. Despite the minimal impact observed in thin-disc configurations, variations in the accretion rate could potentially lead to significant alterations in orbital trajectories.

BIBLIOGRAPHY

[1]R. Abuter, N. Aimar, P. Amaro Seoane, A. Amorim, M. Bauböck, J. P. Berger, H. Bonnet, G. Bourdarot, W. Brandner, V. Cardoso, Y. Clénet, R. Davies, P. T. de Zeeuw, J. Dexter, A. Drescher, A. Eckart, F. Eisenhauer, H. Feuchtgruber, G. Finger, N. M. Förster Schreiber, A. Foschi, P. Garcia, F. Gao, Z. Gelles, E. Gendron, R. Genzel, S. Gillessen, M. Hartl, X. Haubois, F. Haussmann, G. Heißel, T. Henning, S. Hippler, M. Horrobin, L. Jochum, L. Jocou, A. Kaufer, P. Kervella, S. Lacour, V. Lapeyrère, J.-B. Le Bouquin, P. Léna, D. Lutz, F. Mang, N. More, T. Ott, T. Paumard, K. Perraut, G. Perrin, O. Pfuhl, S. Rabien, D. C. Ribeiro, M. Sadun Bordoni, S. Scheithauer, J. Shangguan, T. Shimizu, J. Stadler, O. Straub, C. Straubmeier, E. Sturm, L. J. Tacconi, F. Vincent, S. von Fellenberg, F. Widmann, M. Wielgus, E. Wieprecht, E. Wiezorrek, and J. Woillez, "Polarimetry and astrometry of nir flares as event horizon scale, dynamical probes for the mass of sgr a*," Astronomy & Astrophysics **677**, L10 (2023).

[2]R. Abuter, A. Amorim, M. Bauböck, J. P. Berger, H. Bonnet, W. Brandner, Y. Clénet, R. Davies, P. T. de Zeeuw, J. Dexter, Y. Dallilar, A. Drescher, A. Eckart, F. Eisenhauer, N. M. Förster Schreiber, P. Garcia, F. Gao, E. Gendron, R. Genzel, S. Gillessen, M. Habibi, X. Haubois, G. Heißel, T. Henning, S. Hippler, M. Horrobin, A. Jiménez-Rosales, L. Jochum, L. Jocou, A. Kaufer, P. Kervella, S. Lacour, V. Lapeyrère, J.-B. Le Bouquin, P. Léna, D. Lutz, M. Nowak, T. Ott, T. Paumard, K. Perraut, G. Perrin, O. Pfuhl, S. Rabien, G. Rodríguez-Coira, J. Shangguan, T. Shimizu, S. Scheithauer, J. Stadler, O. Straub, C. Straubmeier, E. Sturm, L. J. Tacconi, F. Vincent, S. von Fellenberg, I. Waisberg, F. Widmann, E. Wieprecht, E. Wiezorrek, J. Woillez, S. Yazici, A. Young, and G. Zins, "Improved gravity astrometric accuracy from modeling optical aberrations," Astronomy and Astrophysics **647**, A59 (2021).

[3]T. Alexander, "Stellar Dynamics and Stellar Phenomena Near a Massive Black Hole," Annual Review of Astron and Astrophysis **55**, 17–57 (2017).

[4]B. Ali, D. Paul, A. Eckart, M. Parsa, M. Zajacek, F. Peißker, M. Subroweit, M. Valencia-S., L. Thomkins, and G. Witzel, "Kinematic structure of the galactic center s cluster," The Astrophysical Journal **896**, 100 (2020).

[5]P. Amaro-Seoane, J. R. Gair, M. Freitag, M. C. Miller, I. Mandel, C. J. Cutler, and S. Babak, "Intermediate and extreme mass-ratio inspirals—astrophysics, science applications and detection using lisa," Classical and Quantum Gravity **24**, R113–R169 (2007).

[6]F. K. Baganoff, "Multiwavelength Monitoring of Sgr A* During Chandra Observations of Multiple X-ray Flares," in Aas/high energy astrophysics division #7, Vol. 7, AAS/High Energy Astrophysics Division (Mar. 2003), p. 03.02.

[7]F. K. Baganoff, M. W. Bautz, W. N. Brandt, G. Chartas, E. D. Feigelson, G. P. Garmire, Y. Maeda, M. Morris, G. R. Ricker, L. K. Townsley, and F. Walter, "Rapid x-ray flaring from the direction of the supermassive black hole at the galactic centre," Nature **413**, 45–48 (2001).

[8]B. Balick and R. L. Brown, "Intense sub-arcsecond structure in the galactic center.," Astrophysical Journal **194**, 265–270 (1974).

[9]H. Bartko, F. Martins, S. Trippe, T. K. Fritz, R. Genzel, T. Ott, F. Eisenhauer, S. Gillessen, T. Paumard, T. Alexander, K. Dodds-Eden, O. Gerhard, Y. Levin, L. Mascetti, S. Nayakshin, H. B. Perets, G. Perrin, O. Pfuhl, M. J. Reid, D. Rouan, M. Zilka, and A. Sternberg, "An Extremely Top-Heavy Initial Mass Function in the Galactic Center Stellar Disks," The Astrophysical Journal **708**, 834–840 (2010).

[10]E. E. Becklin and G. Neugebauer, "Infrared Observations of the Galactic Center," The Astrophysical Journal **151**, 145 (1968).

[11]R. Bender, J. Kormendy, G. Bower, R. Green, J. Thomas, A. C. Danks, T. Gull, J. B. Hutchings, C. L. Joseph, M. E. Kaiser, T. R. Lauer, C. H. Nelson, D. Richstone, D. Weistrop, and B. Woodgate, "HST STIS Spectroscopy of the Triple Nucleus of M31: Two Nested Disks in Keplerian Rotation around a Supermassive Black Hole," The Astrophysical Journal **631**, 280–300 (2005).

[12]R. D. Blum, S. V. Ramirez, K. Sellgren, and K. Olsen, "Really cool stars and the star formation history at the galactic center," The Astrophysical Journal **597**, 323–346 (2003).

[13]A. Boehle, A. M. Ghez, R. Schödel, L. Meyer, S. Yelda, S. Albers, G. D. Martinez, E. E. Becklin, T. Do, J. R. Lu, K. Matthews, M. R. Morris, B. Sitarski, and G. Witzel, "An Improved Distance and Mass Estimate for Sgr A* from a Multistar Orbit Analysis," Astrophysical Journal **830**, 17, 17 (2016).

[14]G. C. Bower, W. M. Goss, H. Falcke, D. C. Backer, and Y. Lithwick, "The intrinsic size of sagittarius a* from 0.35 to 6 cm," The Astrophysical Journal **648**, L127–L130 (2006).

[15]R. L. Branham, "The distance to the Galactic center determined by OB stars," Astronomy and Astrophysics, Supplement **353**, 179–190 (2014).

[16]T. Böker, S. Laine, R. P. van der Marel, M. Sarzi, H.-W. Rix, L. C. Ho, and J. C. Shields, "A hubble space telescope census of nuclear star clusters in late-type spiral galaxies. i. observations and image analysis*," The Astronomical Journal **123**, 1389 (2002).

[17]T. Böker, M. Sarzi, D. E. McLaughlin, R. P. van der Marel, H.-W. Rix, L. C. Ho, and J. C. Shields, "A hubble space telescope census of nuclear star clusters in late-type spiral galaxies. ii. cluster sizes and structural parameter correlations," The Astronomical Journal **127**, 105 (2004).

[18]R. Capuzzo-Dolcetta and A. Mastrobuono-Battisti, "Globular cluster system erosion in elliptical galaxies," Astronomy and Astrophysics Journal **507**, 183–193 (2009).

[19]C. M. Carollo, M. Stiavelli, M. Seigar, P. T. de Zeeuw, and H. Dejonghe, "Spiral Galaxies with HST/NICMOS. I. Nuclear Morphologies, Color Maps, and Distinct Nuclei," The Astronomical Journal **123**, 159–183 (2002).

[20]M. H. Christopher, N. Z. Scoville, S. R. Stolovy, and M. S. Yun, "Hcn and hco+observations of the galactic circumnuclear disk," The Astrophysical Journal **622**, 346–365 (2005).

[21]T. E. H. T. Collaboration, "First sagittarius a* event horizon telescope results. v. testing astrophysical models of the galactic center black hole," The Astrophysical Journal Letters **930** (2022).

[22]T. E. H. T. Collaboration, "First sagittarius a* event horizon telescope results. vii. polarization of the ring," The Astrophysical Journal Letters **964**, L25 (2024).

[23]P. Côté, S. Piatek, L. Ferrarese, A. Jordán, D. Merritt, E. W. Peng, M. Haşegan, J. P. Blakeslee, S. Mei, M. J. West, M. Milosavljević, and J. L. Tonry, "The ACS Virgo Cluster Survey. VIII. The Nuclei of Early-Type Galaxies," The Astrophysical Journal, Supplement **165**, 57–94 (2006).

[24]M. K. Crawford, R. Genzel, A. I. Harris, D. T. Jaffe, J. H. Lacy, J. B. Lugten, E. Serabyn, and C. H. Townes, "Mass distribution in the galactic centre," Nature **315**, 467–470 (1985).

[25]M. B. Davies and A. King, "The stars of the galactic center," The Astrophysical Journal **624**, L25 (2005).

[26]T. Do, A. M. Ghez, M. R. Morris, S. Yelda, L. Meyer, J. R. Lu, S. D. Hornstein, and K. Matthews, "A Near-Infrared Variability Study of the Galactic Black Hole: A Red Noise Source with NO Detected Periodicity," The Astrophysical Journal **691**, 1021–1034 (2009).

[27]T. Do, G. D. Martinez, S. Yelda, A. Ghez, J. Bullock, M. Kaplinghat, J. R. Lu, A. H. G. Peter, and K. Phifer, "Three-dimensional stellar kinematics at the galactic center: measuring the nuclear star cluster spatial density profile, black hole mass, and distance," The Astrophysical Journal **779**, L6 (2013).

[28]T. Do, A. Hees, A. Ghez, G. D. Martinez, D. S. Chu, S. Jia, S. Sakai, J. R. Lu, A. K. Gautam, K. K. O'Neil, E. E. Becklin, M. R. Morris, K. Matthews, S. Nishiyama, R. Campbell, S. Chappell, Z. Chen, A. Ciurlo, A. Dehghanfar, E. Gallego-Cano, W. E. Kerzendorf, J. E. Lyke, S. Naoz, H. Saida, R. Schödel, M. Takahashi, Y. Takamori, G. Witzel, and P. Wizinowich, "Relativistic redshift of the star so-2 orbiting the galactic center supermassive black hole," Science **365**, 664–668 (2019).

[29]K. Dodds-Eden, S. Gillessen, T. K. Fritz, F. Eisenhauer, S. Trippe, R. Genzel, T. Ott, H. Bartko, O. Pfuhl, G. Bower, A. Goldwurm, D. Porquet, G. Trap, and F. Yusef-Zadeh, "The two states of sgr a* in the near-infrared: bright episodic flares on top of low-level continuous variability," The Astrophysical Journal **728**, 37 (2011).

[30]L. J. Dursi and C. Pfrommer, "Draping of cluster magnetic fields over bullets and bubbles—morphology and dynamic effects," The Astrophysical Journal **677**, 993 (2008).

[31]I. Dékány, D. Minniti, M. Catelan, M. Zoccali, R. K. Saito, M. Hempel, and O. A. Gonzalez, "Vvv survey near-infrared photometry of known bulge rr lyrae stars: the distance to the galactic center and absence of a barred distribution of the metal-poor population," The Astrophysical Journal **776**, L19 (2013).

[32]A. Eckart, F. K. Baganoff, R. Schödel, M. Morris, R. Genzel, G. C. Bower, D. Marrone, J. M. Moran, T. Viehmann, M. W. Bautz, W. N. Brandt, G. P. Garmire, T. Ott, S. Trippe, G. R. Ricker, C. Straubmeier, D. A. Roberts, F. Yusef-Zadeh, J. H. Zhao, and R. Rao, "The flare activity of Sagittarius A*. New coordinated mm to X-ray observations," Astronomy and Astrophysics **450**, 535–555 (2006).

[33]A. Eckart and R. Genzel, "Observations of the Galactic Center with SHARP: First Stellar Proper Motions," in The galactic center, Vol. 102, edited by R. Gredel, Astronomical Society of the Pacific Conference Series (Jan. 1996), p. 196.

[34]A. Eckart, R. Genzel, T. Ott, and R. Schodel, "Stellar orbits near sagittarius a," Monthly Notices of the Royal Astronomical Society **331**, 917–934 (2002).

[35]A. Eckart, A. Hüttemann, C. Kiefer, S. Britzen, M. Zajaček, C. Lämmerzahl, M. Stöckler, M. Valencia-S, V. Karas, and M. García-Marín, "The milky way's supermassive black hole: how good a case is it?: a challenge for astrophysics and philosophy of science," Foundations of Physics **47**, 553–624 (2017).

[36]F. Eisenhauer, R. Genzel, T. Alexander, R. Abuter, T. Paumard, T. Ott, A. Gilbert, S. Gillessen, M. Horrobin, S. Trippe, H. Bonnet, C. Dumas, N. Hubin, A. Kaufer, M. Kissler-Patig, G. Monnet, S. Ströbele, T. Szeifert, A. Eckart, R. Schödel, and S. Zucker, "Sinfoni in the galactic center: young stars and infrared flares in the central light-month*," The Astrophysical Journal **628**, 246 (2005).

[37]R. D. Ekers, J. H. van Gorkom, U. J. Schwarz, and W. M. Goss, "The radio structure of SGR A.," Astronomy and Astrophysics **122**, 143–150 (1983).

[38]A. Feldmeier-Krause, N. Neumayer, R. Schödel, A. Seth, M. Hilker, P. T. de Zeeuw, H. Kuntschner, C. J. Walcher, N. Lützgendorf, and M. Kissler-Patig, "Kmos view of the galactic centre," Astronomy and Astrophysics **584**, A2 (2015).

[39]A. Feldmeier, N. Neumayer, A. Seth, R. Schödel, N. Lützgendorf, P. T. de Zeeuw, M. Kissler-Patig, S. Nishiyama, and C. J. Walcher, "Large scale kinematics and dynamical modelling of the Milky Way nuclear star cluster," Astronomy and Astrophysics **570**, A2, A2 (2014).

[40]K. Ferrière, "Interstellar magnetic fields in the galactic center region," Astronomy and Astrophysics **505**, 1183–1198 (2009).

[41]C. Francis and E. Anderson, "Two estimates of the distance to the galactic centre," Monthly Notices of the Royal Astronomical Society **441**, 1105–1114 (2014).

[42]J. Frank, A. King, and D. J. Raine, *Accretion Power in Astrophysics: Third Edition* (2002).

[43]A. M. Fridman, O. V. Khoruzhii, V. V. Lyakhovich, L. Ozernoy, and L. Blitz, "Mini-spiral at the galactic center: a link between its structure and the value of a central point mass," in *Unsolved problems of the milky way: proceedings of the 169th symposium of the international astronomical union, held in the hague, the netherlands, august 23–29, 1994*, edited by L. Blitz and P. Teuben (Springer Netherlands, Dordrecht, 1996), pp. 241–246.

[44]T. K. Fritz, S. Chatzopoulos, O. Gerhard, S. Gillessen, R. Genzel, O. Pfuhl, S. Tacchella, F. Eisenhauer, and T. Ott, "The nuclear cluster of the milky way: total mass and luminosity*," The Astrophysical Journal **821**, 44 (2016).

[45]T. K. Fritz, S. Gillessen, K. Dodds-Eden, D. Lutz, R. Genzel, W. Raab, T. Ott, O. Pfuhl, F. Eisenhauer, and F. Yusef-Zadeh, "Line Derived Infrared Extinction toward the Galactic Center," The Astrophysical Journal **737**, 73, 73 (2011).

[46]R. Genzel, D. Hollenbach, and C. H. Townes, "The nucleus of our Galaxy," Reports on Progress in Physics **57**, 417–479 (1994).

[47]R. Genzel, C. Pichon, A. Eckart, O. E. Gerhard, and T. Ott, "Stellar dynamics in the galactic centre: proper motions and anisotropy," Monthly Notices of the Royal Astronomical Society **317**, 348–374 (2000).

[48]R. Genzel, R. Schödel, T. Ott, A. Eckart, T. Alexander, F. Lacombe, D. Rouan, and B. Aschenbach, "Near-infrared flares from accreting gas around the supermassive black hole at the Galactic Centre," Nature **425**, 934–937 (2003).

[49]R. Genzel, N. Thatte, A. Krabbe, H. Kroker, and L. E. Tacconi-Garman, "The Dark Mass Concentration in the Central Parsec of the Milky Way," Astrophysical Journal **472**, 153 (1996).

[50]R. Genzel and C. H. Townes, "Physical conditions, dynamics, and mass distribution in the center of the galaxy.," Annual Review of Astron and Astrophysis **25**, 377–423 (1987).

[51]R. Genzel, *A forty year journey*, 2021.

[52]R. Genzel, F. Eisenhauer, and S. Gillessen, "The galactic center massive black hole and nuclear star cluster," Reviews of Modern Physics **82**, 3121–3195 (2010).

[53]A. M. Ghez, G. Duchêne, K. Matthews, S. D. Hornstein, A. Tanner, J. Larkin, M. Morris, E. E. Becklin, S. Salim, T. Kremenek, D. Thompson, B. T. Soifer, G. Neugebauer, and I. McLean, "The first measurement of spectral lines in a short-period star bound to the galaxy's central black hole: a paradox of youth," The Astrophysical Journal **586**, L127 (2003).

[54]A. M. Ghez, B. L. Klein, M. Morris, and E. E. Becklin, "High Proper-Motion Stars in the Vicinity of Sagittarius A*: Evidence for a Supermassive Black Hole at the Center of Our Galaxy," Astrophysical Journal **509**, 678–686 (1998).

[55]A. M. Ghez, S. Salim, S. D. Hornstein, A. Tanner, J. R. Lu, M. Morris, E. E. Becklin, and G. Duchêne, "Stellar orbits around the galactic center black hole," The Astrophysical Journal **620**, 744 (2005).

[56]A. M. Ghez, S. Salim, N. N. Weinberg, J. R. Lu, T. Do, J. K. Dunn, K. Matthews, M. R. Morris, S. Yelda, E. E. Becklin, T. Kremenek, M. Milosavljevic, and J. Naiman, "Measuring Distance and Properties of the Milky Way's Central Supermassive Black Hole with Stellar Orbits," Astrophysical Journal **689**, 1044–1062 (2008).

[57]S. Gillessen, F. Eisenhauer, S. Trippe, T. Alexander, R. Genzel, F. Martins, and T. Ott, "Monitoring stellar orbits around the massive black hole in the galactic center," The Astrophysical Journal **692**, 1075 (2009).

[58]S. Gillessen, F. Eisenhauer, S. Trippe, T. Alexander, R. Genzel, F. Martins, and T. Ott, "Monitoring Stellar Orbits Around the Massive Black Hole in the Galactic Center," **692**, 1075–1109 (2009).

[59]S. Gillessen, P. M. Plewa, F. Eisenhauer, R. Sari, I. Waisberg, M. Habibi, O. Pfuhl, E. George, J. Dexter, S. v. Fellenberg, T. Ott, and R. Genzel, "An update on monitoring stellar orbits in the galactic center," The Astrophysical Journal **837**, 30 (2017).

[60]A. W. Graham and L. R. Spitler, "Quantifying the coexistence of massive black holes and dense nuclear star clusters," Monthly Notices of the Royal Astronomical Society **397**, 2148–2162 (2009).

[61]R. Güsten and D. Downes, "The dynamics of the Molecular Gas in the Galactic Center," Mitteilungen der Astronomischen Gesellschaft Hamburg **50**, 76 (1980).

[62]M. Habibi, S. Gillessen, F. Martins, F. Eisenhauer, P. M. Plewa, O. Pfuhl, E. George, J. Dexter, I. Waisberg, T. Ott, S. von Fellenberg, M. Bauböck, A. Jimenez-Rosales, and R. Genzel, "Twelve Years of Spectroscopic Monitoring in the Galactic Center: The Closest Look at S-stars near the Black Hole," The Astrophysical Journal **847**, 120, 120 (2017).

[63]E. Hassani, R. Pazhouhesh, and H. Ebadi, "The effect of dark matter on stars at the galactic center: the paradox of youth problem," International Journal of Modern Physics D **29**, 2050052 (2020).

[64]A. Hees, T. Do, A. Ghez, G. Martinez, S. Naoz, E. Becklin, A. Boehle, S. Chappell, D. Chu, A. Dehghanfar, K. Kosmo, J. Lu, K. Matthews, M. Morris, S. Sakai, R. Schödel, and G. Witzel, "Testing general relativity with stellar orbits around the supermassive black hole in our galactic center," Physical Review Letters **118**, 10.1103/physrevlett.118.211101 (2017).

[65]I. Heywood, I. Rammala, F. Camilo, W. D. Cotton, F. Yusef-Zadeh, T. D. Abbott, R. M. Adam, G. Adams, M. A. Aldera, K. M. B. Asad, E. F. Bauermeister, T. G. H. Bennett, H. L. Bester, W. A. Bode, D. H. Botha, A. G. Botha, L. R. S. Brederode, S. Buchner, J. P. Burger, T. Cheetham, D. I. L. de Villiers, M. A. Dikgale-Mahlakoana, L. J. du Toit, S. W. P. Esterhuyse, B. L. Fanaroff, S. February, D. J. Fourie, B. S. Frank, R. R. G. Gamatham, M. Geyer, S. Goedhart, M. Gouws, S. C. Gumede, M. J. Hlakola, A. Hokwana, S. W. Hoosen, J. M. G. Horrell, B. Hugo, A. I. Isaacson, G. I. G. Józsa, J. L. Jonas, A. F. Joubert, R. P. M. Julie, F. B. Kapp, J. S. Kenyon, P. P. A. Kotzé, N. Kriek, H. Kriel, V. K. Krishnan, R. Lehmensiek, D. Liebenberg, R. T. Lord, B. M. Lunsky, K. Madisa, L. G. Magnus, O. Mahgoub, A. Makhaba, S. Makhathini, J. A. Malan, J. R. Manley, S. J. Marais, A. Martens, T. Mauch, B. C. Merry, R. P. Millenaar, N. Mnyandu, O. J. Mokone, T. E. Monama, M. C. Mphego, W. S. New, B. Ngcebetsha, K. J. Ngoasheng, M. T. Ockards, N. Oozeer, A. J. Otto, S. S. Passmoor, A. A. Patel, A. Peens-Hough, S. J. Perkins, A. J. T. Ramaila, N. M. R. Ramanujam, Z. R. Ramudzuli, S. M. Ratcliffe, A. Robyntjies, S. Salie, N. Sambu, C. T. G. Schollar, L. C. Schwardt, R. L. Schwartz, M. Serylak, R. Siebrits, S. K. Sirothia, M. Slabber, O. M. Smirnov, L. Sofeya, B. Taljaard, C. Tasse, A. J. Tiplady, O. Toruvanda, S. N. Twum, T. J. van Balla, A. van der Byl, C. van der Merwe, V. Van Tonder, R. Van Wyk, A. J. Venter, M. Venter, B. H. Wallace, M. G. Welz, L. P. Williams, and B. Xaia, "The 1.28 ghz meerkat galactic center mosaic," The Astrophysical Journal **925**, 165 (2022).

[66]M. Horrobin, F. Eisenhauer, M. Tecza, N. Thatte, R. Genzel, R. Abuter, C. Iserlohe, J. Schreiber, A. Schegerer, D. Lutz, T. Ott, and R. Schödel, "First results from SPIFFI. I: The Galactic Center," Astronomische Nachrichten **325**, 88–91 (2004).

[67]HubbleSite, *Nasa's great observatories examine the galactic center region*, (2024) https://hubblesite.org/contents/media/images/2009/28/2634-Image.html?news=true (visited on 04/03/2024).

[68]M. Inoue, T. Takahashi, H. Tabara, T. Kato, and M. Tsuboi, "Extremely large Faraday rotation at the radio arc in the galactic center region.," Publications of the Astronomical Society of Japan **36**, 633–638 (1984).

[69]Z. M. Jan Janík, *Obecná astronomie* (2022).

[70]K. G. Jansky, "Electrical disturbances apparently of extraterrestrial origin," Proceedings of the Institute of Radio Engineers **21**, 1387–1398 (1933).

[71]T. W. Jones, "On the Nature of the Nonthermal Radio Emission from the Galactic Center," Astronomy and Astrophysics **30**, 37 (1974).

[72]R. Kannan and P. Saha, "Frame dragging and the kinematics of galactic-center stars," The Astrophysical Journal **690**, 1553 (2008).

[73]R. P. Kerr, "Gravitational field of a spinning mass as an example of algebraically special metrics," Phys. Rev. Lett. **11**, 237–238 (1963).

[74]A. King, "How big can a black hole grow?" Monthly Notices of the Royal Astronomical Society: Letters **456**, L109–L112 (2015).

[75]A. Krabbe, R. Genzel, A. Eckart, F. Najarro, D. Lutz, M. Cameron, H. Kroker, L. E. Tacconi-Garman, N. Thatte, L. Weitzel, S. Drapatz, T. Geballe, A. Sternberg, and R. Kudritzki, "The nuclear cluster of the milky way: star formation and velocity dispersion in the central 0.5 parsec," The Astrophysical Journal **447**, L95 (1995).

[76]P. Kroupa, L. Subr, T. Jerabkova, and L. Wang, "Very high redshift quasars and the rapid emergence of supermassive black holes," Monthly Notices of the Royal Astronomical Society **498**, 5652–5683 (2020).

[77]R. M. Lau, T. L. Herter, M. R. Morris, E. E. Becklin, and J. D. Adams, "Sofia/forcast imaging of the circumnuclear ring at the galactic center," The Astrophysical Journal **775**, 37 (2013).

[78]H. W. Leung, J. Bovy, J. T. Mackereth, J. A. S. Hunt, R. R. Lane, and J. C. Wilson, "A measurement of the distance to the galactic centre using the kinematics of bar stars," Monthly Notices of the Royal Astronomical Society **519**, 948–960 (2022).

[79]Y. Levin and A. M. Beloborodov, "Stellar disk in the galactic center: a remnant of a dense accretion disk?" The Astrophysical Journal **590**, L33 (2003).

[80]Y. Levin and A. M. Beloborodov, "Stellar disk in the galactic center: a remnant of a dense accretion disk?" The Astrophysical Journal **590**, L33 (2003).

[81]K. Y. Lo and M. J. Claussen, "High-resolution observations of ionized gas in central 3 parsecs of the Galaxy: possible evidence for infall," Nature **306**, 647–651 (1983).

[82]J. M. Lotz, R. Telford, H. C. Ferguson, B. W. Miller, M. Stiavelli, and J. Mack, "Dynamical Friction in DE Globular Cluster Systems," The Astrophysical Journal **552**, 572–581 (2001).

[83]J. R. Lu, T. Do, A. M. Ghez, M. R. Morris, S. Yelda, and K. Matthews, "Stellar populations in the central 0.5 pc of the galaxy. ii. the initial mass function," The Astrophysical Journal **764**, 155 (2013).

[84]Y. Maeda, F. K. Baganoff, E. D. Feigelson, M. Morris, M. W. Bautz, W. N. Brandt, D. N. Burrows, J. P. Doty, G. P. Garmire, S. H. Pravdo, G. R. Ricker, and L. K. Townsley, "Achandrastudy of sagittarius a east: a supernova remnant regulating the activity of our galactic center?" The Astrophysical Journal **570**, 671–687 (2002).

[85]D. J. Majaess, D. G. Turner, and D. J. Lane, "Characteristics of the galaxy according to cepheids," Monthly Notices of the Royal Astronomical Society **398**, 263–270 (2009).

[86]Z. M. Malkin, "Analysis of determinations of the distance between the sun and the galactic center," Astronomy Reports **57**, 128–133 (2013).

[87]E. Maoz, "Dynamical constraints on alternatives to supermassive black holes in galactic nuclei," The Astrophysical Journal **494**, L181 (1998).

[88]F. Martins, S. Gillessen, F. Eisenhauer, R. Genzel, T. Ott, and S. Trippe, "On the nature of the fast-moving star s2 in the galactic center*," The Astrophysical Journal **672**, L119 (2007).

[89]M. McCourt, R. M. O'Leary, A.-M. Madigan, and E. Quataert, "Magnetized gas clouds can survive acceleration by a hot wind," Monthly Notices of the Royal Astronomical Society **449**, 2–7 (2015).

[90]D. Merritt, "Evolution of nuclear star clusters," The Astrophysical Journal **694**, 959–970 (2009).

[91]D. Merritt, T. Alexander, S. Mikkola, and C. M. Will, "Testing properties of the galactic center black hole using stellar orbits," Phys. Rev. D **81**, 062002 (2010).

[92]P. G. Mezger, W. J. Duschl, and R. Zylka, "The Galactic Center: a laboratory for AGN?" Astronomy and Astrophysics Reviews **7**, 289–388 (1996).

[93]E. Mills, M. Morris, C. Lang, H. Dong, Q. Wang, A. Cotera, and S. Stolovy, "Properties of the compact hii region complex g-0.02-0.07," (2011).

[94]M. Milosavljevic, "On the origin of nuclear star clusters in late-type spiral galaxies," The Astrophysical Journal **605**, L13–L16 (2004).

[95]M. Morris, "The galactic center magnetosphere," Journal of Physics: Conference Series **54**, 1 (2006).

[96]R. Narayan, R. Mahadevan, J. E. Grindlay, R. G. Popham, and C. Gammie, "Advection-dominated accretion model of sagittarius a*: evidence for a black hole at the galactic center," The Astrophysical Journal **492**, 554–568 (1998).

[97]R. Narayan, I. Yi, and R. Mahadevan, "Explaining the spectrum of Sagittarius A* with a model of an accreting black hole," Nature **374**, 623–625 (1995).

[98]N. Neumayer, A. Seth, and T. Böker, "Nuclear star clusters," The Astronomy and Astrophysics Review **28**, 10.1007/s00159-020-00125-0 (2020).

[99]N. Neumayer, C. J. Walcher, D. Andersen, S. F. Sánchez, T. Böker, and H.-W. Rix, "Two-dimensional halpha kinematics of bulgeless disc galaxies," Monthly Notices of the Royal Astronomical Society **413**, 1875–1888 (2011).

[100]D. D. Nguyen, A. C. Seth, N. Neumayer, S. Iguchi, M. Cappellari, J. Strader, L. Chomiuk, E. Tremou, F. Pacucci, K. Nakanishi, A. Bahramian, P. M. Nguyen, M. den Brok, C. C. Ahn, K. T. Voggel, N. Kacharov, T. Tsukui, C. K. Ly, A. Dumont, and R. Pechetti, "Improved dynamical constraints on the masses of the central black holes in nearby low-mass early-type galactic nuclei and the first black hole determination for ngc 205," The Astrophysical Journal **872**, 104 (2019).

[101]K. S. Oh and D. N. C. Lin, "Nucleation of Dwarf Galaxies in the Virgo Cluster," The Astrophysical Journal **543**, 620–633 (2000).

[102]J. Oort, "The Galactic Center," Annual Review of Astronomy and Astrophysics **15**, 295–362 (1997).

[103]E. C. Ostriker, "Dynamical Friction in a Gaseous Medium," The Astrophysical Journal **513**, 252–258 (1999).

[104]M. Parsa, A. Eckart, B. Shahzamanian, V. Karas, M. Zajaček, J. A. Zensus, and C. Straubmeier, "Investigating the relativistic motion of the stars near the supermassive black hole in the galactic center," The Astrophysical Journal **845**, 22 (2017).

[105]T. Paumard, R. Genzel, F. Martins, S. Nayakshin, A. M. Beloborodov, Y. Levin, S. Trippe, F. Eisenhauer, T. Ott, S. Gillessen, R. Abuter, J. Cuadra, T. Alexander, and A. Sternberg, "The two young star disks in the central parsec of the galaxy: properties, dynamics, and formation*," The Astrophysical Journal **643**, 1011 (2006).

[106]T. Paumard, J.-P. Maillard, and M. Morris, "Kinematic and structural analysis of the minispiral in the galactic center from bear spectro-imagery," Astronomy and Astrophysics **426**, 81–96 (2004).

[107]T. Paumard, J. P. Maillard, M. Morris, and F. Rigaut, "New results on the helium stars in the galactic center using bear spectro-imagery," Astronomy and Astrophysics **366**, 466–480 (2001).

[108]P. M. Plewa, S. Gillessen, F. Eisenhauer, T. Ott, O. Pfuhl, E. George, J. Dexter, M. Habibi, R. Genzel, M. J. Reid, and K. M. Menten, "Pinpointing the near-infrared location of Sgr A* by correcting optical distortion in the NACO imager," Monthly Notices of the Royal Astronomical Society **453**, 3234–3244 (2015).

[109]D. Porquet, N. Grosso, V. Burwitz, I. L. Andronov, B. Aschenbach, P. Predehl, and R. S. Warwick, "Discovery of a bright X-ray transient in the Galactic Center with XMM-Newton," Astronomy and Astrophysics **430**, L9–L12 (2005).

[110]E. Quataert, R. Narayan, and M. J. Reid, "What is the accretion rate in sagittarius a*?" The Astrophysical Journal **517**, L101 (1999).

[111]K. P. Rauch and B. Ingalls, "Resonant tidal disruption in galactic nuclei," Monthly Notices of the Royal Astronomical Society **299**, 1231–1241 (1998).

[112]M. J. Reid, J. A. Braatz, J. J. Condon, K. Y. Lo, C. Y. Kuo, C. M. V. Impellizzeri, and C. Henkel, "The Megamaser Cosmology Project. IV. A Direct Measurement of the Hubble Constant from UGC 3789," Astrophysical Journal **767**, 154, 154 (2013).

[113]M. J. Reid, "The distance to the center of the Galaxy.," Annual Review of Astronomy and Astrophysics **31**, 345–372 (1993).

[114]N. Sabha, A. Eckart, D. Merritt, M. Zamaninasab, G. Witzel, M. García-Marín, B. Jalali, M. Valencia-S., S. Yazici, R. Buchholz, B. Shahzamanian, C. Rauch, M. Horrobin, and C. Straubmeier, "The s-star cluster at the center of the milky way: on the nature of diffuse nir emission in the inner tenth of a parsec," Astronomy and Astrophysics **545**, A70 (2012).

[115]R. H. Sanders, "The circumnuclear material in the Galactic Centre: a clue to the accretion process," Monthly Notices of the Royal Astronomical Society **294**, 35–46 (1998).

[116]R. Schödel, A. Feldmeier, D. Kunneriath, S. Stolovy, N. Neumayer, P. Amaro-Seoane, and S. Nishiyama, "Surface brightness profile of the Milky Way's nuclear star cluster," Astronomy and Astrophysics **566**, A47, A47 (2014).

[117]R. Schödel, T. Ott, R. Genzel, A. Eckart, N. Mouawad, and T. Alexander, "Stellar Dynamics in the Central Arcsecond of Our Galaxy," The Astrophysical Journal **596**, 1015–1034 (2003).

[118]K. Schwarzschild, *On the gravitational field of a mass point according to einstein's theory*, 1916.

[119]R. Schödel, D. Merritt, and A. Eckart, "The nuclear star cluster of the milky way: proper motions and mass," Astronomy and Astrophysics **502**, 91–111 (2009).

[120]R. Schödel, T. Ott, R. Genzel, R. Hofmann, M. Lehnert, A. Eckart, N. Mouawad, T. Alexander, M. J. Reid, R. Lenzen, M. Hartung, F. Lacombe, D. Rouan, E. Gendron, G. Rousset, A.-M. Lagrange, W. Brandner, N. Ageorges, C. Lidman, A. F. M. Moorwood, J. Spyromilio, N. Hubin, and K. M. Menten, "A star in a 15.2-year orbit around the supermassive black hole at the centre of the milky way," Nature **419**, 694–696 (2002).

[121]A. Seth, J. Dalcanton, P. Hodge, and V. Debattista, "Clues to nuclear star cluster formation from edge?on spirals," The Astronomical Journal **132**, 2539–2555 (2006).

[122]H. Shapley, "Studies based on the colors and magnitudes in stellar clusters. VII. The distances, distribution in space, and dimensions of 69 globular clusters.," The Astrophysical Journal **48**, 154–181 (1918).

[123]O. P. Stoyanovskaya, F. A. Okladnikov, E. I. Vorobyov, Y. N. Pavlyuchenkov, and V. V. Akimkin, "Simulations of dynamical gas–dust circumstellar disks: going beyond the epstein regime," Astronomy Reports **64**, 107–125 (2020).

[124]A. Szolgyen, M. MacLeod, and A. Loeb, "Eccentricity evolution in gaseous dynamical friction," Monthly Notices of the Royal Astronomical Society **513**, 5465–5473 (2022).

[125]A. Tanner, D. F. Figer, F. Najarro, R. P. Kudritzki, D. Gilmore, M. Morris, E. E. Becklin, I. S. McLean, A. M. Gilbert, J. R. Graham, J. E. Larkin, N. A. Levenson, and H. I. Teplitz, "High Spectral Resolution Observations of the Massive Stars in the Galactic Center," Astrophysical Journal **641**, 891–904 (2006).

[126]*The lion king*, 1994.

[127]S. D. Tremaine, J. P. Ostriker, and J. Spitzer L., "The formation of the nuclei of galaxies. I. M31.," The Astrophysical Journal **196**, 407–411 (1975).

[128]M. Tsuboi, M. Inoue, T. Handa, H. Tabara, and T. Kato, "Two highly polarized lobes near tge Galactic Center.," Publications of the Astronomical Society of Japan **37**, 359–368 (1985).

[129]M. Tsuboi, M. Inoue, T. Handa, H. Tabara, T. Kato, Y. Sofue, and N. Kaifu, "Prominent polarized plumes in the Galactic Center region and their magnetic field.," The Astronomy Journal **92**, 818–824 (1986).

[130]UCLA, *Take an educational journey to the center of our galaxy*, (2024) https://www.astro.ucla.edu/~ghezgroup/gc_edit/Latest/journey.html (visited on 04/03/2024).

[131]E. Vanhollebeke, M. A. T. Groenewegen, and L. Girardi, "Stellar populations in the Galactic bulge. Modelling the Galactic bulge with TRILEGAL," Astronomy & Astrophysics **498**, 95–107 (2009).

[132]E. Villaver and M. Livio, "The Orbital Evolution of Gas Giant Planets Around Giant Stars," The Astrophysical Journal **705**, L81–L85 (2009).

[133]C. J. Walcher, T. Böker, S. Charlot, L. C. Ho, H. W. Rix, J. Rossa, J. C. Shields, and R. P. van der Marel, "Stellar Populations in the Nuclei of Late-Type Spiral Galaxies," The Astrophysical Journal **649**, 692–708 (2006).

[134]Q. D. Wang, "Chandra large-scale mapping of the Galactic Centre: probing high-energy structures around the central molecular zone," Monthly Notices of the Royal Astronomical Society **504**, 1609–1618 (2021).

[135]J. A. Wheeler, "Our universe: the known and the unknown.," Amer. Sch., 37: 248-74(Spring 1968). (1968).

[136]Wikipedia, *Orbital elements*, (2024) https://en.wikipedia.org/w/index.php?title=Orbital_elements&oldid=1221112683 (visited on 05/06/2024).

[137]E. R. Wollman, T. R. Geballe, J. H. Lacy, C. H. Townes, and D. M. Rank, "Ne II 12.8 micron emission from the galactic center. II.," Astrophysical Journall **218**, L103–L107 (1977).

[138]F. Yusef-Zadeh, M. Morris, and D. Chance, "Large, highly organized radio structures near the galactic centre," Nature **310**, 557–561 (1984).

[139]F. Yusef-Zadeh and M. Morris, "The Linear Filaments of the Radio Arc near the Galactic Center," The Astrophysical Journal **322**, 721 (1987).

[140]M. Zajaček, A. Araudo, V. Karas, B. Czerny, and A. Eckart, "Depletion of Bright Red Giants in the Galactic Center during Its Active Phases," The Astrophysical Journal **903**, 140, 140 (2020).

[141]J.-H. Zhao, M. R. Morris, W. M. Goss, and T. An, "Dynamics of ionized gas at the galactic center: very large array observations of the three-dimensional velocity field and location of the ionized streams in sagittarius a west," The Astrophysical Journal **699**, 186 (2009).

[142]S. Zucker, T. Alexander, S. Gillessen, F. Eisenhauer, and R. Genzel, "Probing Post-Newtonian Physics near the Galactic Black Hole with Stellar Redshift Measurements," The Astrophysical Journal **639**, L21–L24 (2006).